R. & M. No. 3781

PROCUREMENT EXECUTIVE MINISTRY OF DEFENCE

AERONAUTICAL RESEARCH COUNCIL
REPORTS AND MEMORANDA

Interference Problems on Wing–Fuselage Combinations in Inviscid, Incompressible Flow

By J. WEBER AND M. GAYNOR JOYCE

Aerodynamics Dept., R.A.E., Farnborough

LONDON: HER MAJESTY'S STATIONERY OFFICE
1976

£4·50 NET

Interference Problems on Wing–Fuselage Combinations in Inviscid, Incompressible Flow

By J. WEBER AND M. GAYNOR JOYCE

Aerodynamics Dept., R.A.E., Farnborough

Reports and Memoranda No. 3781*

May, 1974

Summary

Some interference effects between fuselage and wing are studied for two classes of configurations. The fuselage is an infinite cylinder of circular cross section with the axis parallel to the main stream. The wings have constant chord and infinite span, they are attached in a midwing position to the fuselage. In the first group of configurations, the wings are non-lifting and have the same symmetrical section shape across the span; in the second group the wings are warped such that, when attached to the fuselage, they produce the same chordwise load distribution across the span. For the first class of wings, the Report deals with the change of the pressure distribution caused by the body interference, and, for the second class, with the change of the required shape of the mean surface.

The problems are solved by considering first the flow field past a single kinked infinite swept source line or a vortex, in the presence of the fuselage, and by computing some velocity components. From the tabulated values of these velocity components, the interference velocities for wings of given thickness distribution or load distribution can be derived by chordwise integration. A few examples demonstrate how the interference effects can vary with the angle of sweep, with the ratio between body radius and wing chord and with the spanwise distance from the wing–body junction.

The present Report summarises the work published previously in four separate reports.[1–4]

* Replaces R.A.E., Technical Report 74073—A.R.C. 35 588

LIST OF CONTENTS

1. Introduction

The aim of this Report is to study some interference effects between fuselage and wing in inviscid incompressible flow. From the large variety of possible wing–fuselage configurations, we select a restricted class, so that we are able to examine in a systematic manner how the interference velocity depends on certain geometric parameters. We intend to provide also the means for deriving, without much further computation, an estimate of some interference effects for configurations which differ from those dealt with in detail.

We consider an infinite cylindrical fuselage of circular cross section, with the axis parallel to the main stream so that the isolated fuselage does not perturb the main stream.

The wings are of constant chord and infinite span; they are attached in a midwing position to the fuselage. Two types of wing are to be considered: either the wings are untwisted and have the same symmetrical section shape across the span, or they are warped (i.e. cambered and twisted) such that, when attached to the fuselage, they produce the same chordwise load distribution across the span.

The thickness- and load-distributions are to be such that they produce small perturbations of the main flow, except near leading and trailing edges. The wings can therefore be represented by singularity distributions in the chordal plane of the wing.

We consider only singularity distributions in a plane which contains the axis of the fuselage. For the configuration with the untwisted, uncambered wing, both wing and fuselage are therefore at zero incidence to the main stream, so that we are dealing with a pure displacement flow. For the configuration with the warped wing, we consider only load distributions which produce small angles of twist near the wing–body junction; we thus ensure that the angle between the wing chord and the body axis is sufficiently small for us to ignore its effect on the interference velocity.

With the configurations chosen, the sides of the fuselage cross the chordal plane at right angles. The fuselage affects the flow near the wing-body junction in a way similar to that of an infinite reflection plate normal to the wing plane; but the flow is influenced also by the finite curvature of the body. The aim of the present Report is to examine this second effect. For the uncambered wing, we determine the difference between the pressure distribution on a wing–fuselage combination and that on the wing when it is attached to an infinite reflection plate. This latter distribution is the same as that on the isolated swept wing with its centre section at the wing-body junction. (In the following, 'isolated wing' is used to describe the nett wing attached to an infinite reflection plate.) For the fuselage in combination with a cambered wing, we examine how the warp of the isolated wing has to be modified in order to retain the given load distribution.

The isolated wings are represented by distributions of singularities (sources and vortices) in the wing plane. To these we must add further singularities so that the total normal velocity on the surface of the fuselage vanishes and the fuselage remains a stream surface. There exist various possible singularity distributions which would solve the problem. One could place all the additional singularities on the surface of the fuselage, or one could place some in the part of the wing plane which is inside the fuselage and some on the surface of the fuselage. We prefer the latter possibility.

We extend the singularities, which represent the isolated wing, inside the fuselage in such a way that the local reflection effect of the body wall is represented. As a consequence, the requirements for the singularity distribution on the fuselage are more easily satisfied than when all singularities are placed on the surface of the fuselage. There exists a choice of singularities inside the fuselage which take account of the local reflection effect. We choose a distribution which simplifies the computation of the induced velocity fields, using inside the fuselage the image (produced by a plane reflection) of that part of the wing source (or vortex) distribution outside the fuselage which has a spanwise width equal to the body radius. For the special case of wings of constant chord and constant section shape (or load distribution), this means that the singularity distribution in the wing plane is equivalent to a chordwise distribution of swept source lines (or vortices) of constant strength which are piecewise straight but have three kinks, namely, at the wing–body junctions and at the axis of the fuselage, as sketched in Fig. 1.

The singularities in the wing plane induce a non-zero normal velocity at the surface of the fuselage. To cancel this, we place a source distribution on the fuselage, the strength of which is determined by solving an integral equation in two variables. The components of the velocity field induced by the various singularities can be determined by evaluating double integrals.

We intend to study configurations with different values of the ratio between wing chord and body diameter, and with wings of different section shape or different chordwise load distribution. To reduce the amount of computation, we determine first the flow field past a single kinked swept source line, or a single kinked swept vortex, in the presence of a fuselage. Using the results for a single source line, or vortex, the interference effect for a complete wing can be derived by means of single integrals. The more laborious task of solving an integral

equation in two variables and of evaluating double integrals has thus to be done only once for a series of configurations with wings of the same angle of sweep.

This procedure has the disadvantage that the singular behaviour of the velocity field near a single line of singularities is more severe than near a planar distribution of singularities. We have therefore determined in detail the singular behaviour of the interference velocity near the point where the source line, or vortex, crosses the fuselage. This task would have been more difficult if the source line or vortex, had not been reflected at the side of the body.

Some values of various interference velocity components for a single source line, and for a single vortex, in the presence of a circular cylindrical fuselage are tabulated for four angles of sweep, $\phi = 0$, 30, 45 and 60 degrees. Further values are given in Refs. 3 and 4.

We use the results for the single source line to determine the effect of the fuselage on the pressure distribution of a symmetrical wing at zero incidence and consider wings of different sweep and configurations for which the ratio between body radius and wing chord varies. The results given refer to only one particular section shape, but results for other section shapes can be derived with a small amount of further effort (*see* also Ref. 3). We derive the results according to first-order theory and study also some of the second-order terms.

In practice, the wing of a wing–fuselage combination differs from the configurations mentioned so far, in that the span is finite, and the thickness distribution may vary across the span. We expect however that the results derived from infinitely long source lines will allow us to obtain a fair estimate of the interference velocity for a general wing shape. This assumption is based on the fact that, with many configurations, the fuselage has an appreciable effect on the displacement flow in only a fairly narrow region near the wing–body junction (measured in terms of the wing span). We consider only the interference velocity and not the total pressure distribution on the wing–fuselage configurations for the following reasons. (1) The interference velocity is of a magnitude which is usually appreciably smaller than the perturbation velocity of the isolated wing so that a crude estimate is often sufficient. (2) The flow field past a wing attached to an infinite reflection plate can be evaluated, to first or higher order accuracy, by existing computer programs (*see* for example J. A. Ledger[5] and C. C. L. Sells[6]).

For two particular configurations, we compare more exact results, derived by means of source distributions on the surface of wing and fuselage,[7–9] with the estimates obtained by means of infinitely long source lines. We have not included any comparisons with experiment since the test results available for pressure distributions near the wing–body junction are strongly influenced by a complicated development of the boundary layer, *see* for example Figs. 2 and 9 of Ref. 10.

Using the values tabulated for the downwash induced by a single vortex in the presence of the fuselage, we determine, by chordwise integration, the required change in the shape of the mean surface, for a given chordwise load distribution. A few examples demonstrate how the additional wing warp can vary with the angle of sweep, with the ratio between body radius and wing chord, and with the spanwise distance from the wing–body junction. For the wing–body junction, we consider also the effect of the finite thickness of the wing on the additional wing warp necessitated by the presence of the fuselage. We cannot yet, however, examine how useful the results for infinite vortices are in deriving an estimate for the additional wing warp in a practical design case, because no results from an accurate design method are available for comparison.

2. A Single Kinked Swept Source Line in the Presence of a Circular Cylindrical Fuselage

2.1. Velocities Induced by the Source Line

Let x, y, z be a cartesian system of coordinates, where $z = 0$ is the plane of the wing and $y = z = 0$ the axis of the fuselage. Let x, r, θ be a system of cylindrical coordinates, where $\theta = 0$ corresponds to $z = 0$ and positive values of y. We consider an infinitely long cylindrical fuselage of circular cross section $y^2 + z^2 = R^2$ and an infinitely long source line in the plane $z = 0$, which is piecewise straight, swept by an angle $\pm\phi$, and which has kinks at $x = 0$, $y = \pm R$ and at $x = R \tan \phi$, $y = 0$ (*see* Fig. 1). The position of the source line is thus given by

$$x = |R - |y|| \tan \phi. \tag{1}$$

The strength of the source line is constant along the span and equal to Q per unit length. In this and the next section, all lengths are made dimensionless by dividing by R.

The velocity field $\mathbf{v}_{MQ}(x, y, z)$ induced by the source line can be obtained from the relation

$$\mathbf{v}_{MQ}(x, y, z) = \frac{Q}{4\pi \cos\phi}\left\{\int_1^\infty \frac{[x-(y'-1)\tan\phi]\mathbf{i}+(y-y')\mathbf{j}+z\mathbf{k}}{\sqrt{[x-(y'-1)\tan\phi]^2+(y-y')^2+z^2}^3}\,dy'\right.$$
$$+\int_0^1 \frac{[x-(1-y')\tan\phi]\mathbf{i}+(y-y')\mathbf{j}+z\mathbf{k}}{\sqrt{[x-(1-y')\tan\phi]^2+(y-y')^2+z^2}^3}\,dy'+$$
$$+\int_0^1 \frac{[x-(1-y')\tan\phi]\mathbf{i}+(y+y')\mathbf{j}+z\mathbf{k}}{\sqrt{[x-(1-y')\tan\phi]^2+(y+y')^2+z^2}^3}\,dy'$$
$$\left.+\int_1^\infty \frac{[x-(y'-1)\tan\phi]\mathbf{i}+(y+y')\mathbf{j}+z\mathbf{k}}{\sqrt{[x-(y'-1)\tan\phi]^2+(y+y')^2+z^2}^3}\,dy'\right\}, \tag{2}$$

where **i**, **j**, **k** are unit vectors parallel to the x, y, z axes.

Expressions for the velocity components parallel to the x, y, z axes, v_{xMQ}, v_{yMQ}, v_{zMQ}, can be written down in analytic form. Using these, one can determine the normal velocity at the fuselage (positive outwards):

$$v_{nQ}(x, \theta) = \cos\theta v_{yMQ}(x, \theta) + \sin\theta v_{zMQ}(x, \theta). \tag{3}$$

An explicit formula for $v_{nQ}(x, \theta)$ is given in Appendix A of Ref. 3.

In the following, we shall require the mean value of the normal velocity at the cross section $x = \text{const}$

$$\bar{v}_{nQ}(x) = \frac{1}{2\pi}\int_0^{2\pi} v_{nQ}(x, \theta)\,d\theta. \tag{4}$$

Using computed values of $v_{nQ}(x, \theta)$, we have determined $\bar{v}_{nQ}(x)$ by numerical integration.

The integral of $v_{nQ}(x, \theta)$ over the fuselage is

$$\int_{-\infty}^{\infty}\int_0^{2\pi} v_{nQ}(x, \theta)\,d\theta\,dx = 2\pi\int_{-\infty}^{\infty} \bar{v}_{nQ}(x)\,dx = 2Q\sqrt{1+\tan^2\phi}, \tag{5}$$

as is to be expected, since the total source strength of that part of the source line which lies inside the fuselage is $2Q\sqrt{1+\tan^2\phi}$.

We may note that the normal velocity at the side of the fuselage, $v_{nQ}(x, \theta = 0)$, has non-zero values for $\phi \neq 0$. As x tends to zero,

$$v_{nQ}(x \to 0, \theta = 0) = \frac{Q}{4\pi}\sin^2\phi.$$

If we were to extend the source line within the fuselage without forming a kink at the body junction, then the normal velocity in $\theta = 0$ would tend to infinity as $-Q\tan\phi/2\pi x$, when x tends to zero; this type of singular behaviour is of course the result of our considering an isolated source line.

2.2. Strength of the Source Distribution on the Fuselage which makes the Fuselage a Stream Surface

As mentioned in the introduction, we cancel the normal velocity $v_{nQ}(x, \theta)$ by a source distribution on the surface of the fuselage of strength $q(x, \theta)$. The function $q(x, \theta)$ must therefore satisfy the equation (*see* equation (A-4) of Appendix A):

$$v_{nq}(x, \theta) = -v_{nQ}(x, \theta), \tag{6}$$

where

$$v_{nq}(x,\theta)=\frac{q(x,\theta)}{2}+\int_{-\infty}^{\infty}\int_{0}^{2\pi}\frac{q(x',\theta')[1-\cos(\theta-\theta')]\,d\theta'\,dx'}{4\pi\sqrt{(x-x')^2+2[1-\cos(\theta-\theta')]}^3}\quad . \tag{7}$$

We introduce the mean value of the source strength $q(x,\theta)$ at a station $x=\text{const}$:

$$\bar{q}(x)=\frac{1}{2\pi}\int_{0}^{2\pi}q(x,\theta)\,d\theta. \tag{8}$$

Using equation (A-14) of Appendix A, we can write equation (7) in the form

$$q(x,\theta)+\bar{q}(x)+\int_{-\infty}^{\infty}\int_{0}^{2\pi}\frac{[q(x',\theta')-q(x,\theta')][1-\cos(\theta-\theta')]\,d\theta'\,dx'}{2\pi\sqrt{(x-x')^2+2[1-\cos(\theta-\theta')]}^3}=-2v_{nQ}(x,\theta). \tag{9}$$

One might consider determining a numerical solution of this equation in a manner similar to the panel method developed by A. M. O. Smith and J. L. Hess (*see* for example Ref. 7) for calculating the pressure distribution on a non-lifting wing-fuselage combination. This would however involve the solution of a large system of linear equations.

Our aim is to determine only an approximate solution but with somewhat less effort. Further we intended to deal with continuous functions for the source distribution, instead of using panels of constant source strength, since with the latter one obtains realistic results only for certain points on the panels. This is particularly important, since we want to perform the lengthy part of the calculation, (i.e. the determination of the source distribution on the fuselage and of the velocity field which it induces) only a few times, namely for single source lines of various angles of sweep and then use the results with a series of chordwise source distributions. The difficulty caused by planar panels of constant source strength could of course be overcome by using curved panels for which the source strength and its first derivatives are continuous, as with the method derived by A. Roberts and K. Rundle.[8,9]

We prefer however to derive an approximate solution of equation (9) by an iteration procedure, since this provides also some information about the accuracy of the solution.

Equation (9) suggests that the nth approximation $q^{(n)}(x,\theta)$ may be derived from the $(n-1)$th approximation by the relation

$$q^{(n)}(x,\theta)+\bar{q}^{(n)}(x)=-2v_{nQ}(x,\theta)-\int_{-\infty}^{\infty}\int_{0}^{2\pi}\frac{[q^{(n-1)}(x',\theta')-q^{(n-1)}(x,\theta')][1-\cos(\theta-\theta')]\,d\theta'\,dx'}{2\pi\sqrt{(x-x')^2+2[1-\cos(\theta-\theta')]}^3}\quad . \tag{10}$$

A first approximation $q^{(0)}(x,\theta)$ can be obtained by neglecting the last term in equation (10). Thus $q^{(0)}(x,\theta)$ satisfies the equation

$$q^{(0)}(x,\theta)+\bar{q}^{(0)}(x)=-2v_{nQ}(x,\theta). \tag{11}$$

Taking the mean value with respect to θ of both sides of equation (11), we see that

$$\bar{q}^{(0)}(x)=-\bar{v}_{nQ}(x) \tag{12}$$

and hence

$$q^{(0)}(x,\theta)=-2v_{nQ}(x,\theta)+\bar{v}_{nQ}(x). \tag{13}$$

The integral of the source strength $q^{(0)}(x,\theta)$ taken over the whole fuselage is

$$\int_{-\infty}^{\infty}\int_{0}^{2\pi}q^{(0)}(x,\theta)\,d\theta\,dx=-\int_{-\infty}^{\infty}\int_{0}^{2\pi}v_{nQ}(x,\theta)\,d\theta\,dx=-2Q\sqrt{1+\tan^2\phi},$$

so that $q^{(0)}(x,\theta)$ satisfies the condition on $q(x,\theta)$ that there is no overall flow through the fuselage.

The second approximation

$$q^{(1)}(x, \theta) = q^{(0)}(x, \theta) + \Delta^{(1)} q(x, \theta) \tag{14}$$

is obtained from

$$\Delta^{(1)} q(x, \theta) + \Delta^{(1)} \bar{q}(x) = K^{(1)}(x, \theta), \tag{15}$$

where

$$K^{(1)}(x, \theta) = -\int_{-\infty}^{\infty} \int_{0}^{2\pi} \frac{[q^{(0)}(x', \theta') - q^{(0)}(x, \theta')][1 - \cos(\theta - \theta')]\, d\theta'\, dx'}{2\pi \sqrt{(x - x')^2 + 2[1 - \cos(\theta - \theta')]^3}} \tag{16}$$

Comparing equation (15) with equation (11), we obtain, similar to equation (13)

$$\Delta^{(1)} q(x, \theta) = K^{(1)}(x, \theta) - \tfrac{1}{2} \bar{K}^{(1)}(x) \tag{17}$$

where

$$\bar{K}^{(1)}(x) = \frac{1}{2\pi} \int_{0}^{2\pi} K^{(1)}(x, \theta)\, d\theta. \tag{18}$$

Using equation (A-11) of Appendix A, we find that $\bar{K}^{(1)}(x)$ can be derived from the relation

$$\bar{K}^{(1)}(x) = -\int_{-\infty}^{\infty} \frac{\bar{q}^{(0)}(x') - \bar{q}^{(0)}(x)}{2\pi} k[\mathbf{K} - \mathbf{E}]\, dx', \tag{19}$$

with $\bar{q}^{(0)}(x)$ from equation (12), where **K** and **E** are the complete elliptic integrals (of the first and second kind respectively) with the modulus

$$k^2 = \frac{4}{4 + (x - x')^2} \tag{20}$$

For $\phi = 0$ and $\phi = 45$ degrees, we have computed values of $\bar{K}^{(1)}(x)$ and of $K^{(1)}(x, \theta)$ for $\theta = 0, 30, 60$ *and* 90 degrees. For $\phi = 0$, it was found that $|K^{(1)}(x, \theta) - \bar{K}^{(1)}(x)|$ is nowhere larger than $0{\cdot}032 \times \bar{q}^{(0)}(x = 0)$ and, for $\phi = 45$ degrees, that $|K^{(1)}(x, \theta) - \bar{K}^{(1)}(x)|$ is nowhere larger than $0{\cdot}05 \times \bar{q}^{(0)}(x = 0)$.

We shall mention in Section 2.3 that, for $\phi = 0$, we have computed the streamwise velocity induced by a source distribution of strength $K^{(1)}(x, \theta) - \bar{K}^{(1)}(x)$ and found that the velocity was nowhere larger than 3 per cent of the magnitude of the velocity induced at $x = 0$, $y = R$ by the source distributions $q^{(0)}(x, \theta)$ or $q^{(1)}(x, \theta)$.

Further, in Section 4, we shall show that the streamwise velocity caused by the wing-body interference effect is of a magnitude not greater than about 20 per cent of the streamwise velocity of the isolated wing.

We aim in this Report only towards an accuracy consistent with a small-perturbation theory approach. To reduce the computational effort, we therefore neglect the term $K^{(1)}(x, \theta) - \bar{K}^{(1)}(x)$ in the source distribution $\Delta^{(1)} q(x, \theta)$ for swept source lines. This means we use the approximation

$$\Delta^{(1)} q(x, \theta) = \tfrac{1}{2} \bar{K}^{(1)}(x). \tag{21}$$

Similarly, we approximate $q^{(n)}(x, \theta)$ by

$$q^{(n)}(x, \theta) = q^{(0)}(x, \theta) + \Delta^{(n)} \bar{q}(x), \tag{22}$$

with

$$\Delta^{(n)} \bar{q}(x) = \tfrac{1}{2} \sum_{\nu=1}^{n} \bar{K}^{(\nu)}(x)$$

where, (*cf.* equation (19)), we determine $\bar{K}^{(\nu)}(x)$ from

$$\bar{K}^{(\nu)}(x) = -\int_{-\infty}^{\infty} \frac{\bar{K}^{(\nu-1)}(x') - \bar{K}^{(\nu-1)}(x)}{4\pi} k[\mathbb{K} - \mathbb{E}]\, dx'. \tag{23}$$

The modulus k, equation (20), is a function of $(x-x')^2$, and since

$$\int_a^b dx \int_a^b dx'[f(x') - f(x)]F((x-x')^2) = 0,$$

it follows that

$$\int_{-\infty}^{\infty} \Delta^{(n)}\bar{q}(x)\, dx = 0,$$

so that $q^{(n)}(x, \theta)$ satisfies the condition that there is no overall flow through the fuselage.

We have computed values of $\bar{K}^{(n)}(x)$ for $1 \leqslant n \leqslant 6$. It was found that

$$|\bar{K}^{(n)}(x)|_{\max} < \tfrac{1}{2}|\bar{K}^{(n-1)}(x)|_{\max}.$$

If the same is true for $n > 6$, then

$$\sum_{n=7}^{\infty} |\bar{K}^{(n)}(x)| < |\bar{K}^{(6)}(x)|_{\max} \sum_{\nu=1}^{\infty} (\tfrac{1}{2})^{\nu} < |\bar{K}^{(6)}(x)|_{\max}.$$

For computing the velocity components induced on the wing and the fuselage, we therefore use the approximate source distribution

$$q(x, \theta) = -2v_{nQ}(x, \theta) + \bar{v}_{nQ}(x) + \tfrac{1}{2}\sum_{n=1}^{6} \bar{K}^{(n)}(x). \tag{24}$$

The function $q(x, \theta)$ has the same properties of symmetry as $v_{nQ}(x, \theta)$, i.e.

$$q(x, \theta) = q(x, \pi - \theta) = q(x, -\theta). \tag{25}$$

2.3. Streamwise Velocity in the Plane through the Source Line and the Axis of the Fuselage

We consider now the streamwise velocity in the plane $z = 0$, i.e. the plane through the source line and the axis of the fuselage.

The source distribution $q(x, \theta)$ produces the streamwise velocity (*see* equation (A-1))

$$v_{xq}(x, y, 0) = \int_{-\infty}^{\infty} \int_0^{2\pi} \frac{q(x', \theta')(x - x')\, d\theta'\, dx'}{4\pi\sqrt{(x-x')^2 + y^2 + 1 - 2y\cos\theta'}^3} \tag{26}$$

For the numerical evaluation of v_{xq}, we write this relation in the form of equation (A-16) of Appendix A.

The evaluation of the integrals in equation (A-16) does not cause any difficulty, except for $y = 1$ and small values of $|x|$. It is shown in Appendix B that the velocity v_{xq} for $y = 1$ behaves as

$$\frac{v_{xq}(x, y = 1, 0)}{Q} = -\frac{\cos^3\phi - 1 + \frac{3}{2}\sin^2\phi}{4\pi\sin^3\phi}\log|x| + \frac{x}{|x|}J_4(\phi) + f(x; \phi), \tag{27}$$

where $J_4(\phi)$ can be evaluated numerically from a single integral and $f(x;\phi)$ is a finite continuous function. For $\phi = 45$ degrees values of $v_{xq}(x, 1, 0)$ are plotted in Fig. 2.

Our aim is to determine the difference between the velocity fields past a swept wing attached to a circular fuselage and past a swept wing attached to an infinite reflection plate. To obtain the corresponding interference velocity field for a single source line $\mathbf{v}_{IQ}$, we have to add to the velocity field induced by the source distribution $q(x, \theta)$ on the fuselage, the velocity field produced by the source line with three kinks, $\mathbf{v}_{\curlywedge Q}$, and to subtract the velocity field produced by the ordinary swept source line, $\mathbf{v}_{\wedge Q}$. We therefore derive v_{xIQ} in the plane $z = 0$ from

$$v_{xIQ}(x, y, 0) = v_{xq}(x, y, 0) + v_{x\curlywedge Q}(x, y, 0) - v_{x\wedge Q}(x, y, 0). \tag{28}$$

Values for $v_{x\curlywedge Q}(x, y, 0)$ can be derived from equation (2) and values for $v_{x\wedge}(x, y, 0)$ from the relation

$$\mathbf{v}_{\wedge Q}(x, y, z) = \frac{Q}{4\pi \cos\phi}\left\{\int_1^\infty \frac{[x-(y'-1)\tan\phi]\mathbf{i}+(y-y')\mathbf{j}+z\mathbf{k}}{\sqrt{[x-(y'-1)\tan\phi]^2+(y-y')^2+z^2}^3}\,dy' + \right.$$

$$\left. + \int_{-\infty}^1 \frac{[x-(1-y')\tan\phi]\mathbf{i}+(y-y')\mathbf{j}+z\mathbf{k}}{\sqrt{[x-(1-y')\tan\phi]^2+(y-y')^2+z^2}^3}\,dy\right\}. \tag{29}$$

Explicit formulae for $v_{x\curlywedge Q}(x, y, 0)$ and $v_{x\wedge}(x, y, 0)$ are given in Appendices A and C of Ref. 3.

For $\phi = 45$ degrees, values for v_{xIQ} in the wing-body junction are plotted in Fig. 2. The figure shows that, for most values of x, the sign of the term $v_{x\curlywedge} - v_{x\wedge}$ is opposite to that of v_{xq}. To judge the magnitude of the interference velocity the term $-0{\cdot}2v_{x\wedge Q}$ is also plotted.

We have computed values of v_{xIQ} for the angles of sweep $\phi = 0$, 30, 45 and 60 degrees and for the spanwise stations $y/R = 1{\cdot}0$, $1{\cdot}25$ and $2{\cdot}0$. Values of v_{xIQ} are tabulated in Table 1. (Further values of v_{xIQ} are given in Table 1 of Ref. 3.) Fig. 3 illustrates how the interference velocity in the wing-body junction varies with the angle of sweep.

For $\phi = 45$ degrees, we have plotted, in Fig. 4, v_{xIQ} for various spanwise stations. Since chordwise distributions of isolated source lines will be used to represent swept wings and since the pressure distributions on swept wings are usually given as functions of the chordwise coordinate ξ, where ξ is zero at the leading edge of the wing, this coordinate is used in Fig. 4. Note that

$$\xi/R = x/R - (|y/R| - 1)\tan\phi. \tag{30}$$

We have mentioned in Section 2.2 that a more accurate approximation to $q(x, \theta)$ would be obtained, if we were to add to the values given by equation (24) the term $K^{(1)}(x, \theta) - \bar{K}^{(1)}(x)$. To judge the importance of the term $K^{(1)}(x, \theta) - \bar{K}^{(1)}(x)$, we have expressed $K^{(1)}(x, \theta)$, for $\phi = 0$, as a Fourier series with respect to θ. Using the numerical values of $K^{(1)}(x, \theta)$ for $\theta = 0$, 30, 60 and 90 degrees, we found that it was sufficient to consider only the first two terms of the Fourier series, i.e. we have used the approximation

$$K^{(1)}(x, \theta) - \bar{K}^{(1)}(x) = F_1(x)\cos 2\theta + F_2(x)\cos 4\theta \tag{31}$$

where

$$F_1(x) = \tfrac{1}{3}K^{(1)}(x, 0) + \tfrac{1}{3}K^{(1)}(x, 30°) - \tfrac{1}{3}K^{(1)}(x, 60°) - \tfrac{1}{3}K^{(1)}(x, 90°)$$

and

$$F_2(x) = \tfrac{1}{3}K^{(1)}(x, 0) - \tfrac{1}{3}K^{(1)}(x, 30°) - \tfrac{1}{3}K^{(1)}(x, 60°) + \tfrac{1}{3}K^{(1)}(x, 90°).$$

For the source distribution $\Delta^* q(x, \theta) = F_1(x)\cos 2\theta + F_2(x)\cos 4\theta$, we have computed the streamwise velocity, $\Delta v_x^*(x, y = 1, 0)$, in the wing–body junction. Δv_x^* has the largest value, $0{\cdot}0015$, at $x/R = 0{\cdot}15$ and the smallest value, $-0{\cdot}0009$, at $x/R = 1$. These values are small compared to $|v_{xIQ}(x = 0, y = 1, 0)| = 0{\cdot}0530$. We have therefore computed the interference velocity from the approximate source distribution given by equation (24).

2.4. Streamwise Velocity on the Fuselage

The isolated infinitely long fuselage does not produce any perturbation to the free stream. Thus the pressure distribution on the fuselage is entirely due to the presence of the wing.

On the fuselage, the source distribution $q(x, \theta)$ produces the streamwise velocity

$$v_{xq}(x, \theta) = \int_{-\infty}^{\infty} \int_{0}^{2\pi} \frac{q(x', \theta')(x - x')\, d\theta'\, dx'}{4\pi\sqrt{(x-x')^2 + 2[1 - \cos(\theta - \theta')]}^3} \tag{32}$$

For the numerical evaluation of $v_{xq}(x, \theta)$, we write equation (32) in the form of equation (A-18).

The total velocity v_{xQ} at the surface of the fuselage is given by

$$v_{xQ}(x, \theta) = v_{xq}(x, \theta) + v_{x\curlywedge Q}(x, \theta), \tag{33}$$

where $v_{x\curlywedge Q}(x, \theta) = v_{x\curlywedge Q}(x, y = \cos\theta, z = \sin\theta)$ can be derived from equation (2).

As for the flow in the plane of the wing, we define an interference velocity on the fuselage

$$v_{xIQ}(x, \theta) = v_{xq}(x, \theta) + v_{x\curlywedge Q}(x, \theta) - v_{x\wedge Q}(x, y = 1, z = \sin\theta). \tag{34}$$

Values of $v_{xIQ}(x, \theta)$ are quoted in Table 2, and, for $\phi = 45$ degrees, are plotted in Fig. 5.

We have not computed values of $v_{xIQ}(x, y > R, z \neq 0)$ at spanwise stations away from the wing-body junction; to do so would require the evaluation of further double integrals, *see* equation (A-1).

2.5. The Velocity Component v_z

The source distribution $q(x, \theta)$ is a symmetrical function with respect to the plane $z = 0$ and therefore it does not produce a velocity normal to that plane: i.e. $v_{zq}(x, y, z = 0) = 0$ and $v_{zIQ}(x, y, z = 0) = 0$. However, at $z \neq 0$ the velocity components v_{zq} and v_{zIQ} do not vanish.

To determine the pressure distribution on a wing in the presence of a fuselage to second-order accuracy, we require the velocity components at the surface of the wing to second-order accuracy. We therefore need to know the velocity component v_z at $z \neq 0$ which is induced by the single source line in the presence of the fuselage.

The velocity component $v_{zq}(x, y, z \neq 0)$, induced by the source distribution $q(x, \theta)$, can be derived from equation (A-3). We have computed values of $v_{zq}(x, y, z)$ only at the fuselage. In Ref. 3, we indicated how we computed first the circumferential velocity component $v_{\theta q}(x, \theta)$, using equation (A-15), and then determined $v_{zq}(x, \theta)$ by means of the relation

$$v_{zq}(x, \theta) = \cos\theta v_{\theta q} + \sin\theta v_{nq} = \cos\theta v_{\theta q} - \sin\theta v_{nQ}. \tag{35}$$

We again determined the interference velocity v_{zIQ}, where

$$v_{zIQ}(x, \theta) = v_{zq}(x, \theta) + v_{z\curlywedge Q}(x, \theta) - v_{z\wedge Q}(x, y = 1, \sin\theta). \tag{36}$$

Values of $v_{zIQ}(x, \theta)$ are quoted in Table 3 and, for $\phi = 45$ degrees, are plotted in Fig. 6, together with values of $v_{z\wedge Q}$, induced by the ordinary swept source line.

For the complete velocity field, we would also require values for the spanwise velocity component. We have not computed any values, but those on the fuselage are known since

$$v_{yq} + v_{y\curlywedge Q} = -\sin\theta(v_{\theta q} + v_{\theta\curlywedge Q}) = -\tan\theta(v_{zq} + v_{z\curlywedge Q}). \tag{37}$$

3. A Single Kinked Swept Vortex in the Presence of a Circular Cylindrical Fuselage

3.1. Velocities Induced by the Vortex

We consider an infinitely long kinked swept vortex, the shape of which is given by equation (1). The strength of the vortex is constant along the span and equal to Γ per unit length.

The velocity field $\mathbf{v}_{M\Gamma}(x, y, z)$ induced by the vortex can be obtained from the relation

$$\mathbf{v}_{M\Gamma}(x, y, z) = -\frac{\Gamma}{4\pi}\left\{\int_1^\infty \frac{-z\mathbf{i}+z\tan\phi\,\mathbf{j}+[x-(y-1)\tan\phi]\mathbf{k}}{\sqrt{[x-(y'-1)\tan\phi]^2+(y-y')^2+z^2}^3}\,dy' + \int_0^1 \frac{-z\mathbf{i}-z\tan\phi\,\mathbf{j}+[x+(y-1)\tan\phi]\mathbf{k}}{\sqrt{[x-(1-y')\tan\phi]^2+(y-y')^2+z^2}^3}\,dy'\right.$$
$$\left. + \int_0^1 \frac{-z\mathbf{i}+z\tan\phi\,\mathbf{j}+[x-(y+1)\tan\phi]\mathbf{k}}{\sqrt{[x-(1-y')\tan\phi]^2+(y+y')^2+z^2}^3}\,dy' + \int_1^\infty \frac{-z\mathbf{i}-z\tan\phi\,\mathbf{j}+[x+(y+1)\tan\phi]\mathbf{k}}{\sqrt{[x-(y'-1)\tan\phi]^2+(y+y')^2+z^2}^3}\,dy'\right\}. \tag{38}$$

Using this relation one can derive analytical expressions for $v_{yM\Gamma}$ and $v_{zM\Gamma}$ and also for the normal velocity $v_{n\Gamma}$ at the surface of the fuselage. An explicit formula for $v_{n\Gamma}$ is given in Appendix A of Ref. 4. The normal velocity $v_{n\Gamma}$ is an antisymmetric function with respect to the plane $z = 0$, i.e. $v_{n\Gamma}(x, \theta) = -v_{n\Gamma}(x, -\theta)$; therefore the mean value $\bar{v}_{n\Gamma}(x)$ vanishes at any cross section $x = \text{const}$.

3.2. Strength of the Source Distribution on the Fuselage which makes the Fuselage a Stream Surface

The strength $q(x, \theta)$ of the source distribution on the fuselage must be such that the normal velocity on the surface of the fuselage is cancelled, i.e.

$$v_{nq}(x, \theta) = -v_{n\Gamma}(x, \theta). \tag{39}$$

The function $q(x, \theta)$ has the same planes of symmetry or antisymmetry as $v_{n\Gamma}(x, \theta)$, therefore the mean values $\bar{q}(x)$ vanish. It follows from equation (A-14) that $q(x, \theta)$ has to satisfy the equation

$$q(x, \theta) + \int_{-\infty}^{\infty}\int_0^{2\pi} \frac{[q(x', \theta')-q(x, \theta')][1-\cos(\theta-\theta')]\,d\theta'\,dx'}{2\pi\sqrt{(x-x')^2+2[1-\cos(\theta-\theta')]}^3} = -2v_{n\Gamma}(x, \theta). \tag{40}$$

An approximate solution of equation (40) can again be derived by an iterative procedure, where the initial approximation is given by

$$q^{(0)}(x, \theta) = -2v_{n\Gamma}(x, \theta). \tag{41}$$

The first step in the iteration procedure leads to

$$q^{(1)}(x, \theta) = q^{(0)}(x, \theta) + \Delta^{(1)}q(x, \theta), \tag{42}$$

where

$$\Delta^{(1)}q(x, \theta) = -\int_{-\infty}^{\infty}\int_0^{2\pi} \frac{[q^{(0)}(x', \theta')-q^{(0)}(x, \theta')][1-\cos(\theta-\theta')]\,d\theta'\,dx'}{2\pi\sqrt{(x-x')^2+2[1-\cos(\theta-\theta')]}^3}. \tag{43}$$

We have computed values of $\Delta^{(1)}q(x, \theta)$ for $\theta = 15$, 45 and 90 degrees; for $\phi = 30$, 45 and 60 degrees. When $\Delta^{(1)}q(x', \theta)$ is approximated by the function

$$\Delta^{(1)}q(x, \theta) = A_1(x)\sin\theta + A_3(x)\sin 3\theta + A_5(x)\sin 5\theta, \tag{44}$$

numerical values for $A_1(x)$, $A_3(x)$, $A_5(x)$ can be derived from the computed values $\Delta^{(1)}q(x, \theta = 15°)$, $\Delta^{(1)}q(x, \theta = 45°)$, $\Delta^{(1)}q(x, \theta = 90°)$. It was found that the maximum values of $|A_1(x; \phi)|$ are approximately the same for all values of ϕ. The ratio $|A_1(x; \phi)|_{max}/|q^{(0)}(x, \theta; \phi)|_{max}$ decreases from about 0·18 for $\phi = 0$ to about 0·11 for $\phi = 60$ degrees. The functions $|A_3(x)|$ and $|A_5(x)|$ have appreciably smaller values than $|A_1(x)|_{max}$. The ratio $|A_3|_{max}/|A_1|_{max}$ is about 0·15 and $|A_5|_{max}/|A_1|_{max}$ is about 0·05, for all values of ϕ; this means that $|A_3(x)|/|q^{(0)}(x, \theta)|_{max} < 0{\cdot}03$ and $|A_5(x)|/|q^{(0)}(x, \theta)|_{max} < 0{\cdot}01$.

These values suggest that for the second term in the iteration procedure

$$\Delta^{(2)}q(x, \theta) = -\int_{-\infty}^{\infty}\int_0^{2\pi} \frac{[\Delta^{(1)}q(x', \theta')-\Delta^{(1)}q(x, \theta')][1-\cos(\theta-\theta')]\,d\theta'\,dx'}{2\pi\sqrt{(x-x')^2+2[1-\cos(\theta-\theta')]}^3}, \tag{45}$$

it is sufficient to derive an approximate value by substituting for $\Delta^{(1)}q(x, \theta)$ the term $A_1(x) \sin \theta$. We therefore determine an approximate value of $\Delta^{(2)}q(x, \theta)$ in the form

$$\Delta^{(2)}q(x, \theta) = B(x) \sin \theta, \tag{46}$$

where

$$\begin{aligned} B(x) &= \Delta^{(2)}q(x, \theta = 90°) \\ &= -\int_{-\infty}^{\infty} \int_{0}^{2\pi} \frac{[A_1(x') - A_1(x)] \sin \theta' (1 - \sin \theta')\, d\theta'\, dx'}{2\pi \sqrt{(x - x')^2 + 2(1 - \sin \theta')^3}} \\ &= \int_{-\infty}^{\infty} \frac{[A_1(x') - A_1(x)]}{4\pi} \sqrt{(x - x')^2 + 4}[(4 - k^2)\mathbf{E} + (3k^2 - 4)\mathbf{K}]\, dx', \end{aligned} \tag{47}$$

with

$$k^2 = \frac{4}{4 + (x - x')^2}. \tag{48}$$

We have computed values of $B(x)$; it was found that the maximum values of $|B(x; \phi)|$ are nearly independent of the value of ϕ and that the ratio $|B(x; \phi)|_{max}/|A_1(x; \phi)|_{max}$ is about 0·15. We conclude from this that the source distribution

$$q(x, \theta) = q^{(0)}(x, \theta) + \Delta^{(1)}q(x, \theta) + \Delta^{(2)}q(x, \theta)$$

is a sufficiently accurate solution of equation (40). We therefore consider in the following the velocity field induced by the source distribution

$$q(x, \theta) = -2v_{n1}(x, \theta) + [A_1(x) + B(x)] \sin \theta + A_3(x) \sin 3\theta + A_5(x) \sin 5\theta. \tag{49}$$

3.3. Downwash in the Plane through the Vortex and the Axis of the Fuselage

We consider now the velocity which the source distribution $q(x, \theta)$ on the fuselage induces in the plane $z = 0$, i.e. the plane through the vortex and the axis of the fuselage.

Since the source distribution $q(x, \theta)$ is asymmetrical with respect to the plane $z = 0$, it produces no velocity component tangential to that plane, that is

$$v_{xq}(x, y, z = 0) = 0$$

and

$$v_{yq}(x, y, z = 0) = 0.$$

The velocity normal to the plane $z = 0$ is

$$v_{zq}(x, y, 0) = -\int_{-\infty}^{\infty} \int_{0}^{2\pi} \frac{q(x', \theta)}{4\pi} \frac{\sin \theta\, d\theta\, dx'}{\sqrt{(x - x')^2 + y^2 + 1 - 2y \cos \theta}^3} \tag{50}$$

For the numerical evaluation of v_{zq}, we write equation (50) in the form of equation (A-17). The evaluation of the integrals in equation (A-17) does not cause any difficulty, except for $y = 1$ and small values of $|x|$. It can be shown, by a technique similar to the one used in Appendix B, (*see* also Refs. 2–4), that the function $v_{zq}(x, y = 1, 0)$ behaves as

$$v_{zq}(x, y = 1, 0) = -\frac{1}{8\pi} \frac{\sin \phi \cos \phi}{(1 + \cos \phi)^2} \log |x| + \frac{x}{|x|} J_5(\phi) + g(x; \phi), \tag{51}$$

where $J_5(\phi)$ can be evaluated numerically from single integrals and $g(x; \phi)$ is a finite continuous function. We

have computed the following values for $J_5(\phi)$:

ϕ	J_5
0	−0·10610
30°	−0·10283
45°	−0·09906
60°	−0·09337

To obtain the interference term for the downwash of a single vortex, $v_{zI\Gamma}$, we have to add to v_{zq} the downwash from the vortex with three kinks, $v_{z\curlywedge\Gamma}$, and to subtract the downwash from the swept vortex (with one kink at $y = 1$), $v_{z\wedge\Gamma}$:

$$v_{zI\Gamma}(x, y, 0) = v_{zq}(x, y, 0) + v_{z\curlywedge\Gamma}(x, y, 0) - v_{z\wedge\Gamma}(x, y, 0). \tag{52}$$

Values of $v_{z\curlywedge\Gamma}(x, y, 0)$ can be derived from equation (38) and values of $v_{z\wedge\Gamma}(x, y, 0)$ from the relation

$$\mathbf{v}_{\wedge\Gamma}(x, y, z) = -\frac{\Gamma}{4\pi}\left\{\int_1^\infty \frac{-z\mathbf{i} + z\tan\phi\,\mathbf{j} + [x-(y-1)\tan\phi]\mathbf{k}}{\sqrt{[x-(y'-1)\tan\phi]^2 + (y-y')^2 + z^2}^3}\,dy' + \right.$$

$$\left. + \int_{-\infty}^1 \frac{-z\mathbf{i} - z\tan\phi\,\mathbf{j} + [x+(y-1)\tan\phi]\mathbf{k}}{\sqrt{[x-(1-y')\tan\phi]^2 + (y-y')^2 + z^2}^3}\,dy'\right\}. \tag{53}$$

For $\phi = 45$ degrees and $y = 1$, we have plotted values of v_{zq} and $v_{zI\Gamma}$ in Fig. 7. To provide a measure for the importance of the interference downwash, we have plotted also the term $0{\cdot}2v_{z\wedge\Gamma}$. Comparing Fig. 7 with Fig. 2, which shows the corresponding results for a source line in the presence of a fuselage, we note that the interference effect is more important with respect to the downwash from a vortex than with respect to the streamwise velocity component from a source line.

We have computed values of $v_{zI\Gamma}$ for the angles of sweep $\phi = 0$, 30, 45 and 60 degrees and for the spanwise stations $y/R = 1{\cdot}0$, $1{\cdot}25$, $2{\cdot}0$. Values of $v_{zI\Gamma}$ are tabulated in Table 4. (Further values of $v_{zI\Gamma}$ are given in Table 1 of Ref. 4.) Fig. 8 illustrates how the interference velocity $v_{zI\Gamma}$ in the wing-body junction varies with the angle of sweep.

For $\phi = 45$ degrees, we have plotted, in Fig. 9, $v_{zI\Gamma}$ for various spanwise stations as a function of ξ/R, *see* equation (30). Comparing Fig. 9 with the corresponding figure for a source-line, Fig. 4, we note that $|v_{zI\Gamma}|$ decreases more rapidly with increasing distance from the wing-body junction than the interference velocity $|v_{xIQ}|$.

3.4. Downwash at Points away from the Plane $z=0$

In practice, we are interested in designing wing-fuselage combinations with wings of finite thickness. We therefore require the variation of the interference velocity away from the plane $z = 0$.

The velocity component $v_{zq}(x, y, z)$ induced by the source distribution $q(x, \theta)$ on the fuselage can be obtained from equation (A-3). We are particularly interested in the downwash at the junction of a thick wing with the fuselage. The value of $v_{zq}(x, \theta)$ can be derived from equation (A-19). We have again determined the interference term

$$v_{zI\Gamma}(x, \theta) = v_{zq}(x, \theta) + v_{z\curlywedge\Gamma}(x, y = \cos\theta, z = \sin\theta) - v_{z\wedge\Gamma}(x, y = 1, z = \sin\theta). \tag{54}$$

Values of $v_{zI\Gamma}(x, \theta)$ are quoted in Table 5, and, for $\phi = 45$ degrees, are plotted in Fig. 10.

From the known values of $v_{zq}(x, \theta)$, the spanwise interference velocity at the fuselage can easily be found since

$$v_{yq}(x, \theta) + v_{y\curlywedge\Gamma}(x, \theta) = -\tan\theta[v_{zq}(x, \theta) + v_{z\curlywedge\Gamma}(x, \theta)].$$

We have not computed values of $v_{zI\Gamma}(x, y > R, z \neq 0)$ nor of $v_{yI\Gamma}(x, y > R, z \neq 0)$ at spanwise stations away from the fuselage. Neither have we determined the streamwise velocity component $v_{xI\Gamma}(x, y, z \neq 0)$ at points off the wing plane; in $z = 0$, $v_{xI\Gamma}$ vanishes. We note that, for an unswept vortex in the presence of a circular cylinder, Kramer[11] has computed (by an approximate method which differs from the present one) the pressure distribution at the fuselage and has tabulated values of the pressure coefficient, $C_p(x, \theta)$. Using Kramer's

values of $C_p(x, \theta)$, one can derive values of $v_{xI\Gamma}(x, \theta; \phi = 0)$:

$$v_{xI\Gamma}(x, \theta; \phi = 0) = \tfrac{1}{4}[C_p(x, -\theta) - C_p(x, \theta)] - \frac{1}{2\pi} \frac{\sin \theta}{x^2 + \sin^2 \theta}. \tag{55}$$

We shall see in Section 5.2 that if we intend to determine, to second-order accuracy, only the shape of a wing with finite thickness, for which the vorticity distribution in the wing plane is given, then we do not require to know the values of the streamwise and spanwise interference velocities, which implies that we do not need the values of $v_{xI\Gamma}(x, y, z)$ and of $v_{yI\Gamma}(x, y, z)$. However, if we wish to determine the pressure distribution at the fuselage and at the surface of the wing, and in particular the difference, ΔC_p, between the pressure coefficients on the upper and the lower surfaces of the wing, to second-order, then a knowledge of $v_{xI\Gamma}(x, y, z)$ (and for large angles of sweep perhaps also of $v_{yI\Gamma}(x, y, z)$) will be required.

4. Pressure Distribution on a Symmetrical Wing at Zero Incidence Attached to a Circular Cylindrical Fuselage

4.1. Pressure Distribution on the Wing according to First-Order Theory

We consider an uncambered untwisted wing at zero angle of incidence. The wing is attached in a midwing position to a fuselage. The wing has constant chord and constant section shape, $z = z_t(x, y)$, across the span, so that

$$z_t(x, y) = z_t(\xi = x - (|y| - R) \tan \phi). \tag{56}$$

The wing is in a main stream of velocity V_0 parallel to the wing chord. In the following, we make all velocity components dimensionless by taking $V_0 = 1$. We want to examine how the pressure distribution on the wing is altered by the presence of the fuselage.

Within first-order theory, we have to satisfy the boundary condition

$$v_z^{(1)}(x, y, z = 0) = \frac{\partial z_t(x, y)}{\partial x} = \frac{dz_t(\xi)}{d\xi} \tag{57}$$

to first-order accuracy. We use the superscript (1) to denote terms derived by first-order theory. The isolated wing can be represented by a source distribution $q_w^{(1)}(x, y)$ in the wing plane of strength

$$q_w^{(1)}(x, y) = q_w^{(1)}(\xi) = 2\frac{dz_t}{d\xi}. \tag{58}$$

We have seen in Section 2 that the source distribution on the fuselage, which makes the fuselage a stream surface, does not produce a velocity component $v_z(x, y, z = 0)$ in the plane $z = 0$. Therefore, in first-order theory, the strength of the source distribution in the plane $z = 0$ for the wing–fuselage combination is the same as for the wing alone, equation (58). Thus for the configurations considered the source distribution can be derived from a chord-wise distribution of the type of source lines studied in Section 2.

The formulae in Section 2 are derived for a single source line for which the strength per unit length along the source line is Q. To derive the velocity components produced by a source distribution $q(\xi)$ from the results for the single source line, we have to replace Q by $Q\,dn = \cos \phi q(\xi)\, d\xi$ and perform the integration with respect to ξ.

To determine the change in the pressure distribution due to the fuselage—to first-order accuracy—we have to determine only the change in the streamwise velocity, $\Delta v_x^{(1)}(x, y, z = 0)$. Values of $\Delta v_x^{(1)}$ can be determined from the relation

$$\begin{aligned} \Delta v_x^{(1)}(x, y, z = 0) &= \cos \phi \int_0^{c/R} q_w^{(1)}(x') \frac{v_{xIQ}[(x - x')/R, y/R, 0]}{Q/R} d\left(\frac{x'}{R}\right) \\ &= 2 \cos \phi \frac{c}{R} \int_0^1 \frac{d(z_t/c)}{d(x'/c)} \frac{v_{xIQ}[(x - x')/R, y/R, 0]}{Q/R} d\left(\frac{x'}{c}\right), \end{aligned} \tag{59}$$

where c is the wing chord and values of $v_{xIQ}/(Q/R)$ are taken from Table 1.

It has been stated above, *see* equation (27), that, for $y = R$, the values of v_{xq} and v_{xIQ} tend logarithmically to infinity when x' tends to x. In computing values of $\Delta v_x^{(1)}(x, y = R, z = 0)$, we therefore write equation (59) in a somewhat different form and make use of the known singular behaviour of $v_{xIQ}(x, y = R, 0)$.

For the 10 per cent thick R.A.E. 101 section, we have computed values of the velocity change in the wing–body junction, $\Delta v_{xJ}^{(1)} = \Delta v_x^{(1)}(x, y = R, 0)$, for several values of the ratio between wing chord and body radius, c/R, and for various angles of sweep. Some results are plotted in Figs. 11 and 12 (further results are given in Refs. 2 and 3). For comparison, we have also plotted values of $-0{\cdot}1 v_{xt}^{(1)}(x)$ where $v_{xt}^{(1)}$ is the velocity at the junction of the wing with an infinite reflection plate.

The figures show that, except near the leading and trailing edges, the velocity is reduced (a fact which is well-known from experiment). The velocity decrement, $-\Delta v_{xJ}$, vanishes when c/R tends to zero since $c/R \to 0$ represents the case of a wing attached to an infinite reflection plate. For the range $0 < c/R \leqslant 10$ considered in Fig. 11, the velocity decrement $-\Delta v_{xJ}$ increases with increasing value of the ratio c/R. We note that the value $c/R = 10$ is larger than the values which occur generally on civil aircraft. We have therefore not derived values of $-\Delta v_{xJ}$ for values of c/R larger than 10 and do not know how $-\Delta v_{xJ}$ varies when c/R tends to infinity, i.e. when the radius vanishes for a wing of given chord. (We may expect that the interference velocity evaluated from equation (59) by means of the velocity $v_{xIQ}(x, y, z = 0)$ in the plane $z = 0$, i.e. $\theta = 0$, can only be a reasonably accurate estimate for configurations where the ratio between the wing thickness and the body diameter is small; we note that for the configuration $t/c = 0{\cdot}1$, $c/R = 10$, considered in Fig. 11, $t/2R = 0{\cdot}5$.)

We see from Figs. 11 and 12 that, according to first-order theory, the interference velocity is not larger than 20 per cent of the perturbation velocity of the wing with the reflection plate.

Fig. 12 shows that, for wings with the same streamwise section shape, the velocity decrement in the wing-body junction, $-\Delta v_{xJ}^{(1)}$, decreases with increasing value of ϕ. For the unswept wing, the maximum velocity decrement occurs in the neighbourhood of the position of the maximum thickness of the wing, but with increasing sweep the position of the maximum value of $-\Delta v_{xJ}^{(1)}$ moves rearwards.

In Fig. 13, we have plotted the total streamwise velocity (from first-order theory) in the junction of the wing with a fuselage, v_{xJ}, and in the junction of the wing with an infinite reflection plate, v_{xt}. We note that the difference in the type of velocity distribution between a swept and an unswept wing is not much affected by the finite body radius. (Near the leading edge, the values of the velocity from first-order theory are of course not representative of the actual velocity.)

For the case $c/R = 5$, we have plotted in Fig. 14 the interference velocity at two spanwise stations outboard of the wing-body junction as function of the coordinate $\xi = [x - x_{LE}(y)]/c$. We note that, for both stations, the maximum value of the velocity decrement varies approximately as $\cos \phi$; Fig. 12 shows a similar variation in the wing-body junction. The results suggest that near the junction, $R \leqslant y \leqslant 2R$, the values of the maximum velocity decrement decrease approximately linearly with the distance from the junction.

4.2. Pressure Distribution on the Wing According to Second-Order Theory

It is of some interest to know the interference velocity somewhat more accurately than the result from first-order theory. To obtain the pressure distribution to second-order accuracy, one has first to determine singularity distributions which satisfy the boundary condition to second order and then to determine the induced velocities at the wing surface to second-order accuracy. This requires the evaluation of, at least, some velocity components at $z \neq 0$.

We consider first the boundary condition. For a swept wing of constant chord and constant section shape, the velocity field has to satisfy the equation

$$[1 + v_x(x, y, z_t) - \tan \phi v_y(x, y, z_t)] \frac{\partial z_t}{\partial x} = v_z(x, y, z_t). \tag{60}$$

An approximation correct to second order is obtained by replacing the terms v_x and v_y in equation (60) by $v_{xt}^{(1)}(x, y, 0) + \Delta v_x^{(1)}(x, y, 0)$ and $v_{yt}^{(1)}(x, y, 0) + \Delta v_y^{(1)}(x, y, 0)$ respectively. As above, we denote the various velocity components for the wing attached to an infinite reflection plate by the suffix t and the interference terms by the symbol Δ; the superscript (1) denotes again terms computed from the first-order source distribution.

We have seen above, *see* Figs. 11 and 12, that in the wing-body junction the interference term $\Delta v_x^{(1)}$ is of a magnitude of only about $0{\cdot}1 v_{xt}^{(1)}$. Further outboard $-\Delta v_{x\,\max}^{(1)}$ is smaller than the value in the junction $(-\Delta v_{xJ}^{(1)})_{\max}$; thus within the accuracy required we can neglect the term Δv_x in the boundary condition (even though it is formally a term of order t/c). We propose to neglect the term Δv_y, which is zero in the wing-body junction, for all spanwise stations.

We therefore approximate the left-hand side of equation (60) by the term that applies to the isolated wing, and the approximate boundary condition on the wing of the wing–fuselage combination then reads:

$$[1+v_{xt}^{(1)}(x, y, 0)-\tan\phi v_{yt}^{(1)}(x, y, 0)]\frac{\partial z_t}{\partial x}=v_z(x, y, z_t). \tag{61}$$

The solution of equation (61) for the wing-fuselage combination differs however from the solution for the isolated wing because the velocity $v_z(x, y, z_t)$ contains not only a contribution from the second-order source distribution of the isolated wing but also the interference velocity $\Delta v_z(x, y, z_t)$.

We consider next the determination of source distributions in the wing plane and on the fuselage which satisfy equation (61) approximately. We express the source distribution in the wing plane as the sum of two terms $q_w^{(2)}(x, y)+\Delta q(x, y)$, where $q_w^{(2)}(x, y)$ satisfies the boundary condition, correct to second order, of the wing attached to an infinite reflection plate and $\Delta q(x, y)$ is an interference term.

There exist several possibilities for determining a source distribution $q_w^{(2)}$ (*see*, for example, Refs. 6 and 12) which satisfies the equation

$$[1+v_{xt}^{(1)}(x, y, 0)-\tan\phi v_{yt}^{(1)}(x, y, 0)]\frac{\partial z_t}{\partial x}=v_{zt}^{(2)}(x, y, z_t)\approx v_{zt}^{(1)}(x, y, z_t)+\tfrac{1}{2}[q_w^{(2)}(x, y)-q_w^{(1)}(x, y)]. \tag{62}$$

For the present purpose of deriving only the interference velocity field it seems sufficient to use an approximate expression for $q_w^{(2)}$ derived by means of a Taylor series expansion of $v_{zt}^{(1)}(x, y, z_t)$ with respect to z (even though such an expansion is not strictly permissible at the centre section of the wing, *see* Ref. 12). The resulting relation for $q_w^{(2)}$ reads

$$q_w^{(2)}(x, y)=2\frac{\partial}{\partial x}\{z_t[1+v_{xt}^{(1)}(x, y, 0)]\}+2\frac{\partial}{\partial y}\{z_t v_{yt}^{(1)}(x, y, 0)\}.$$

When we use for $v_{xt}^{(1)}$ and $v_{yt}^{(1)}$ the approximate values given by the R.A.E. Standard Method,[13] we obtain

$$q_w^{(2)}(x, y)=q_w^{(2)}(\xi)+\frac{1-|K_2|\sin^2\phi}{\cos\phi}2\frac{d(z_t S^{(1)})}{d\xi}-$$
$$-2K_2 f(\phi)\cos\phi\frac{d}{d\xi}\left(z_t\frac{dz_t}{d\xi}\right)+2\frac{dK_2}{dy}z_t S^{(1)}\sin\phi. \tag{63}$$

(For details concerning the terms $S^{(1)}(\xi)$, $K_2(y)$, $f(\phi)$ *see* Refs. 6 and 13.) For spanwise stations sufficiently far away from the reflection plate (i.e. from the wing-body junction), where $K_2=0$, $dK_2/dy=0$, we obtain

$$q_{ws}^{(2)}(\xi)=q_w^{(2)}(x, y\gg R)$$
$$=q_w^{(1)}(\xi)+\frac{2}{\cos\phi}\frac{d(z_t S^{(1)})}{d\xi}; \tag{64}$$

for the wing-body junction we obtain with $K_2=1$:

$$q_{wJ}^{(2)}(x)=q_w^{(2)}(x, y=R)$$
$$=q_w^{(1)}(\xi)+2\cos\phi\frac{d(z_t S^{(1)})}{d\xi}-2f(\phi)\cos\phi\frac{d}{d\xi}\left(z_t\frac{dz_t}{d\xi}\right)+2\left(\frac{dK_2}{dy}\right)_J z_t S^{(1)}\sin\phi. \tag{65}$$

(The function $K_2(y)$ suggested by Sells[6] gives $(dK_2/dy)_J=-8$.) The interference velocity $\Delta v_z(x, y, z)$, related to $q_w^{(1)}$ or $q_w^{(2)}$, does not vanish at $z=z_t\neq 0$. We shall see that $\Delta v_z^{(1)}(x, y, z_t)$ is numerically small; it is therefore sufficient to determine Δv_z from $q_w^{(1)}$. For the wing–fuselage combination the velocity $v_z(x, y, z_t)$ can be written, to second-order accuracy, as the sum

$$v_z(x, y, z_t)=v_{zt}^{(2)}(x, y, z_t)+\Delta v_z^{(1)}(x, y, z_t)+\Delta v_z^*(x, y, z_t), \tag{66}$$

where Δv_z^* is produced by a source distribution $\Delta q(x, y)$, yet to be determined, in the wing plane. When we combine equations (61), (62) and (66), we find that the source distribution Δq has to produce a velocity Δv_z^*

which satisfies the equation

$$\Delta v_z^*(x, y, z_t; \Delta q) = -\Delta v_z^{(1)}(x, y, z_t). \tag{67}$$

For the case of a wing, swept by 45 degrees, with the section R.A.E. 101, $t/c = 0{\cdot}1$, attached to a fuselage with the radius $R/c = 0{\cdot}2$, we have computed values of $\Delta v_z^{(1)}(x, \theta)$ for various values of θ, using the values of $v_{zIQ}(x, \theta)$ derived in Section 2.5. By graphical interpolation, we have determined values of $\Delta v_{zJ}^{(1)}$ in the wing-body junction, i.e. for $\theta_J = \sin^{-1}[(c/R)(z_t/c)]$. These values are plotted in Fig. 15, together with the values of $0{\cdot}1 v_{zt}^{(1)}(x, y; 0) = 0{\cdot}1\, dz_t/dx$. The figure shows that $\Delta v_{xJ}^{(1)}$ is of a magnitude comparable to $0{\cdot}1 v_{zt}^{(1)}$ (which confirms that we need not consider the source distribution $q_w^{(2)} - q_w^{(1)}$ when we compute Δv_z).

We have not computed values of $v_{zIQ}(x, y > R, z \neq 0)$ for spanwise stations outboard of the junction. We can therefore make only an estimate of the source distribution $\Delta q(x, y)$ which would cancel the interference velocity $\Delta v_z^{(1)}(x, y, z_t)$ at all spanwise stations. We can expect that $\Delta v_z^{(1)}$ varies rapidly across the span; this would imply that the strength of the source distribution Δq also varies rapidly across the span. Such a source distribution induces at $z \neq 0$ a velocity component $\Delta v_z^*(x, y, z)$ which can be quite different from the velocity induced in $z = 0$,

$$\Delta v_z^*(x, y, 0) = \tfrac{1}{2}\Delta q(x, y).$$

The aim of deriving an estimate of Δq is of course to estimate its effect on the pressure distribution of the wing, which means on v_x. In view of the uncertainty about the spanwise variation of the interference velocity $\Delta v_z^{(1)}$, we may attempt to obtain an estimate of the effect on v_x by means of a distribution of three-dimensional sources along the line $0 < x < c$, $y = R$, $z = 0$. We ignore the fact that such a source distribution produces a normal velocity at the fuselage and determine the strength of the line source distribution such that it induces the velocity

$$\Delta v_z^*(x, y = R, z_t) = -\Delta v_{zJ}^{(1)}(x). \tag{68}$$

By approximating the line source distribution by one which varies piecewise linearly, the distribution can be determined by solving a system of linear equations.

We are not able to say whether the streamwise velocity produced by the line source distribution is a fair estimate of the velocity produced by Δq. It is possible that the interference velocity $\Delta v_z^{(1)}$ varies more rapidly across the span than the velocity $\Delta v_z^*(x, y, z_t)$ produced by the line source distribution in $y = R$, $z = 0$. If this were the case, then we could derive an over-estimate of the effect of Δq on v_x. We therefore consider Δv_x^* induced by the line source distribution to be only a measure of the possible error in v_x if we neglect the interference velocity $\Delta v_z^{(1)}(x, y, z_t)$ in the boundary condition.

To evaluate the interference velocity Δv_x at the wing surface to second-order accuracy, we have both to take account of the change in the source distributions and to determine the velocity at the wing surface instead of in the plane $z = 0$.

We consider first the effect of the additional source distribution $q_w^{(2)} - q_w^{(1)}$. We can only make an estimate of the change in Δv_x because this source distribution is no longer of the type considered above, since it varies across the span, *see* equation (63). To obtain an estimate for the magnitude of the effect of $q_w^{(2)} - q_w^{(1)}$, we have calculated values of $\Delta v_x(x, y = R, z = 0)$ for two different source distributions, each of which is of constant strength across the span. We have considered the two extreme cases, firstly the distribution which pertains to the source distributions far away from the fuselage:

$$q_{ws}^{(2)} - q_w^{(1)} = \frac{2}{\cos\phi}\frac{d(z_t S^{(1)})}{d\xi}$$

and secondly the distribution which pertains to the wing-body junction: $q_{wJ}^{(2)} - q_w^{(1)}$ given by equation (65). Results are shown in Fig. 16.

Next, we examine how the values of Δv_x at the wing surface $z = z_t$ differ from those in the plane $z = 0$. From a Taylor series expansion of Δv_x with respect to z we obtain

$$\Delta v_x(x, y, z) = \Delta v_x(x, y, 0) + z\left(\frac{\partial \Delta v_x(x, y, z)}{\partial z}\right)_{z=0} + \ldots = \Delta v_x(x, y, 0) + z\frac{\partial \Delta v_z(x, y, 0)}{\partial x} + \ldots \tag{69}$$

The component $\Delta v_z(x, y, 0)$ in the plane $z = 0$ vanishes, because v_{zIQ} vanishes in $z = 0$, except for $x = 0$, $y = R$ where v_{zIQ} is finite. The difference $\Delta v_x(x, y, z_t) - \Delta v_x(x, y, 0)$ is therefore a term of third order. Nevertheless, we have computed values of $\Delta v_{xJ}^{(2)}(x, z_t)$ in the junction, using the values of the velocity component $v_{xIQ}(x, \theta)$ given in Table 2 and the source distribution $q_{ws}^{(2)}$. By graphical interpolation, we have derived values of $\Delta v_{xJ}^{(2)}(x, \theta_J)$ and plotted these in Fig. 17 together with the values of $\Delta v_{xJ}^{(2)}(x, \theta = 0)$ and $\Delta v_{xJ}^{(1)}(x, \theta = 0)$. The figure shows that, for the particular case considered, the maximum velocity decrement is increased by about the same amount when evaluating Δv_x at $z = z_t$ instead of at $z = 0$ as when evaluating Δv_x from $q_{ws}^{(2)}$ instead of from $q_w^{(1)}$; the ratio between $(-\Delta v_{xJ}^{(2)}(x, \theta_J)_{\max}$ and $(-\Delta v_{xJ}^{(1)}(x, 0))_{\max}$ is about 1·5.

Finally, we have determined the strength of the line source distribution, which satisfies equation (68) for the values of $\Delta v_{zJ}^{(1)}$ given in Fig. 15, and have computed the streamwise velocity component $\Delta v_x^*(x, y = R, z_t)$ induced by the line source distribution. Values of the sum $\Delta v_{xJ}^{(2)}(x, \theta_J) + \Delta v_x^*(x, R, z_t)$ are also plotted in Fig. 17. We note that the ratio between $-\Delta v_{x\,\max}^*$ and $\Delta v_{xJ\,\max}^{(1)}$ is about $\frac{1}{3}$. We have however to stress again the uncertainty of the estimated Δv_x^* which means of the effect of $\Delta v_z^{(1)}$ in the boundary condition.

In comparing the difference between the values of Δv_x computed from $q_{ws}^{(2)} - q_w^{(1)}$ and from $q_{wJ}^{(2)} - q_w^{(1)}$, given in Fig. 16, with the magnitude of the somewhat uncertain value of Δv_x^*, it seems justified to ignore the spanwise variation of $q_w^{(2)}$ and to use only the simpler term $q_{ws}^{(2)}$ in evaluating the interference velocity Δv_x.

In order to compute the pressure coefficient C_p to second-order accuracy, we ought to take account also of the velocity components Δv_y and Δv_z. We have not computed values of the spanwise interference velocity Δv_y away from the wing–body junction. The approximate boundary condition of equation (61) states that the velocity component v_z at the surface of the wing attached to the fuselage is the same as for the isolated wing. Within the present approximations, the change in the pressure distribution caused by the fuselage is therefore only produced by the change in the streamwise velocity.

4.3. Pressure Distribution on the Fuselage

The pressure distribution on the fuselage, to first-order accuracy, can be derived by computing the values of $\Delta v_x^{(1)}(x, \theta)$, using the values of $v_{xIQ}(x, \theta)$ of Table 2 and $q_w^{(1)}$, and adding these to the velocity $v_{xt}^{(1)}$ at the reflection plate at $z = R \sin \theta$ (computed from $v_{x\wedge Q}$, using $q_w^{(1)}$). For $\theta = 90$ degrees, values of

$$v_x^{(1)}(x, \theta) = v_{xt}^{(1)}(x, y = R, z = R \sin \theta) + \Delta v_x^{(1)}(x, \theta)$$

are plotted in Fig. 18.

More accurate values of v_{xt} can be derived by using $q_w^{(2)}(x, y)$ instead of $q_w^{(1)}$ with Ledger's program[5] or by means of the iteration technique developed by Sells.[6] However, without further effort, we are not in a position to determine more accurate values of Δv_x.

Fig. 18 shows that for the configuration considered, with $c/R = 5$, the maximum perturbation velocity at the top of the fuselage is about half the velocity in the flow past the isolated wing in the plane of symmetry at $z = R$. A reduction of the perturbation velocity is to be expected since the fuselage straightens the streamlines past the isolated wing. The maximum velocity at the top of the fuselage decreases with increasing sweep, as for the isolated wing, and the position of the maximum velocity moves rearwards.

4.4. Comparison of Results using the Present Method with those derived by Other Methods for Particular Configurations

The configurations considered so far deal with wings of constant chord and infinite span. We have mentioned in the introduction that we assume that the tabulated values of v_{xIQ} for infinitely long source lines can also be used to estimate the interference on wings of finite span (when the span is larger than say five times the diameter of the fuselage). One may also expect that wings of moderate taper can be dealt with. In order to examine the validity of these assumptions, comparisons can be made of the results derived by the present method with those from more exact methods. Such comparisons can also provide information about the accuracy of the estimate for Δv_x^*.

For symmetrical wing–fuselage configurations at zero lift, it is generally assumed that nominally-exact pressure distributions can be derived by means of singularity distributions on the surface of the wing and the fuselage, the strengths of which are chosen such that the exact boundary condition is satisfied at certain points of the surface. A method for solving the problem by means of planar source panels, each of constant source strength, was devised by A. M. O. Smith and J. Hess (*see* for example Ref. 7). Recently A. Roberts and K. Rundle[8,9] have produced a computer program for solving the problem by means of curved panels where the geometry of the panels and the strength of the source distribution vary continuously between adjacent panels.

Using both methods, calculations have been done (unpublished work by A. F. Jones, R.A.E. and A. Roberts, B.A.C.) for two particular wing–fuselage combinations and for the related gross wing without fuselage. Geometric details are given in Fig. 19. The velocity components have been computed by Roberts' program for a freestream Mach number $M_0 = 0{\cdot}4$. In the following analysis, we compare only the streamwise perturbation velocity component pertaining to incompressible flow, which we have derived from the values of v_x computed by Roberts' program by multiplying them by the factor $\beta = \sqrt{1-0{\cdot}4^2}$. Somewhat different values would be obtained if Roberts' program were applied for incompressible flow. We may however expect that the difference is small because for the wing alone, the values of v_x derived in this way from the Roberts' program are very similar to those computed by the A. M. O. Smith program for $M = 0$. Unfortunately, the two programs have produced values for v_x at different spanwise and chordwise positions, so that we have to interpolate or extrapolate the computed values before we can make a comparison. In particular, we have to extrapolate the values of v_x into the junction. In the neighbourhood of the wing-body junction, the two programs produce different values for v_x, as shown in Fig. 20. It seems reasonable to assume that Roberts' program, which uses continuous singularity distributions, produces the more reliable results. (We note also that in Roberts' method special singular source 'modes' are used near the wing-body junction, in accordance with the results of Craggs and Mangler.[14] This feature should also increase the accuracy in this region.)

Some further justification for the assumption can be derived by an examination of the values for the spanwise velocity component obtained by the two methods. The velocity components v_y and v_z at the junction are related by the condition

$$v_{nJ}(x, \theta_J) = \cos\theta_J v_y(x, y_J, z_t) + \sin\theta_J v_z(x, y_J, z_t) = 0.$$

The values of $v_y(x, y > R, z_t)$ given by Roberts' program extrapolate readily to the approximate values at the junction,

$$v_y = -\tan\theta_J v_{zt}^{(1)}(x, y, 0) = -\frac{z_t/c}{R/c}\frac{dz_t}{d\xi}.$$

However, values from the A. M. O. Smith program for the examples considered, though following the same trends as the Robert's results away from the junction, diverge from them for stations within about 2 per cent chord of the junction and consequently do not tend to the values given above.

To determine the interference velocity, we strictly require the velocity on the nett wing, when attached to an infinite reflection plate. We have not in fact determined this but have assumed that we may neglect the difference between the gross and nett wings (aspect ratio 6 and 5·65 respectively) and thus obtain the interference velocity by subtracting the values of $v_{xt}(\xi, \eta = 0)$ at the centre section of the gross wing from the $v_{xJ}(\xi, y_J)$ in the wing-body junction at the same percentage-chord point $\xi = [x - x_{LE}(y)]/c(y)$ (where $c(y)$ is the local chord and $x_{LE}(y)$ the coordinate of the leading edge). Values of Δv_{xJ} are plotted in Fig. 21.

To derive an estimate for Δv_x by the method of the present Report, we have approximated the tapered wing by an untapered wing of 30 degrees sweep and the same chord c_J as the tapered wing in the wing-body junction; the ratio between body radius and wing chord is $R/c_J = 0{\cdot}24$. For this configuration, we have computed values of $\Delta v_x^{(2)}(x, \theta_J)$ using the source distribution $q_{ws}^{(2)}(\xi)$, given by equation (64).

The fuselage is non-cylindrical at a distance greater than one diameter forward of the apex of the gross wing. To estimate the effect of the body nose, we have computed, by slender-body theory, values of the streamwise velocity v_{xB} for the isolated fuselage and have added these to $\Delta v_{xJ}^{(2)}$.

In Fig. 21, we compare the values of $\Delta v_{xJ}^{(2)} + v_{xB}$ with the values of Δv_{xJ} derived by the two panel methods. We note that, for $0{\cdot}1 < x/c_J < 0{\cdot}6$ say, the values of $\Delta v_{xJ}^{(2)} + v_{xB}$ agree fairly well with those derived from the Roberts' program. It is likely that the differences over the rearward part of the chord are taper effects. We have seen in Fig. 12 that the position where Δv_x vanishes moves forward with decreasing angle of sweep. An improved estimate of Δv_x, at the chordwise position x, could probably be derived if the wing were to be represented by one with the local sweep $\phi(x)$ instead of the sweep of the midchord line. Unfortunately, we cannot draw definite conclusions because we cannot estimate the accuracy of the interpolated values of v_{xt}. We do not compare the various values of Δv_x near the leading edge because the interpolated values of v_{xt} can be rather inaccurate and because the present method is based on a small perturbation theory (without leading-edge corrections) which is by nature unreliable near the leading edge.

We have computed values of $\Delta v_{zJ}^{(1)}$ and hence, by means of a line source distribution, values of the corresponding change in the streamwise velocity Δv_x^*. If we consider the values of Δv_x derived from Roberts'

program as reliable, then Fig. 21 suggests that the change in Δv_x, which is related to the change Δv_z at the surface of the wing, is smaller than Δv_x^*; this could imply that the interference term Δv_z decreases more rapidly away from the wing–body junction than $\Delta v_z^*(x, y, z_t)$ induced by the line source distribution.

A calculation by Roberts' program has also been done for a combination of the same gross wing A with a fuselage, B_0, for which the diameter of fuselage B_1 has been reduced by the factor $\sqrt{0{\cdot}5}$. For this configuration, the ratio between the wing chord in the wing-body junction and the body radius, $c_J/R \approx 6$. From the computed results we have derived values of Δv_{xJ} in the same way as for the larger fuselage. These are plotted in Fig. 22 together with the values for the thicker body B_1. The maximum velocity decrement is larger for the thinner body because the projection of the junction shape into the chord plane, $y_J(x)$, departs more from a straight line. We have also plotted in Fig. 22 the values of $\Delta v_{xJ}^{(2)}(x, \theta_J) + v_{xB}$. The values of $\Delta v_x^{(2)}$ are again determined with $q_{ws}^{(2)}$. For the body B_0 we have taken for v_{xB} half the values of v_{xB} for the body B_1. Fig. 22 shows that the difference between the values of Δv_{xJ} for the two bodies is well predicted by the estimates. The maximum value $-\Delta v_x^*$, derived from $\Delta v_{zJ}^{(1)}$, is 20 per cent larger for the configuration AB_0 than for AB_1. If we consider the values of Δv_{xJ}, derived from the Roberts results, as being correct, then Fig. 22 suggests again that the change in Δv_x, related to $\Delta v_z(x, y, z_t)$, is negligible.

We have also derived values of Δv_x for the spanwise stations $y_J + 0{\cdot}25R$ and $y_J + R$ and have plotted them in Fig. 23 together with the estimates of the present method; note that, for $y > R$, $\Delta v_x^{(2)}$ has been computed at $z = 0$, using $q_{ws}^{(2)}$. The differences between the results from the two panel methods decrease away from the junction, *see* Fig. 20. The output of the A. M. O. Smith program enables us to derive values of Δv_x at more chordwise points than the output of Roberts' program. In Fig. 23, we have therefore shown mainly the Δv_x from the A. M. O. Smith program, they agree fairly well with the estimate, $\Delta v_x^{(2)}(x, y, z = 0) + v_{xB}$.

Summarising, we can say that the comparison of the present method with the results from Roberts' program for two particular configurations suggests that a fair estimate of the interference velocity Δv_{xJ} is given by $\Delta v_x^{(2)}(x, \theta_J)$ and of $\Delta v_x(x, y > R)$ by $\Delta v_x^{(2)}(x, y, 0)$, when the terms $\Delta v_x^{(2)}$ are computed from the second-order source distribution and the velocity component Δv_{xIQ} related to an infinitely long source line.

The recommended procedure for estimating the change of the streamwise velocity Δv_x due to the presence of the fuselage is therefore as follows. For the given section shape $z_t(x)$, one determines the strength of the second-order source distribution $q_{ws}^{(2)}(x)$ of the related infinite sheared wing:

$$q_{ws}^{(2)}(x) = 2\frac{d}{dx}\left[z_t(x)\left(1 + \frac{S^{(1)}(x)}{\cos\phi}\right)\right], \tag{70}$$

where

$$S^{(1)}(x) = \frac{1}{\pi}\int_0^c \frac{dz_t(x')}{dx'}\frac{dx'}{x - x'}. \tag{71}$$

Using $q_{ws}^{(2)}$ one evaluates $\Delta v_x^{(2)}$ from the single integral

$$\Delta v_x^{(2)}(x, y, z) = \cos\phi \int_0^{c/R} q_{ws}^{(2)}(x') \frac{v_{xIQ}\left(\frac{x - x'}{R}, \frac{y}{R}, z\right)}{Q/R} d\left(\frac{x'}{R}\right); \tag{72}$$

values of v_{xIQ} are given in Tables 1 and 2 (further values are given in Tables 1 and 2 of Ref. 3). Using the values of $v_{xIQ}(x, y, z = 0)$ given in Table 1, one can determine the interference velocity in the wing plane. To obtain an improved estimate of Δv_{xJ} in the wing–body junction, it is recommended that firstly the integral of equation (72) be evaluated for various values of θ using the values of $v_{xIQ}(x, \theta)$ from Table 2 and that secondly one interpolates between the values of $\Delta v_x^{(2)}(x, \theta)$ to derive the value applicable to $\theta_J(x) = \sin^{-1}(z_t(x)/R)$. When the required angle of sweep differs from the values for which v_{xIQ} is tabulated, it seems advisable to compute $\Delta v_x^{(2)}$ with the tabulated values of v_{xIQ} and to interpolate between the values of $\Delta v_x^{(2)}(x, y, z; \phi)$ to derive $\Delta v_x^{(2)}$ for the required value of ϕ.

5. Design of a Wing with Given Load Distribution when Attached to a Circular Cylindrical Fuselage

5.1. Mean Surface according to First-Order Theory

We consider now the design problem for a wing of constant chord, c, and infinite aspect ratio attached in a midwing position to a circular fuselage.

We consider first the isolated wing which has a camber surface $z_s^{(1)}(x, y)$ and a twist distribution, $\alpha^{(1)}(y)$, such that it produces a chordwise load distribution which is constant across the span:

$$-\Delta C_p(x, y) = -\Delta C_p(\xi = x - (|y| - R) \tan \phi) = l(\xi). \tag{73}$$

(The superscript (1) denotes that the wing warp is to be obtained by first-order theory.) In first-order theory, such a load distribution can be represented by a chordwise distribution of infinite swept vortices in the chordal plane of strength $\gamma(\xi)$, where the vorticity is related to the pressure difference by the relation

$$l(\xi) = 2 \cos \phi \gamma(\xi). \tag{74}$$

Thus, the strength of an elemental strip of vortices, which are parallel to the leading edge, is

$$\gamma(\xi)\, dn = \gamma(\xi) \cos \phi\, d\xi = \tfrac{1}{2} l(\xi)\, d\xi \tag{75}$$

where dn is a length measured normal to the leading edge.

In first-order wing theory, the assumption is usually made that the normal velocity at the wing surface can be approximated by the velocity component $v_z(x, y, 0)$ in the chordal plane, so that the first-order boundary condition reads

$$\frac{\partial z^{(1)}(x, y)}{\partial x} = \frac{\partial z_s^{(1)}(x, y)}{\partial x} - \alpha^{(1)}(y) = \frac{v_z(x, y, z = 0)}{V_0} \tag{76}$$

where V_0 is the magnitude of the freestream velocity, taken again as unity.

For load distributions like those considered in this Report, where the direction of the vorticity vectors changes somewhere discontinuously, the downwash induced in the plane $z = 0$ tends logarithmically to infinity as the station is approached where the vorticity vectors have a kink. In a practical design, this difficulty can be avoided since the mean surface for a wing of finite thickness, $z_t(x, y)$, is to be determined; for this the first-order boundary condition can also be written in the form

$$\frac{\partial z_s^{(1)}(x, y)}{\partial x} - \alpha^{(1)}(y) = v_z(x, y, z_t(x, y)). \tag{77}$$

The design of the isolated wing can therefore be performed by means of equation (77).

We examine in the following only how the presence of the fuselage modifies the required shape of the mean surface. The interference downwash, $\Delta v_z(x, y, 0)$, in the plane $z = 0$ is everywhere finite, including the wing–body junction. We therefore consider first the interference downwash in the plane $z = 0$.

It follows from equation (75) that

$$\Delta v_z(x, y, 0) = \frac{1}{2} \frac{c}{R} \int_0^1 l\left(\frac{x'}{c}\right) \frac{v_{z\Gamma}[(x - x')/R, y/R, 0])}{\Gamma/R} d\left(\frac{x'}{R}\right); \tag{78}$$

values of $v_{z\Gamma}$ are given in Table 4. For $y = R$, the values of v_{zq} and $v_{z\Gamma}$ tend logarithmically to infinity when x' tends to x (*see* equation (51)). In computing values of $\Delta v_z(x, y = R, 0)$, we therefore write equation (78) in a different form and make use of this known singular behaviour of $v_{z\Gamma}(x, y = R, 0)$.

As an example, we choose the load distribution

$$l\left(\frac{\xi}{c}\right) = 4\alpha \cos \phi \sqrt{\frac{1 - \xi/c}{\xi/c}}, \quad 0 < \frac{\xi}{c} < 1; \tag{79}$$

which produces at spanwise stations far away from the fuselage, $|y| \gg R$, the downwash

$$v_z(\xi, y \gg R, 0) = -\alpha.$$

Values of $\Delta v_z(x, y = R, 0)/\alpha$ for various values of ϕ and $c/R = 5$ are plotted in Fig. 24, and for $\phi = 45$ degrees and various values of c/R in Fig. 25. The figures show that the body interference can increase the downwash

considerably and that, for the flat-plate load distribution, the interference downwash does not depend much on the angle of sweep. The relatively weak dependence of Δv_z on the angle of sweep differs appreciably from the variation of the interference velocity Δv_x for the displacement flow with the angle of sweep, shown in Fig. 12. The dependence of Δv_z on the angle of sweep varies of course somewhat with the type of chordwise load distribution and with the ratio c/R.

For $\phi = 45$ degrees, $c/R = 5$ and the flat-plate load distribution, the interference downwash has also been determined at spanwise stations away from the wing-body junction. In Fig. 26, we have plotted Δv_z as function of ξ/c. We note that the magnitude of $|\Delta v_z(x, y, 0)|$ decreases more rapidly with increasing y/R than the magnitude of $|\Delta v_x^{(1)}(x, y, 0)|$ given in Fig. 14; this different behaviour was to be expected from the different variation of $v_{xIO}(x, y, 0)$ and $v_{zII}(x, y, 0)$ with increasing y, shown in Figs. 4 and 9.

When $\Delta v_z(x, y, 0)$ is known, the required change of the wing surface can be derived from the first-order boundary condition, *see* equation (76)

$$\frac{\partial \Delta z^{(1)}(x, y)}{\partial x} = \frac{\partial \Delta z_s^{(1)}(x, y)}{\partial x} - \Delta\alpha^{(1)}(y)$$

$$= \Delta v_z(x, y, 0). \tag{80}$$

If we keep the z-coordinate at the trailing edge, $z_{TE}(y) = z(\xi/c = 1, y)$, the same as for the isolated wing, then the additional wing warp $\Delta z^{(1)}$ is given by the relation

$$\frac{\Delta z^{(1)}(\xi, y)}{c} = -\int_{\xi/c}^{1} \Delta v_z\left(\frac{x}{c} = \left(\frac{|y|}{c} - \frac{R}{c}\right)\tan\phi + \frac{\xi'}{c}, y, 0\right) d\left(\frac{\xi'}{c}\right). \tag{81}$$

Values of $\Delta z^{(1)}$, derived from equation (81) and the downwash Δv_z given in Fig. 26, are shown in Fig. 27. The additional wing warp can be expressed as a change in twist, $\Delta\alpha^{(1)}(y)$, and a change of the camber shape, $\Delta z_s^{(1)}$, where

$$\Delta\alpha^{(1)}(y) = -\int_0^1 \Delta v_z(\xi', y, 0)\, d\left(\frac{\xi'}{c}\right) \tag{82}$$

and

$$\frac{\Delta z_s^{(1)}(\xi, y)}{c} = \int_0^{\xi/c} \Delta v_z(\xi', y, 0)\, d\left(\frac{\xi'}{c}\right) + \frac{\xi}{c}\Delta\alpha^{(1)}(y). \tag{83}$$

When the values of Δv_{zJ}, given in Fig. 25 for various values of c/R, are inserted into equations (82), (83), we find that the additional wing warp increases with increasing c/R, or for given chord with decreasing body radius. We have, however, to remind ourselves of the assumption made above that the mean surface of the wing does not depart much from the plane $z = 0$; this requires in particular $|\Delta z^{(1)}| \ll R$, $\Delta\alpha^{(1)} \ll R/c$, $|\Delta z_s^{(1)}/c| \ll R/c$. To achieve this it is necessary that $|l(\xi)|$ or α tend to zero when R/c tends to zero. When c/R tends to zero, the interference downwash and the additional wing warp vanish, since $c/R \to 0$ represents a wing attached to an infinite reflection plate.

For an unswept wing, which, when attached to a fuselage, produces a flat-plate load distribution, the mean surface has the twist distribution $\Delta\alpha^{(1)}(y)$ and the camber $\Delta z_s^{(1)}(x, y)$. For a swept wing the mean surface of the isolated wing is already twisted and cambered.

To illustrate the magnitude of the interference downwash for a combination of a swept wing and a fuselage, we have computed values of the downwash at the centre section of the isolated wing, at a station far away from the centre section and at the wing–body junction. We have mentioned that, with a load distribution which is constant across the span, the downwash at the centre section must not be computed at $z = 0$. We have therefore computed the downwash for a constant finite value of z, namely $z/c = (R/c)\sin 10° = 0{\cdot}2 \sin 10° \approx 0{\cdot}035$. To allow a proper comparison, we have computed also the interference downwash and the downwash of the sheared wing at $z \neq 0$. For $\phi = 45$ degrees, $c/R = 5$ and the flat-plate load distribution, the various downwash distributions are shown in Fig. 28. The figure shows that, for a wing with 45 degrees sweep, more of the difference between the required wing shape in the wing–body junction and the shape far away from the junction is produced by the reflection-plate effect than by the effects of the curvature of the body.

for the wing–body junction the approximate equation

$$\frac{d\Delta z_J^{(2)}}{dx} = \Delta v_{zl}(x, \theta_J) - \frac{d\Delta z_{sJ}^{(1)}}{dx}\left[S^{(1)} \cos\phi - f(\phi)\cos\phi \frac{dz_t}{d\xi}\right]$$
$$- \Delta z_{sJ}^{(1)}\left[\frac{dS^{(1)}}{d\xi}\cos\phi - f(\phi)\cos\phi \frac{d^2 z_t}{d\xi^2} - 8S^{(1)}\sin\phi\right]. \tag{86}$$

For the flat-plate load distribution and $c/R = 5$, values of $d\Delta z_J^{(2)}/dx$ are plotted in Figs. 30 and 31. (The small discontinuity in the curves at $x/c = 0{\cdot}3$ is a consequence of the discontinuity in the slope $dS^{(1)}(x)/dx$ at $x/c = 0{\cdot}3$.) For the swept wing, we note that taking account of the wing thickness reduces the interference downwash considerably; in particular the additional twist is much reduced. We have not derived the effect of the second-order terms on the wing shape away from the junction, but we may assume that they are less important, because the fact that the linear term in the Taylor series expansion of $\Delta v_{zl}(x, y, z)$ with respect to z vanishes is likely to have a more decisive influence on the difference between $\Delta v_{zl}(x, y, z_t)$ and $\Delta v_{zl}(x, y, z = 0)$ for $y > R$ than for $y = R$. As a consequence, it may be expected that the change in the wing warp caused by the body interference varies less rapidly across the span when it is determined by second-order theory than by first-order theory.

In a practical design case, the thickness distribution and the pressure distribution on the upper surface of the wing attached to a fuselage at zero incidence may be prescribed. From this one can derive a first-order load distribution $l^{(1)}(x, y)$ by a procedure similar to that of equation (85) in Ref. 12, by substituting for $v_{xl}^{(1)}$ the sum $v_{xl}^{(1)} + \Delta v_{xl}^{(1)}$. The resulting load distribution will presumably vary across the span and the effect of the trailing vortices on the normal velocity at the surface of the fuselage has also to be taken into account. By applying the method developed in this Report, we can derive therefore only an estimate of the additional wing warp Δz. If the interference velocities Δv_{xl} and Δv_{yl} at the surface of the wing are neglected the accuracy of the load distribution and of the mean surface of the isolated wing can be improved by a procedure similar to that suggested in Section 3.2 of Ref. 12. We expect that $\Delta v_{xl}(x, y, z)$ will contain a term of order (zC_L) and that the wing-body angle will not be small, so that the application of the present method, which neglects the effect of the wing-body angle, will produce an error in Δz which may be of a magnitude similar to that of the second- and third-term on the right-hand side of equation (84). In a practical application of the present method, we therefore suggest that these terms should be ignored and that in the wing-body junction Δz_J should be derived from the interference downwash $\Delta v_{zl}(x, \theta_J)$ computed at θ_J

$$\frac{d\Delta z_J}{dx} = \Delta v_{zl}(x, \theta_J) \tag{87}$$

and not from $\Delta v_{zl}(x, \theta = 0)$ computed at $\theta = 0$, i.e. not from equation (80). For spanwise stations away from the fuselage, equation (80) should produce a sufficiently accurate estimate of $\Delta z(x, y > R)$.

The accuracy of the proposed procedure has not been examined because the pressure distribution on a wing–body configuration, designed by the suggested procedure has not been computed by a relatively accurate method, like the Roberts' program. It is to be expected that the estimate for Δz is less accurate than the estimated values of Δv_{xl} for the displacement flow, because, in a practical design case, it is likely that the load distribution in the neighbourhood of the wing–body junction changes fairly rapidly to avoid too rapid changes of the wing shape.

Since we do not yet know how useful the present method is for deriving an estimate of Δz in a practical design, it does not seem important to extend the present work, on wings with infinite aspect ratio and constant spanwise load distribution, to the computation of the streamwise interference velocity at points away from the wing plane nor of the interference downwash at points away from the fuselage and the wing plane. It seems more desirable to extend the present method to general vorticity distributions in the plane $\theta = 0$, even though this extension can provide an estimate of the required Δz only for wing–fuselage combinations, where the wing is mounted near the centre line of a circular cylindrical fuselage.

6. Résumé

The present Report gives tabulated values of the difference between the streamwise velocity component induced by a single swept source line in the presence of a circular cylindrical fuselage and the streamwise velocity induced by the source line when it is reflected at an infinite plate. The tables have been used to

compute the streamwise velocity on symmetrical wings at zero angle of incidence attached in a midwing position to a cylindrical fuselage.

It is shown that the streamwise velocity in the wing–body junction can be about 25 per cent lower than the maximum perturbation velocity at the centre section of the corresponding isolated wing. For the section shape chosen in the numerical examples (10 per cent thick R.A.E. 101 section) and a given ratio between wing chord and body radius, the maximum decrease of the velocity in the wing–body junction measured in terms of the maximum perturbation velocity at the centre section of the isolated wing does not vary a great deal with the angle of sweep. The reduction of the velocity is of course less when the ratio between the body diameter and the wing chord is increased.

It is also shown that the value for the velocity decrease is appreciably larger when it is computed at the surface of the wing using the second-order source distribution of the isolated wing than when it is computed in the wing plane using the first-order source distribution. It is further shown that, by means of the tabulated values for infinite source lines, fairly accurate estimates can be derived of the streamwise interference velocity for wing–fuselage configurations, where the wings are of finite span, have some taper and are of uniform section.

The Report gives also tabulated values of the difference between the downwash induced by a single swept vortex in the presence of a circular cylindrical fuselage and the downwash induced by the vortex when it is reflected at an infinite plate. These tables have been used to design wings of constant chord and infinite aspect ratio, attached in a midwing position to a fuselage, such that the wing–fuselage combination produces the same flat-plate load distribution across the span.

It is found that the interference downwash in the wing–body junction can be of a magnitude comparable to the downwash of the related sheared wing; the required additional wing twist can be 60 per cent of the angle of incidence of the sheared wing. It is shown that the interference downwash in the wing–body junction, computed in the wing plane, does not depend a great deal on the angle of sweep. As with the displacement flow, the interference effect is of course reduced when the ratio between the body diameter and the wing chord is increased.

For the flat-plate load distribution, it is shown that the magnitude of the interference downwash in the wing–body junction is less, when it is computed at the surface of a wing with finite thickness than when it is computed in the wing plane. The effect of the wing thickness increases with the angle of sweep.

With increasing spanwise distance from the wing–body junction, the interference downwash in the wing plane decreases more rapidly than does the decrement of the streamwise velocity for the displacement flow.

No statement can be made about the usefulness of the tabulated values for infinite vortices with respect to practical design requirements, where the chordwise load distribution may be expected to change more rapidly near the wing–body junction than the chordwise thickness distribution. But since the present work has shown that the interference downwash can be large, both for swept and unswept wings, it seems even more important to take account of the wing–body interference for lifting wing–fuselage configurations than for pure displacement flows.

LIST OF SYMBOLS

c	Wing chord
$c(y)$	Local wing chord
C_L	Lift coefficient
$K^{(1)}(x, \theta)$	*See* equations (15), (16)
$\bar{K}^{(1)}(x)$	*See* equations (18), (19)
$\bar{K}^{(\nu)}(x)$	*See* equation (23)
$l(x, y)$	Strength of the distribution of lifting singularities
Q	Strength of single infinite source line
$q(x, \theta)$	Strength of source distribution on the fuselage related to a single source line (or vortex) with triple kink in the plane $z = 0$
$q^{(0)}(x, \theta)$	First approximation to $q(x, \theta)$, *see* equation (13) or equation (41)
$q^{(1)}(x, \theta)$	Second approximation to $q(x, \theta)$, *see* equations (14)–(18) or equations (42)–(44)
$\bar{q}(x)$	Mean value of source strength $q(x, \theta)$ at a station x, *see* equation (8)
$q_w(x, y)$	Strength of source distribution in the wing plane representing the wing attached to an infinite reflection plate
$q_{ws}^{(2)}, q_{wJ}^{(2)}$	*See* equations (64), (65)
$\Delta q(x, y)$	Interference term of source distribution in the plane $z = 0$, which cancels the velocity $\Delta v_z^{(1)}(x, y, z_t)$, *see* equation (67)
R	Radius of fuselage
t/c	Thickness-to-chord-ratio
V_0	Free stream velocity, taken as unity
$\mathbf{v}$	Perturbation velocity
$\mathbf{v}_{\curlywedge}$	Velocity induced by single source line (or vortex) with three kinks *see* equation (2) (or equation (38))
$\mathbf{v}_{\wedge}$	Velocity induced by single source line (or vortex) with one kink *see* equation (29) (or equation (53))
$\mathbf{v}_q$	Velocity induced by source distribution $q(x, \theta)$ on fuselage
$\mathbf{v}_I$	$= \mathbf{v}_q + \mathbf{v}_{\curlywedge} - \mathbf{v}_{\wedge}$, interference velocity related to single source line (or vortex)
$\mathbf{v}_l$	Velocity field induced by load distribution $l(x, y)$ with an infinite reflection plate
$\mathbf{v}_t$	Velocity field past the thick unwarped wing attached to an infinite reflection plate
v_n	Velocity component normal to the surface of the fuselage
$\bar{v}_n$	Mean value of $v_n(x, \theta)$
v_x, v_y, v_z	Components of the perturbation velocity with respect to the various axes
v_θ	Circumferential velocity component at the surface of the fuselage
v_{xB}	Streamwise velocity on isolated fuselage
$\Delta\mathbf{v}$	Difference between the velocity field past the wing–fuselage combination and the velocity field past the wing attached to an infinite reflection plate
Δv_x^*	Streamwise velocity induced by line source distribution in $y = R$, $z = 0$, for which $\Delta v_z^*(x, y = R, z_t) = -\Delta v_{zJ}^{(1)}(x)$

x, y, z	Rectangular coordinate system, x-axis coincides with the axis of the fuselage
x, r, θ	System of cylindrical coordinates
$x_{LE}(y), x_{TE}(y)$	Ordinate of the wing leading edge or trailing edge, respectively
$z_s(x, y)$	Camber distribution of isolated wing
$2z_t(x, y)$	Thickness distribution
$\Delta z(x, y)$	$=\Delta z_s(x, y)+\Delta\alpha(y)(x_{TE}-x)$, change in wing warp produced by the body interference
$\Delta z_s(x, y)$	Additional camber produced by the body interference
$\alpha(y)$	Twist distribution of isolated wing
$\Delta\alpha(y)$	Additional twist produced by the body interference
Γ	Strength of single vortex
$\gamma(\xi)$	Strength of vorticity distribution
$\theta_J(x)$	$=\sin^{-1}\left(\frac{c}{R}\frac{z_t(x)}{c}\right)$
ξ	$=x-(\lvert y\rvert-R)\tan\phi$
ϕ	Angle of sweep
	Suffices
Q	Related to single source line
Γ	Related to single vortex
J	Refers to wing–body junction
l	Related to load distribution $l(x, y)$
t	Related to the source distribution in the wing plane which represents the isolated wing
	Superscripts
(1)	Term derived by first-order theory
(2)	Term derived by second-order theory

REFERENCES

No.	Author(s)	Title, etc.
1	J. Weber	Interference problems on wing–fuselage combinations. Part I: Lifting unswept wing attached to a cylindrical fuselage at zero incidence in midwing position. R.A.E. Technical Report 69130 A.R.C. C.P. 1331 (1969)
2	J. Weber and M. Gaynor Joyce	Interference problems on wing–fuselage combinations. Part II: Symmetrical unswept wing at zero incidence attached to a cylindrical fuselage at zero incidence in midwing position. R.A.E. Technical Report 71119 A.R.C. C.P. 1332 (1971)
3	J. Weber and M. Gaynor Joyce	Interference problem on wing–fuselage combinations. Part III: Symmetrical swept wing at zero incidence attached to a cylindrical fuselage. A.R.C. C.P. 1333 (1974)
4	J. Weber and M. Gaynor Joyce	Interference problems on wing–fuselage combinations. Part IV: The design problem for a lifting swept wing attached to a cylindrical fuselage. A.R.C. C.P. 1334 (1974)
5	J. A. Ledger	Computation of the velocity field induced by a planar source distribution, approximating a symmetrical non-lifting wing in subsonic flow. A.R.C. R. & M. 3751 (1972)
6	C. C. L. Sells	Iterative solution for thick symmetrical wings at incidence in incompressible flow. R.A.E. Technical Report 73047 A.R.C. 34959 (1974)
7	J. L. Hess and A. M. O. Smith	Calculation of potential flow about arbitrary bodies. Progress in Aeron. Scs., Vol. 8 (1967)
8	A. Roberts and K. Rundle	Computation of incompressible flow about bodies and thick wings using the spline mode system. B.A.C. Weybridge, Ma Report 19 (1972), A.R.C. 33775
9	A. Roberts and K. Rundle	The computation of first order compressible flow about wing–body configurations. B.A.C. Weybridge, Ma Report 20 (1973)
10	D. Küchemann	Some remarks on the interference between a swept wing and a fuselage. R.A.E. Technical Report 70093 A.R.C. 32307 (1970)
11	H. Kramer	Some analytical and numerical calculations for a cylinder-vortex combination in incompressible flow. NLR-TR 69057U (1969)

REFERENCES—*continued*

No.	Author(s)	Title, etc.
12	J. Weber	Second-order small-perturbation theory for finite wings in incompressible flow. A.R.C. R. & M. 3759 (1972)
13	.....	Method for predicting the pressure distribution on swept wings with subsonic attached flow. Roy. Aero. Soc. Trans. Data Memo. 6312 (1963) [Revised version to be issued as TDM 73012]
14	J. W. Craggs and K. W. Mangler	Some remarks on the behaviour of surface source distributions near the edge of a body. R.A.E. Technical Report 71085 A.R.C. 33185 (1971) *Aeron. Quarterly*, Vol. 24, p. 25 (1973)

APPENDIX A

The Velocity Field Induced by a Source Distribution on the Fuselage

We consider the velocity field $\mathbf{v}_q(x, y, z)$ induced by a source distribution of strength $q(x, \theta)$ on the surface of the fuselage. The streamwise component of $\mathbf{v}_q$ is

$$v_{xq}(x, y, z) = \int_{-\infty}^{\infty} \int_{0}^{2\pi} \frac{q(x', \theta')(x - x')\, d\theta'\, dx'}{4\pi\sqrt{(x-x')^2 + (y - \cos\theta')^2 + (z - \sin\theta')^2}^3}, \tag{A-1}$$

the spanwise component is

$$v_{yq}(x, y, z) = \int_{-\infty}^{\infty} \int_{0}^{2\pi} \frac{q(x', \theta')(y - \cos\theta')\, d\theta'\, dx'}{4\pi\sqrt{(x-x')^2 + (y - \cos\theta')^2 + (z - \sin\theta')^2}^3}, \tag{A-2}$$

the component normal to the wing plane is

$$v_{zq}(x, y, z) = \int_{-\infty}^{\infty} \int_{0}^{2\pi} \frac{q(x', \theta')(z - \sin\theta')\, d\theta'\, dx'}{4\pi\sqrt{(x-x')^2 + (y - \cos\theta')^2 + (z - \sin\theta')^2}^3}. \tag{A-3}$$

For the velocity component normal to the fuselage, v_{nq}, we obtain from equations (A-2) and (A-3):

$$v_{nq}(x, \theta) = v_{yq}\cos\theta + v_{zq}\sin\theta = \frac{q(x, \theta)}{2} + \int_{-\infty}^{\infty} \int_{0}^{2\pi} \frac{q(x', \theta')[1 - \cos(\theta - \theta')]\, d\theta'\, dx'}{4\pi\sqrt{(x-x')^2 + 2[1 - \cos(\theta - \theta')]}^3}. \tag{A-4}$$

For the circumferential velocity component, $v_{\theta q}$, on the fuselage, we obtain

$$v_{\theta q} = -v_{yq}\sin\theta + v_{zq}\cos\theta = \int_{-\infty}^{\infty} \int_{0}^{2\pi} \frac{q(x', \theta')\sin(\theta - \theta')\, d\theta'\, dx'}{4\pi\sqrt{(x-x')^2 + 2[1 - \cos(\theta - \theta')]}^3}. \tag{A-5}$$

In order to simplify the numerical evaluation of the various velocity components, we make use of the relations

$$\int_{-\infty}^{\infty} \frac{(x - x')\, dx'}{\sqrt{(x-x')^2 + a^2}^3} = 0, \tag{A-6}$$

$$\int_{-\infty}^{\infty} \frac{dx'}{\sqrt{(x-x')^2 + a^2}^3} = \frac{2}{a^2}, \tag{A-7}$$

$$\int_{0}^{2\pi} \frac{\sin(\theta - \theta')\, d\theta'}{\sqrt{(x-x')^2 + 2[1 - \cos(\theta - \theta')]}^3} = 0, \tag{A-8}$$

$$\int_{0}^{2\pi} \frac{d\theta'}{\sqrt{(x-x')^2 + 2[1 - \cos(\theta - \theta')]}^3} = \frac{4\mathbb{E}(k)}{(x-x')^2\sqrt{(x-x')^2 + 4}}, \tag{A-9}$$

where $\mathbb{E}$ is the complete elliptic integral of the second kind, with the modulus

$$k^2 = \frac{4}{4 + (x - x')^2}, \tag{A-10}$$

$$\int_{0}^{2\pi} \frac{[1 - \cos(\theta - \theta')]\, d\theta'}{\sqrt{(x-x')^2 + 2[1 - \cos(\theta - \theta')]}^3} = k[\mathbb{K}(k) - \mathbb{E}(k)], \tag{A-11}$$

where **K** is the complete elliptic integral of the first kind, with the modulus

$$k^2 = \frac{4}{4+(x-x')^2},$$

$$\int_0^{2\pi} \frac{d\theta'}{\sqrt{(x-x')^2+y^2+1-2y\cos\theta}^3} = \frac{4\mathbf{E}(k)}{[(x-x')^2+(y-1)^2]\sqrt{(x-x')^2+(y+1)^2}} \tag{A-12}$$

where

$$k^2 = \frac{4y}{(x-x')^2+(y+1)^2}. \tag{A-13}$$

We evaluated $v_{nq}(x, \theta)$ from the relation

$$v_{nq}(x,\theta) = \frac{q(x,\theta)}{2} + \int_0^{2\pi} \frac{q(x,\theta')\,d\theta'}{4\pi} + \int_{-\infty}^{\infty}\int_0^{2\pi} \frac{[q(x',\theta')-q(x,\theta')][1-\cos(\theta-\theta')]\,d\theta'\,dx'}{4\pi\sqrt{(x-x')^2+2[1-\cos(\theta-\theta')]}^3}. \tag{A-14}$$

$v_{\theta q}(x, \theta)$ can be evaluated from the relation

$$v_{\theta q}(x,\theta) = \int_{-\infty}^{\infty}\int_0^{2\pi} \frac{[q(x',\theta')-q(x,\theta')-q(x',\theta)+q(x,\theta)]\sin(\theta-\theta')\,d\theta'\,dx'}{4\pi\sqrt{(x-x')^2+2[1-\cos(\theta-\theta')]}^3} + \int_0^{2\pi} \frac{[q(x,\theta')-q(x,\theta)][1+\cos(\theta-\theta')]\,d\theta'}{4\pi\sin(\theta-\theta')}. \tag{A-15}$$

With the special configurations considered in this Report, we are only interested in two types of source distribution: either the symmetrical one, $q(x, \theta) = q(x, -\theta)$, or the antisymmetrical one, $q(x, \theta) = -q(x, -\theta)$, For the symmetrical distribution, we evaluate the streamwise velocity component in the plane $z = 0$ from the relation

$$v_{xq}(x,y,0) = \int_{-\infty}^{\infty}\int_0^{\pi} \frac{[q(x',\theta')-q(x,\theta')-q(x',\theta=0)+q(x,\theta=0)](x-x')\,d\theta'\,dx'}{2\pi\sqrt{(x-x')^2+y^2+1-2y\cos\theta'}^3} + \int_{-\infty}^{\infty} \frac{[q(x',\theta=0)-q(x,\theta=0)](x-x')\mathbf{E}(k)\,dx'}{\pi[(x-x')^2+(y-1)^2]\sqrt{(x-x')^2+(y+1)^2}}, \tag{A-16}$$

with k from equation (A-13). For the antisymmetrical source distribution, the streamwise velocity component, $v_{xq}(x, y, 0)$, in the plane $z = 0$ vanishes.

The velocity component $v_{zq}(x, y, 0)$ in the plane $z = 0$ vanishes when $q(x, \theta)$ is a symmetrical distribution. For the antisymmetrical source distribution, we evaluated $v_{zq}(x, y, 0)$ from the relation

$$v_{zq}(x,y,0) = -\int_{-\infty}^{\infty}\int_0^{\pi} \frac{[q(x',\theta)-q(x,\theta)]\sin\theta\,d\theta\,dx'}{2\pi\sqrt{(x-x')^2+y^2+1-2y\cos\theta}^3} - \int_0^{\pi} \frac{q(x,\theta)\sin\theta\,d\theta}{\pi[y^2+1-2y\cos\theta]}. \tag{A-17}$$

The streamwise velocity component on the fuselage $v_{xq}(x, \theta)$ can be evaluated from the relation

$$v_{xq}(x,\theta) = \int_{-\infty}^{\infty}\int_0^{2\pi} \frac{[q(x',\theta')-q(x,\theta')-q(x',\theta)+q(x,\theta)](x-x')\,d\theta'\,dx'}{4\pi\sqrt{(x-x')^2+2[1-\cos(\theta-\theta')]}^3} + \int_{-\infty}^{\infty} \frac{[q(x',\theta)-q(x,\theta)]\mathbf{E}(k)\,dx'}{\pi(x-x')\sqrt{(x-x')^2+4}} \tag{A-18}$$

with k from equation (A-10).

The velocity component $v_{zq}(x, \theta)$ on the fuselage can be evaluated from the relation

$$v_{zq}(x,\theta)=\int_{-\infty}^{\infty}\int_{0}^{2\pi}\frac{[q(x',\theta')-q(x,\theta')-q(x',\theta)+q(x,\theta)][\sin\theta-\sin\theta']\,d\theta'\,dx'}{4\pi\sqrt{(x-x')^2+2[1-\cos(\theta-\theta')]}^3}+$$
$$+\int_{0}^{2\pi}\frac{[q(x,\theta')-q(x,\theta)][\sin\theta-\sin\theta']\,d\theta'}{4\pi[1-\cos(\theta-\theta')]}+\sin\theta\,q(x,\theta)+$$
$$+\sin\theta\int_{-\infty}^{\infty}\frac{q(x',\theta)-q(x,\theta)}{2\pi\sqrt{(x-x')^2+4}}[\mathbb{K}(k)-\mathbb{E}(k)]\,dx' \qquad \text{(A-19)}$$

with k from equation (A-10).

APPENDIX B

The Behaviour of $v_{xq}(x, y = 1, 0)$ for Small Values of $|x|$

Inserting $q(x, \theta)$ from equation (24) into equation (26), and using equations (A-6) and (A-9), we obtain for $v_{xq}(x, 1, 0)$ the equation

$$v_{xq}(x, y=1, 0) = -\int_{-\infty}^{\infty} \int_0^{\pi} \frac{v_{nQ}(x', \theta)(x-x')\, d\theta\, dx'}{\pi\sqrt{(x-x')^2+2(1-\cos\theta)}^3} + \\ + \int_{-\infty}^{\infty} \frac{[\bar{v}_{nQ}(x') - \bar{v}_{nQ}(x) + \frac{1}{2}\sum \bar{K}^{(n)}(x') - \frac{1}{2}\sum \bar{K}^{(n)}(x)]\mathbf{E}(k)\, dx'}{\pi(x-x')\sqrt{(x-x')^2+4}}. \tag{B-1}$$

The single integral is a finite continuous function for all values of x. The singular behaviour of the double integral for small values of $|x|$ arises from

$$J_1(x) = -\int_{-a}^{b} dx' \int_0^{\delta} \frac{v_{nQ}(x', \theta)(x-x')\, d\theta}{\pi\sqrt{(x-x')^2+2(1-\cos\theta)}^3}, \tag{B-2}$$

where a, b, δ are large compared to $|x|$. It can be shown that, for $\theta \ll 1$ and $x \ll 1/\sin 2\phi$, the leading terms in $v_{nQ}(x, \theta)$ are

$$v_{nQ}(x, \theta) = \frac{Q}{4\pi}\left\{2 - \frac{x^2\cos^2\phi(2\cos^2\phi - \sin^2\phi)}{x^2\cos^2\phi + \theta^2} - \frac{2x^4\sin^2\phi\cos^4\phi}{[x^2\cos^2\phi+\theta^2]^2} + \right. \\ \left. + \frac{x\sin\phi[3x^2\theta^2\cos^2\phi + \theta^4(1+2\cos^2\phi)]}{\sqrt{x^2+\theta^2}[x^2\cos^2\phi+\theta^2]^2} + 0(x, \theta^2)\right\}. \tag{B-3}$$

We consider first the contribution J_2 to $v_{xq}(x, 1, 0)$, where

$$J_2(x) = -\frac{1}{4\pi^2}\int_{-d}^{d}\int_0^{d} \frac{x'\sin\phi[3x'^2\theta^2\cos^2\phi + \theta^4(1+2\cos^2\phi)](x-x')\, d\theta\, dx'}{\sqrt{x'^2+\theta^2}[x'^2\cos^2\phi+\theta^2]^2\sqrt{(x-x')^2+\theta^2}^3}.$$

We introduce the variable σ, defined by

$$\theta = \sigma x',$$

$$J_2 = -\frac{\sin\phi}{4\pi^2}\left\{\int_0^1 d\sigma \frac{3\sigma^2\cos^2\phi + \sigma^4(1+2\cos^2\phi)}{[\cos^2\phi+\sigma^2]^2\sqrt{1+\sigma^2}} \times \int_0^d \left[\frac{x'(x-x')}{\sqrt{(x-x')^2+\sigma^2x'^2}^3} - \frac{x'(x+x')}{\sqrt{(x+x')^2+\sigma^2x'^2}^3}\right] dx' + \right. \\ \left. + \int_1^{\infty} d\sigma \frac{3\sigma^2\cos^2\phi + \sigma^4(1+2\cos^2\phi)}{[\cos^2\phi+\sigma^2]^2\sqrt{1+\sigma^2}} \times \int_0^{d/\sigma}\left[\frac{x'(x-x')}{\sqrt{(x-x')^2+\sigma^2x'^2}^3} - \frac{x'(x+x')}{\sqrt{(x+x')^2+\sigma^2x'^2}^3}\right] dx'\right\}. \tag{B-4}$$

The integrals

$$\int_0^d \left[\frac{x'(x-x')}{\sqrt{(x-x')^2+\sigma^2x'^2}^3} - \frac{x'(x+x')}{\sqrt{(x+x')^2+\sigma^2x'^2}^3}\right] dx'$$

and

$$\int_0^{d/\sigma}\left[\frac{x'(x-x')}{\sqrt{(x-x')^2+\sigma^2x'^2}^3} - \frac{x'(x+x')}{\sqrt{(x+x')^2+\sigma^2x'^2}^3}\right] dx'$$

contain the term $\frac{2}{\sqrt[3]{1+\sigma^2}}\log|x|$. This means that J_2 contains the term $\kappa \log|x|$, where

$$\kappa = -\frac{\sin\phi}{4\pi^2}\int_0^\infty 2\frac{3\sigma^2\cos^2\phi+\sigma^4(1+2\cos^2\phi)}{[\cos^2\phi+\sigma^2]^2[1+\sigma^2]^2}d\sigma = -\frac{\cos^3\phi-1+\frac{3}{2}\sin^2\phi}{4\pi\sin^3\phi}. \tag{B-5}$$

We now consider the contribution J_3 to $v_{xq}(x, 1, 0)$, where

$$J_3(x) = -\frac{1}{4\pi^2}\int_{x-\epsilon}^{x+\epsilon}\int_0^\delta \left\{\frac{-x'^2\cos^2\phi(2\cos^2\phi-\sin^2\phi)}{x'^2\cos^2\phi+\theta^2} - \frac{2x'^4\sin^2\phi\cos^4\phi}{[x'^2\cos^2\phi+\theta^2]^2}\right\}\times\frac{(x-x')\,d\theta\,dx'}{\sqrt{(x-x')^2+\theta^2}^3}. \tag{B-6}$$

$J_3(x)$ is discontinuous at $x = 0$. The value

$$J_4(\phi) = \lim_{x\to 0} J_3(x>0;\phi) \tag{B-7}$$

can be determined by performing the integration with respect to θ, introducing the variable τ by the relation $x' = x(1+\tau)$ and taking the limit as x/δ tends to zero (*see* Appendix A of Ref. 2). This leads to the expression

$$J_4(\phi) = -\frac{\cos^2\phi}{4\pi^2}\int_{-\infty}^{\infty}\left\{\frac{(1+\tau)^2[2(\sin^2\phi-\cos^2\phi)\tau^2+(2-\sin^2\phi)\cos^2\phi(1+\tau)^2]}{\tau[\tau^2-(1+\tau)^2\cos^2\phi]^2} + \right.$$
$$\left. + \frac{\tau|1+\tau|[2\tau^2-(2+\sin^2\phi)(1+\tau)^2]}{\sqrt{|\tau^2-(1+\tau)^2\cos^2\phi|}^5}f(\tau)\right\}d\tau, \tag{B-8}$$

where

$$f(\tau) = \tan^{-1}\frac{\sqrt{\tau^2-(1+\tau)^2\cos^2\phi}}{|1+\tau|\cos\phi} \quad \text{for} \quad -\infty<\tau<-\frac{\cos\phi}{1+\cos\phi} \quad \text{and} \quad \frac{\cos\phi}{1-\cos\phi}<\tau<\infty$$

and

$$f(\tau) = \frac{1}{2}\log\frac{(1+\tau)\cos\phi+\sqrt{(1+\tau)^2\cos^2\phi-\tau^2}}{(1+\tau)\cos\phi-\sqrt{(1+\tau)^2\cos^2\phi-\tau^2}} \quad \text{for} \quad -\frac{\cos\phi}{1+\cos\phi}<\tau<\frac{\cos\phi}{1-\cos\phi}.$$

We have evaluated the integral in equation (B-8) numerically and have obtained the values

ϕ	$J_4(\phi)$
0	−0·05305
30°	−0·04853
45°	−0·04240
60°	−0·03288

The remaining contributions to $v_{xq}(x, 1, 0)$ are finite continuous functions. Thus $v_{xq}(x, 1, 0)$ behaves as

$$\frac{v_{xq}(x, y=1, 0)}{Q} = -\frac{\cos^3\phi-1+\frac{3}{2}\sin^2\phi}{4\pi\sin^3\phi}\log|x|+\frac{x}{|x|}J_4(\phi)+f(x;\phi),$$

where $f(x;\phi)$ is a finite continuous function.

TABLE 1

Streamwise Component of the Interference Velocity on the Wing, $[v_{xIQ}(x, y, z=0)]/[Q/R]$, for a Single Source Line

y/R / x/R	$\phi=0$			$\phi=30°$			$\phi=45°$			$\phi=60°$		
	1	1·25	2	1	1·25	2	1	1·25	2	1	1·25	2
−10	0·0014	0·0015	0·0015	0·0011	0·0011	0·0011	0·0009	0·0009	0·0009	0·0008	0·0007	0·0008
−5	0·0051	0·0052	0·0045	0·0041	0·0041	0·0038	0·0037	0·0037	0·0035	0·0034	0·0033	0·0032
−4	0·0072	0·0072	0·0059	0·0060	0·0060	0·0053	0·0055	0·0055	0·0050	0·0050	0·0049	0·0046
−3	0·0104	0·0102	0·0078	0·0093	0·0091	0·0077	0·0087	0·0085	0·0074	0·0081	0·0080	0·0067
−2	0·0160	0·0152	0·0100	0·0152	0·0146	0·0108	0·0147	0·0143	0·0110	0·0143	0·0138	0·0111
−1·5	0·0202	0·0187	0·0106	0·0201	0·0191	0·0127	0·0199	0·0191	0·0133	0·0196	0·0190	0·0138
−1·0	0·0259	0·0228	0·0101	0·0275	0·0254	0·0139	0·0282	0·0263	0·0155	0·0286	0·0270	0·0169
−0·8	0·0288	0·0243	0·0092	0·0319	0·0286	0·0141	0·0332	0·0303	0·0161	0·0342	0·0316	0·0179
−0·6	0·0321	0·0252	0·0077	0·0378	0·0322	0·0137	0·0401	0·0350	0·0163	0·0419	0·0373	0·0188
−0·4	0·0364	0·0243	0·0056	0·0464	0·0356	0·0127	0·0503	0·0402	0·0159	0·0536	0·0443	0·0191
−0·2	0·0423	0·0181	0·0030	0·0612	0·0358	0·0109	0·0685	0·0437	0·0148	0·0749	0·0510	0·0187
−0·1	0·0467	0·0106	0·0015	0·0742	0·0320	0·0097	0·0850	0·0422	0·0139	0·0967	0·0519	0·0182
−0·05	0·0495	0·0056	0·0008	0·0869	0·0284	0·0091	0·1033	0·0397	0·0134	0·1185	0·0510	0·0179
0	±0·0530	0	0	—	0·0237	0·0084	—	0·0362	0·0128	—	0·0488	0·0175
0·05	−0·0495	−0·0056	−0·0008	−0·0066	0·0185	0·0077	0·0213	0·0316	0·0122	0·0547	0·0454	0·0170
0·1	−0·0467	−0·0106	−0·0015	−0·0152	0·0128	0·0070	0·0066	0·0264	0·0116	0·0341	0·0412	0·0165
0·2	−0·0423	−0·0181	−0·0030	−0·0220	0·0029	0·0055	−0·0058	0·0161	0·0102	0·0161	0·0317	0·0155
0·4	−0·0364	−0·0243	−0·0056	−0·0246	−0·0093	0·0025	−0·0150	0·0013	0·0073	−0·0004	0·0154	0·0129
0·6	−0·0321	−0·0252	−0·0077	−0·0237	−0·0145	−0·0002	−0·0176	−0·0066	0·0045	−0·0073	0·0049	0·0101
0·8	−0·0288	−0·0243	−0·0092	−0·0222	−0·0164	−0·0027	−0·0179	−0·0105	0·0018	−0·0107	−0·0014	0·0074
1·0	−0·0259	−0·0228	−0·0101	−0·0208	−0·0169	−0·0044	−0·0175	−0·0124	−0·0004	−0·0123	−0·0053	0·0049
1·5	−0·0202	−0·0187	−0·0106	−0·0179	−0·0161	−0·0070	−0·0160	−0·0137	−0·0041	−0·0130	−0·0095	0·0002
2	−0·0160	−0·0152	−0·0100	−0·0156	−0·0145	−0·0079	−0·0147	−0·0133	−0·0060	−0·0125	−0·0107	−0·0028
3	−0·0104	−0·0102	−0·0078	−0·0116	−0·0113	−0·0076	−0·0120	−0·0114	−0·0069	−0·0113	−0·0107	−0·0053
4	−0·0072	−0·0072	−0·0059	−0·0086	−0·0087	−0·0063	−0·0093	−0·0095	−0·0063	−0·0096	−0·0102	−0·0057
5	−0·0051	−0·0052	−0·0045	−0·0064	−0·0067	−0·0052	−0·0070	−0·0077	−0·0054	−0·0076	−0·0089	−0·0054
10	−0·0014	−0·0015	−0·0015	−0·0018	−0·0022	−0·0020	−0·0019	−0·0028	−0·0024	−0·0019	−0·0038	−0·0030

TABLE 2

Streamwise Component of the Interference Velocity on the Fuselage, $[v_{xIQ}(x, \theta)]/[Q/R]$, for a Single Source Line

x/R \ θ	$\phi = 0$					$\phi = 30°$				
	5°	10°	30°	60°	90°	5°	10°	30°	60°	90°
−10	0·0014	0·0014	0·0015	0·0018	0·0019	0·0010	0·0011	0·0011	0·0011	0·0012
−5	0·0051	0·0052	0·0055	0·0062	0·0066	0·0041	0·0041	0·0042	0·0045	0·0046
−4	0·0072	0·0073	0·0079	0·0091	0·0098	0·0060	0·0060	0·0062	0·0067	0·0070
−3	0·0104	0·0106	0·0119	0·0147	0·0159	0·0093	0·0094	0·0099	0·0111	0·0117
−2	0·0161	0·0165	0·0199	0·0263	0·0289	0·0152	0·0154	0·0174	0·0212	0·0230
−1·5	0·0205	0·0212	0·0272	0·0365	0·0396	0·0202	0·0206	0·0243	0·0313	0·0343
−1	0·0265	0·0282	0·0395	0·0492	0·0506	0·0279	0·0288	0·0370	0·0477	0·0508
−0·8	0·0297	0·0323	0·0466	0·0530	0·0524	0·0325	0·0340	0·0452	0·0557	0·0576
−0·6	0·0338	0·0380	0·0545	0·0528	0·0498	0·0388	0·0415	0·0562	0·0631	0·0630
−0·4	0·0399	0·0477	0·0584	0·0451	0·0404	0·0486	0·0539	0·0692	0·0668	0·0642
−0·2	0·0535	0·0642	0·0446	0·0269	0·0229	0·0686	0·0787	0·0764	0·0627	0·0586
−0·1	0·0683	0·0603	0·0254	0·0141	0·0118	0·0916	0·0943	0·0713	0·0565	0·0529
−0·05	0·0629	0·0384	0·0131	0·0072	0·0059	0·1064	0·0932	0·0653	0·0526	0·0496
0	0	0	0	0	0	0·0845	0·0735	0·0574	0·0478	0·0464
0·05	−0·0629	−0·0384	−0·0131	−0·0072	−0·0059	0·0121	0·0391	0·0471	0·0433	0·0419
0·1	−0·0683	−0·0603	−0·0254	−0·0141	−0·0118	−0·0280	0·0026	0·0345	0·0377	0·0377
0·2	−0·0535	−0·0642	−0·0446	−0·0269	−0·0229	−0·0366	−0·0351	0·0111	0·0256	0·0273
0·4	−0·0399	−0·0477	−0·0584	−0·0451	−0·0404	−0·0301	−0·0389	−0·0254	0·0003	0·0060
0·6	−0·0338	−0·0380	−0·0545	−0·0528	−0·0498	−0·0264	−0·0325	−0·0392	−0·0201	−0·0133
0·8	−0·0297	−0·0323	−0·0466	−0·0530	−0·0524	−0·0238	−0·0278	−0·0407	−0·0326	−0·0284
1	−0·0265	−0·0282	−0·0395	−0·0492	−0·0506	−0·0218	−0·0246	−0·0379	−0·0385	−0·0357
1·5	−0·0205	−0·0212	−0·0272	−0·0365	−0·0396	−0·0184	−0·0199	−0·0290	−0·0375	−0·0390
2	−0·0161	−0·0165	−0·0199	−0·0263	−0·0289	−0·0158	−0·0167	−0·0226	−0·0309	−0·0336
3	−0·0104	−0·0106	−0·0119	−0·0147	−0·0159	−0·0116	−0·0121	−0·0147	−0·0198	−0·0214
4	−0·0072	−0·0073	−0·0079	−0·0091	−0·0098	−0·0086	−0·0088	−0·0100	−0·0130	−0·0139
5	−0·0051	−0·0052	−0·0055	−0·0062	−0·0066	−0·0064	−0·0065	−0·0073	−0·0090	−0·0097
10	−0·0014	−0·0014	−0·0015	−0·0018	−0·0019	−0·0018	−0·0018	−0·0021	−0·0028	−0·0032

TABLE 2—*continued*

θ / x/R	ϕ=45°					ϕ=60°				
	5°	10°	30°	60°	90°	5°	10°	30°	60°	90°
−10	0·0009	0·0009	0·0009	0·0009	0·0009	0·0008	0·0008	0·0008	0·0008	0·0008
−5	0·0037	0·0037	0·0037	0·0038	0·0038	0·0034	0·0034	0·0034	0·0033	0·0033
−4	0·0055	0·0055	0·0056	0·0058	0·0059	0·0051	0·0051	0·0051	0·0051	0·0050
−3	0·0087	0·0087	0·0090	0·0097	0·0101	0·0082	0·0082	0·0083	0·0086	0·0087
−2	0·0148	0·0149	0·0162	0·0190	0·0203	0·0143	0·0144	0·0151	0·0170	0·0180
−1·5	0·0200	0·0203	0·0231	0·0286	0·0309	0·0196	0·0199	0·0218	0·0259	0·0277
−1	0·0285	0·0292	0·0356	0·0449	0·0478	0·0288	0·0293	0·0341	0·0416	0·0442
−0·8	0·0337	0·0349	0·0438	0·0536	0·0557	0·0345	0·0354	0·0423	0·0504	0·0525
−0·6	0·0408	0·0429	0·0552	0·0628	0·0634	0·0425	0·0441	0·0537	0·0603	0·0612
−0·4	0·0520	0·0562	0·0700	0·0702	0·0685	0·0549	0·0581	0·0691	0·0697	0·0687
−0·2	0·0743	0·0827	0·0832	0·0720	0·0693	0·0794	0·0860	0·0855	0·0755	0·0721
−0·1	0·1000	0·1032	0·0840	0·0697	0·0664	0·1074	0·1090	0·0903	0·0759	0·0722
−0·05	0·1198	0·1090	0·0877	0·0676	0·0646	0·1300	0·1188	0·0907	0·0755	0·0718
0	0·1165	0·1012	0·0773	0·0651	0·0624	0·1388	0·1184	0·0896	0·0749	0·0711
0·05	0·0606	0·0775	0·0710	0·0619	0·0594	0·1054	0·1067	0·0864	0·0732	0·0698
0·1	0·0090	0·0449	0·0628	0·0583	0·0566	0·0586	0·0844	0·0818	0·0713	0·0684
0·2	−0·0198	−0·0044	0·0428	0·0494	0·0489	0·0097	0·0386	0·0687	0·0661	0·0647
0·4	−0·0219	−0·0286	0·0036	0·0276	0·0318	−0·0086	−0·0063	0·0368	0·0510	0·0525
0·6	−0·0211	−0·0277	−0·0201	0·0061	0·0128	−0·0121	−0·0168	0·0102	0·0334	0·0379
0·8	−0·0201	−0·0249	−0.0299	−0·0109	−0·0031	−0·0137	−0·0187	−0·0069	0·0170	0·0226
1	−0·0189	−0·0224	−0·0322	−0·0222	−0·0166	−0·0143	−0·0185	−0·0165	0·0035	0·0098
1·5	−0·0167	−0·0183	−0·0285	−0·0324	−0·0317	−0·0139	−0·0164	−0·0235	−0·0168	−0·0128
2	−0·0151	−0·0162	−0·0236	−0·0308	−0·0318	−0·0131	−0·0146	−0·0224	−0·0237	−0·0219
3	−0·0122	−0·0125	−0·0163	−0·0219	−0·0236	−0·0116	−0·0125	−0·0176	−0·0225	−0·0237
4	−0·0094	−0·0096	−0·0118	−0·0152	−0·0166	−0·0099	−0·0104	−0·0136	−0·0178	−0·0190
5	−0·0071	−0·0072	−0·0086	−0·0111	−0·0120	−0·0078	−0·0080	−0·0104	−0·0138	−0·0149
10	−0·0019	−0·0020	−0·0026	−0·0037	−0·0038	−0·0019	−0·0021	−0·0033	−0·0055	−0·0063

TABLE 3

z-Component of the Interference Velocity on the Fuselage, $[v_{zIQ}(x, \theta)]/[Q/R]$, for a Single Source Line

x/R \ ϑ	$\phi=0$				$\phi=30°$			
	5°	10°	20°	30°	5°	10°	20°	30°
−10	0·0001	0·0003	0·0004	0·0004	0·0000	0·0000	0·0000	−0·0001
−5	0·0006	0·0011	0·0017	0·0016	0·0001	0·0002	0·0002	−0·0001
−4	0·0009	0·0017	0·0027	0·0026	0·0002	0·0004	0·0005	−0·0001
−3	0·0016	0·0030	0·0048	0·0045	0·0005	0·0008	0·0011	0·0003
−2	0·0034	0·0063	0·0099	0·0090	0·0013	0·0024	0·0035	0·0024
−1·5	0·0054	0·0102	0·0154	0·0131	0·0023	0·0044	0·0065	0·0046
−1·0	0·0098	0·0179	0·0248	0·0173	0·0049	0·0090	0·0123	0·0075
−0·8	0·0131	0·0235	0·0298	0·0167	0·0068	0·0124	0·0159	0·0079
−0·6	0·0184	0·0317	0·0343	0·0115	0·0101	0·0177	0·0198	0·0057
−0·4	0·0285	0·0442	0·0327	−0·0040	0·0164	0·0264	0·0214	−0·0035
−0·2	0·0508	0·0543	0·0110	−0·0321	0·0316	0·0375	0·0095	−0·0262
−0·1	0·0646	0·0401	−0·0075	−0·0451	0·0452	0·0327	−0·0066	−0·0418
−0·05	0·0545	0·0256	−0·0144	−0·0490	0·0440	0·0218	−0·0158	−0·0491
0	0·0355	0·0181	−0·0169	−0·0504	0·0264	0·0098	−0·0234	−0·0552
0·05	0·0545	0·0256	−0·0144	−0·0490	0·0389	0·0087	−0·0273	−0·0593
0·1	0·0646	0·0401	−0·0075	−0·0451	0·0680	0·0219	−0·0265	−0·0610
0·2	0·0508	0·0543	0·0110	−0·0321	0·0735	0·0541	−0·0121	−0·0566
0·4	0·0285	0·0442	0·0327	−0·0040	0·0479	0·0643	0·0257	−0·0291
0·6	0·0184	0·0317	0·0343	0·0115	0·0329	0·0526	0·0422	−0·0019
0·8	0·0131	0·0235	0·0298	0·0167	0·0243	0·0418	0·0444	0·0142
1·0	0·0098	0·0179	0·0248	0·0173	0·0189	0·0336	0·0412	0·0215
1·5	0·0054	0·0102	0·0154	0·0131	0·0114	0·0209	0·0300	0·0233
2·0	0·0034	0·0063	0·0099	0·0090	0·0075	0·0141	0·0216	0·0191
3	0·0016	0·0030	0·0048	0·0045	0·0040	0·0076	0·0122	0·0119
4	0·0009	0·0017	0·0027	0·0026	0·0024	0·0047	0·0076	0·0078
5	0·0006	0·0011	0·0017	0·0016	0·0017	0·0032	0·0052	0·0055
10	0·0001	0·0003	0·0004	0·0004	0·0005	0·0009	0·0015	0·0016

TABLE 3—*continued*

x/R \ θ	ϕ=45°				ϕ=60°			
	5°	10°	20°	30°	5°	10°	20°	30°
−10	0·0000	0·0000	−0·0001	−0·0002	0·0000	−0·0001	−0·0002	−0·0003
−5	0·0000	−0·0001	−0·0003	−0·0006	−0·0001	−0·0003	−0·0006	−0·0010
−4	0·0000	0·0000	−0·0004	−0·0007	−0·0002	−0·0003	−0·0007	−0·0013
−3	0·0001	0·0001	−0·0003	−0·0007	−0·0001	−0·0003	−0·0009	−0·0017
−2	0·0006	0·0011	0·0013	0·0000	0·0001	0·0001	−0·0003	−0·0022
−1·5	0·0014	0·0025	0·0033	0·0013	0·0006	0·0010	0·0007	−0·0015
−1·0	0·0032	0·0058	0·0074	0·0029	0·0019	0·0033	0·0035	−0·0011
−0·8	0·0047	0·0084	0·0101	0·0029	0·0030	0·0052	0·0052	−0·0017
−0·6	0·0072	0·0124	0·0130	0·0008	0·0048	0·0082	0·0070	−0·0044
−0·4	0·0120	0·0192	0·0140	−0·0075	0·0085	0·0131	0·0069	−0·0127
−0·2	0·0239	0·0280	0·0035	−0·0288	0·0174	0·0191	−0·0040	−0·0336
−0·1	0·0348	0·0239	−0·0118	−0·0448	0·0252	0·0141	−0·0193	−0·0505
−0·05	0·0340	0·0139	−0·0215	−0·0531	0·0231	0·0039	−0·0296	−0·0592
0	0·0162	0·0005	−0·0309	−0·0610	0·0038	−0·0110	−0·0403	−0·0683
0·05	0·0187	−0·0064	−0·0381	−0·0676	−0·0062	−0·0230	−0·0501	−0·0769
0·1	0·0520	0·0007	−0·0414	−0·0723	0·0172	−0·0250	−0·0575	−0·0843
0·2	0·0810	0·0361	−0·0348	−0·0750	0·0700	−0·0009	−0·0616	−0·0943
0·4	0·0629	0·0696	0·0041	−0·0563	0·0809	0·0553	−0·0366	−0·0920
0·6	0·0454	0·0655	0·0334	−0·0266	0·0652	0·0726	−0·0008	−0·0705
0·8	0·0345	0·0556	0·0454	−0·0026	0·0521	0·0712	0·0254	−0·0443
1·0	0·0273	0·0466	0·0478	0·0125	0·0425	0·0647	0·0404	−0·0214
1·5	0·0171	0·0309	0·0406	0·0255	0·0281	0·0481	0·0499	0·0128
2·0	0·0117	0·0217	0·0315	0·0248	0·0201	0·0360	0·0450	0·0243
3	0·0065	0·0124	0·0193	0·0179	0·0119	0·0220	0·0319	0·0252
4	0·0042	0·0080	0·0128	0·0128	0·0080	0·0149	0·0229	0·0207
5	0·0029	0·0056	0·0091	0·0094	0·0057	0·0108	0·0172	0·0165
10	0·0009	0·0017	0·0028	0·0031	0·0019	0·0036	0·0060	0·0065

TABLE 4

Downwash Component of the Interference Velocity on the Wing, $[v_{zII}(x, y, z=0)]/[\Gamma/R]$ for a Single Vortex

y/R / x/R	$\phi=0$			$\phi=30°$			$\phi=45°$			$\phi=60°$		
	1	1·25	2	1	1·25	2	1	1·25	2	1	1·25	2
−10	0·0161	0·0104	0·0041	0·0102	0·0067	0·0029	0·0077	0·0052	0·0024	0·0054	0·0038	0·0018
−5	0·0314	0·0200	0·0075	0·0208	0·0137	0·0058	0·0162	0·0108	0·0049	0·0116	0·0079	0·0038
−4	0·0378	0·0238	0·0087	0·0256	0·0168	0·0070	0·0200	0·0134	0·0059	0·0145	0·0099	0·0047
−3	0·0466	0·0288	0·0098	0·0324	0·0210	0·0083	0·0257	0·0169	0·0072	0·0188	0·0127	0·0058
−2	0·0589	0·0347	0·0104	0·0425	0·0267	0·0096	0·0343	0·0220	0·0087	0·0254	0·0168	0·0073
−1·5	0·0670	0·0374	0·0099	0·0496	0·0300	0·0099	0·0404	0·0252	0·0092	0·0303	0·0196	0·0080
−1·0	0·0768	0·0384	0·0083	0·0584	0·0326	0·0094	0·0483	0·0283	0·0093	0·0368	0·0228	0·0084
−0·8	0·0812	0·0375	0·0072	0·0626	0·0332	0·0089	0·0522	0·0292	0·0090	0·0401	0·0238	0·0085
−0·6	0·0861	0·0350	0·0058	0·0674	0·0328	0·0081	0·0567	0·0296	0·0085	0·0439	0·0247	0·0083
−0·4	0·0914	0·0295	0·0041	0·0731	0·0306	0·0070	0·0623	0·0287	0·0077	0·0489	0·0248	0·0080
−0·2	0·0979	0·0186	0·0021	0·0812	0·0242	0·0055	0·0704	0·0249	0·0068	0·0561	0·0232	0·0075
−0·1	0·1018	0·0101	0·0011	0·0875	0·0181	0·0047	0·0772	0·0206	0·0062	0·0628	0·0211	0·0071
−0·05	0·1039	0·0052	0·0005	0·0926	0·0141	0·0042	0·0831	0·0178	0·0058	0·0689	0·0196	0·0069
0	±0·1061	0·0	0·0	—	0·0094	0·0038	—	0·0143	0·0054	—	0·0177	0·0067
0·05	−0·1039	−0·0052	−0·0005	−0·1097	0·0053	0·0033	−0·1121	0·0105	0·0051	−0·1157	0·0146	0·0064
0·1	−0·1018	−0·0101	−0·0011	−0·1111	0·0006	0·0028	−0·1154	0·0064	0·0047	−0·1202	0·0116	0·0062
0·2	−0·0979	−0·0186	−0·0021	−0·1107	−0·0086	0·0018	−0·1167	−0·0021	0·0039	−0·1232	0·0052	0·0056
0·4	−0·0914	−0·0295	−0·0041	−0·1071	−0·0229	−0·0002	−0·1151	−0·0166	0·0023	−0·1237	−0·0077	0·0044
0·6	−0·0861	−0·0350	−0·0058	−0·1034	−0·0317	−0·0021	−0·1125	−0·0268	0·0005	−0·1221	−0·0183	0·0031
0·8	−0·0812	−0·0375	−0·0072	−0·0995	−0·0370	−0·0038	−0·1094	−0·0337	−0·0012	−0·1200	−0·0262	0·0017
1·0	−0·0768	−0·0384	−0·0083	−0·0957	−0·0401	−0·0053	−0·1062	−0·0382	−0·0028	−0·1179	−0·0321	0·0003
1·5	−0·0670	−0·0374	−0·0099	−0·0864	−0·0426	−0·0080	−0·0980	−0·0434	−0·0059	−0·1117	−0·0408	−0·0027
2	−0·0589	−0·0347	−0·0104	−0·0782	−0·0417	−0·0095	−0·0901	−0·0442	−0·0079	−0·1050	−0·0444	−0·0050
3	−0·0466	−0·0288	−0·0098	−0·0646	−0·0371	−0·0103	−0·0763	−0·0414	−0·0096	−0·0923	−0·0451	−0·0077
4	−0·0378	−0·0238	−0·0087	−0·0540	−0·0322	−0·0098	−0·0654	−0·0372	−0·0098	−0·0816	−0·0428	−0·0088
5	−0·0314	−0·0200	−0·0075	−0·0460	−0·0280	−0·0090	−0·0568	−0·0332	−0·0095	−0·0726	−0·0397	−0·0092
10	−0·0161	−0·0104	−0·0041	−0·0253	−0·0158	−0·0057	−0·0328	−0·0201	−0·0067	−0·0452	−0·0267	−0·0078

TABLE 5

Downwash Component of the Interference Velocity on the Fuselage, $[v_{z\Pi}(x, \theta)]/[\Gamma/R]$, for a Single Vortex

x/R \ θ	$\phi=0°$				$\phi=30°$			
	0	5°	10°	15°	0	5°	10°	15°
−10	0·0161	0·0158	0·0151	0·0140	0·0102	0·0100	0·0096	0·0089
−5	0·0314	0·0309	0·0294	0·0271	0·0208	0·0205	0·0196	0·0182
−4	0·0378	0·0372	0·0354	0·0324	0·0256	0·0252	0·0241	0·0223
−3	0·0466	0·0458	0·0434	0·0395	0·0324	0·0319	0·0304	0·0281
−2	0·0589	0·0577	0·0542	0·0485	0·0425	0·0418	0·0397	0·0363
−1·5	0·0670	0·0654	0·0606	0·0530	0·0496	0·0486	0·0458	0·0413
−1·0	0·0768	0·0741	0·0663	0·0545	0·0584	0·0569	0·0525	0·0458
−0·8	0·0812	0·0776	0·0673	0·0522	0·0626	0·0606	0·0550	0·0465
−0·6	0·0861	0·0805	0·0656	0·0453	0·0674	0·0646	0·0567	0·0453
−0·4	0·0914	0·0811	0·0563	0·0283	0·0731	0·0681	0·0550	0·0387
−0·2	0·0979	0·0682	0·0235	−0·0036	0·0812	0·0665	0·0408	0·0212
−0·1	0·1018	0·0343	−0·0030	−0·0126	0·0875	0·0520	0·0241	0·0125
−0·05	0·1039	0·0049	−0·0071	−0·0086	0·0926	0·0343	0·0185	0·0129
0	±0·1061	0·0	0·0	0·0	—	0·0266	0·0217	0·0185
0·05	−0·1039	−0·0049	0·0071	0·0086	−0·1097	0·0337	0·0319	0·0277
0·1	−0·1018	−0·0343	0·0030	0·0126	−0·1111	0·0090	0·0369	0·0366
0·2	−0·0979	−0·0682	−0·0235	0·0036	−0·1107	−0·0481	0·0168	0·0398
0·4	−0·0914	−0·0811	−0·0563	−0·0283	−0·1071	−0·0845	−0·0372	0·0054
0·6	−0·0861	−0·0805	−0·0656	−0·0453	−0·1034	−0·0914	−0·0617	−0·0260
0·8	−0·0812	−0·0776	−0·0673	−0·0522	−0·0995	−0·0919	−0·0714	−0·0437
1·0	−0·0768	−0·0741	−0·0663	−0·0545	−0·0957	−0·0902	−0·0750	−0·0531
1·5	−0·0670	−0·0654	−0·0606	−0·0530	−0·0864	−0·0834	−0·0744	−0·0605
2·0	−0·0589	−0·0577	−0·0542	−0·0485	−0·0782	−0·0766	−0·0696	−0·0596
3	−0·0466	−0·0458	−0·0434	−0·0395	−0·0646	−0·0630	−0·0589	−0·0524
4	−0·0378	−0·0372	−0·0354	−0·0324	−0·0540	−0·0529	−0·0499	−0·0450
5	−0·0314	−0·0309	−0·0294	−0·0271	−0·0460	−0·0452	−0·0428	−0·0388
10	−0·0161	−0·0158	−0·0151	−0·0140	−0·0253	−0·0249	−0·0237	−0·0217

TABLE 5—*continued*

x/R \ θ	ϕ=45°				ϕ=60°			
	0	5°	10°	15°	0	5°	10°	15°
−10	0·0077	0·0076	0·0072	0·0067	0·0054	0·0053	0·0051	0·0047
−5	0·0162	0·0160	0·0153	0·0142	0·0116	0·0114	0·0110	0·0102
−4	0·0200	0·0198	0·0189	0·0176	0·0145	0·0143	0·0137	0·0128
−3	0·0257	0·0253	0·0242	0·0225	0·0188	0·0185	0·0178	0·0166
−2	0·0343	0·0338	0·0322	0·0296	0·0254	0·0251	0·0240	0·0222
−1·5	0·0404	0·0397	0·0376	0·0343	0·0303	0·0298	0·0284	0·0261
−1·0	0·0483	0·0472	0·0441	0·0392	0·0368	0·0361	0·0340	0·0307
−0·8	0·0522	0·0508	0·0468	0·0406	0·0401	0·0392	0·0365	0·0323
−0·6	0·0567	0·0547	0·0491	0·0408	0·0439	0·0426	0·0389	0·0334
−0·4	0·0623	0·0588	0·0496	0·0378	0·0489	0·0465	0·0405	0·0327
−0·2	0·0704	0·0603	0·0420	0·0270	0·0561	0·0498	0·0378	0·0275
−0·1	0·0772	0·0526	0·0311	0·0206	0·0628	0·0470	0·0322	0·0238
−0·05	0·0831	0·0411	0·0267	0·0205	0·0689	0·0411	0·0296	0·0238
0	—	0·0353	0·0289	0·0246	—	0·0378	0·0309	0·0264
0·05	−0·1121	0·0470	0·0383	0·0325	−0·1157	0·0492	0·0378	0·0320
0·1	−0·1154	0·0367	0·0477	0·0421	−0·1202	0·0555	0·0476	0·0398
0·2	−0·1167	−0·0219	0·0423	0·0540	−0·1232	0·0206	0·0584	0·0556
0·4	−0·1151	−0·0778	−0·0122	0·0334	−0·1237	−0·0537	0·0283	0·0606
0·6	−0·1125	−0·0928	−0·0479	−0·0015	−0·1221	−0·0836	−0·0135	0·0419
0·8	−0·1094	−0·0970	−0·0655	−0·0267	−0·1200	−0·0956	−0·0420	0·0118
1·0	−0·1062	−0·0974	−0·0739	−0·0423	−0·1179	−0·1008	−0·0594	−0·0125
1·5	−0·0980	−0·0932	−0·0795	−0·0592	−0·1117	−0·1026	−0·0783	−0·0470
2·0	−0·0901	−0·0868	−0·0774	−0·0628	−0·1050	−0·0991	−0·0826	−0·0603
3	−0·0763	−0·0743	−0·0685	−0·0597	−0·0923	−0·0889	−0·0791	−0·0648
4	−0·0654	−0·0639	−0·0597	−0·0528	−0·0816	−0·0792	−0·0723	−0·0617
5	−0·0568	−0·0557	−0·0523	−0·0468	−0·0726	−0·0708	−0·0655	−0·0570
10	−0·0328	−0·0323	−0·0306	−0·0279	−0·0452	−0·0444	−0·0418	−0·0377

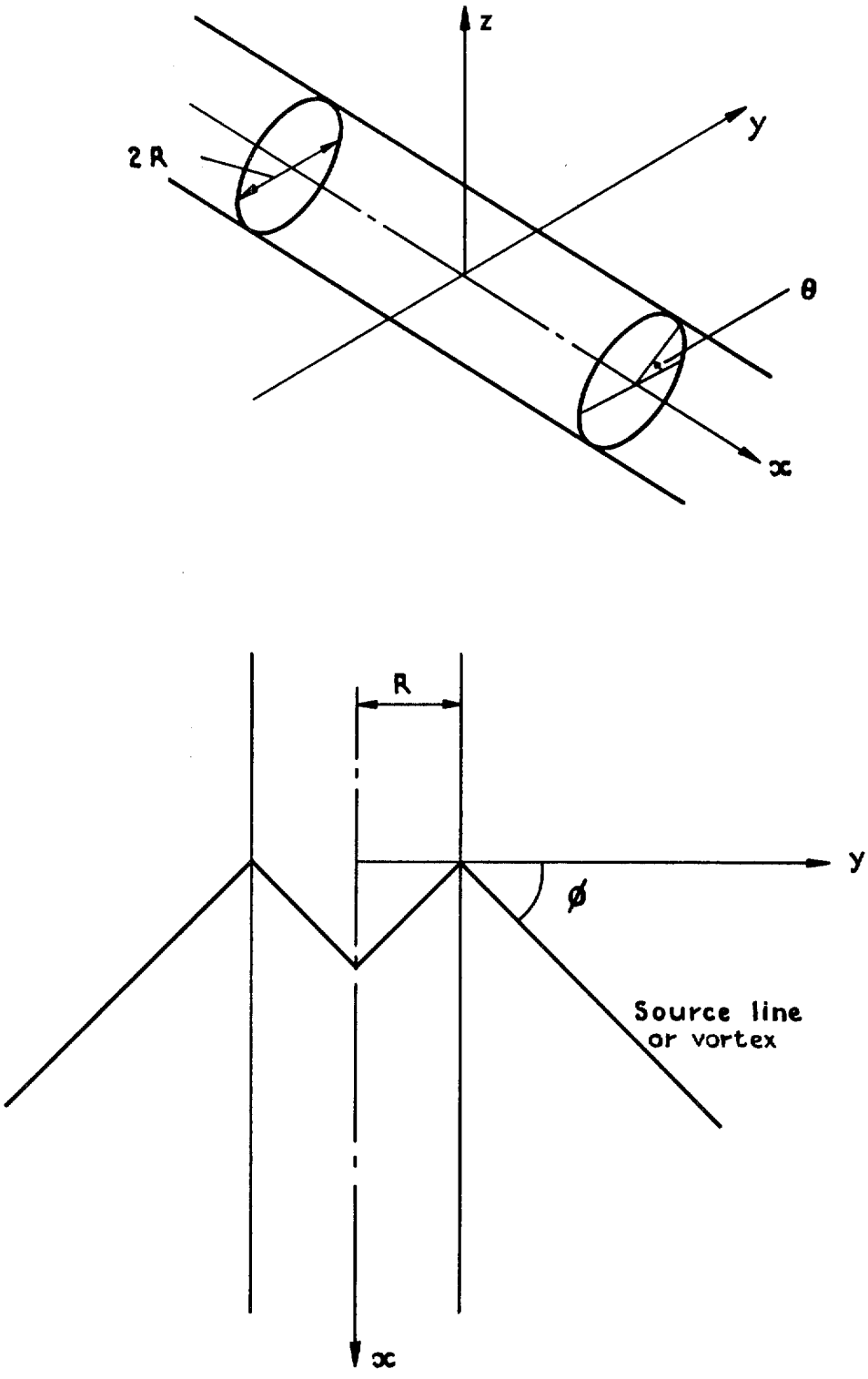

Fig. 1. Notation.

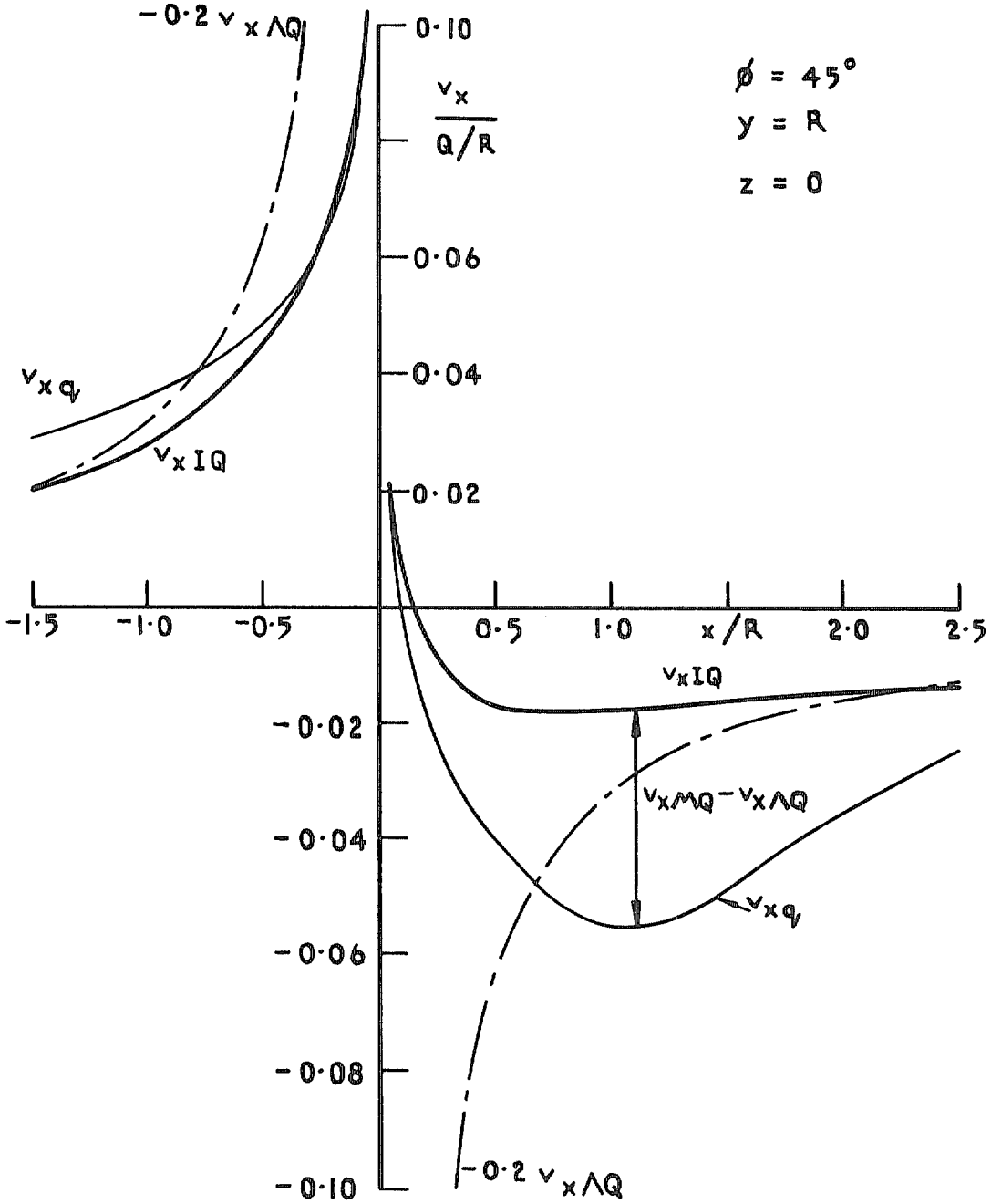

Fig. 2. Additional streamwise velocity in the wing–body junction.

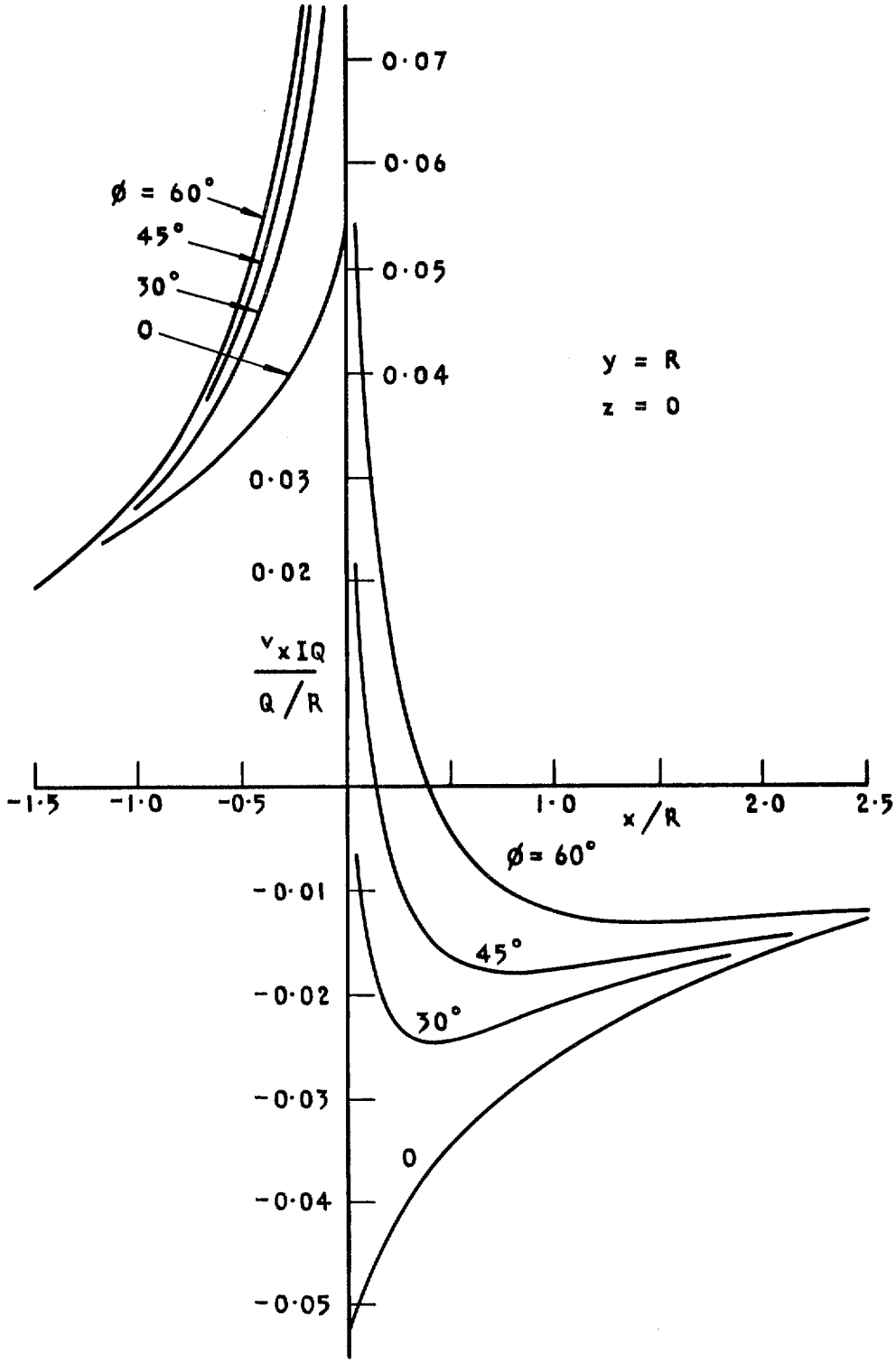

Fig. 3. Additional streamwise velocity in the wing–body junction.

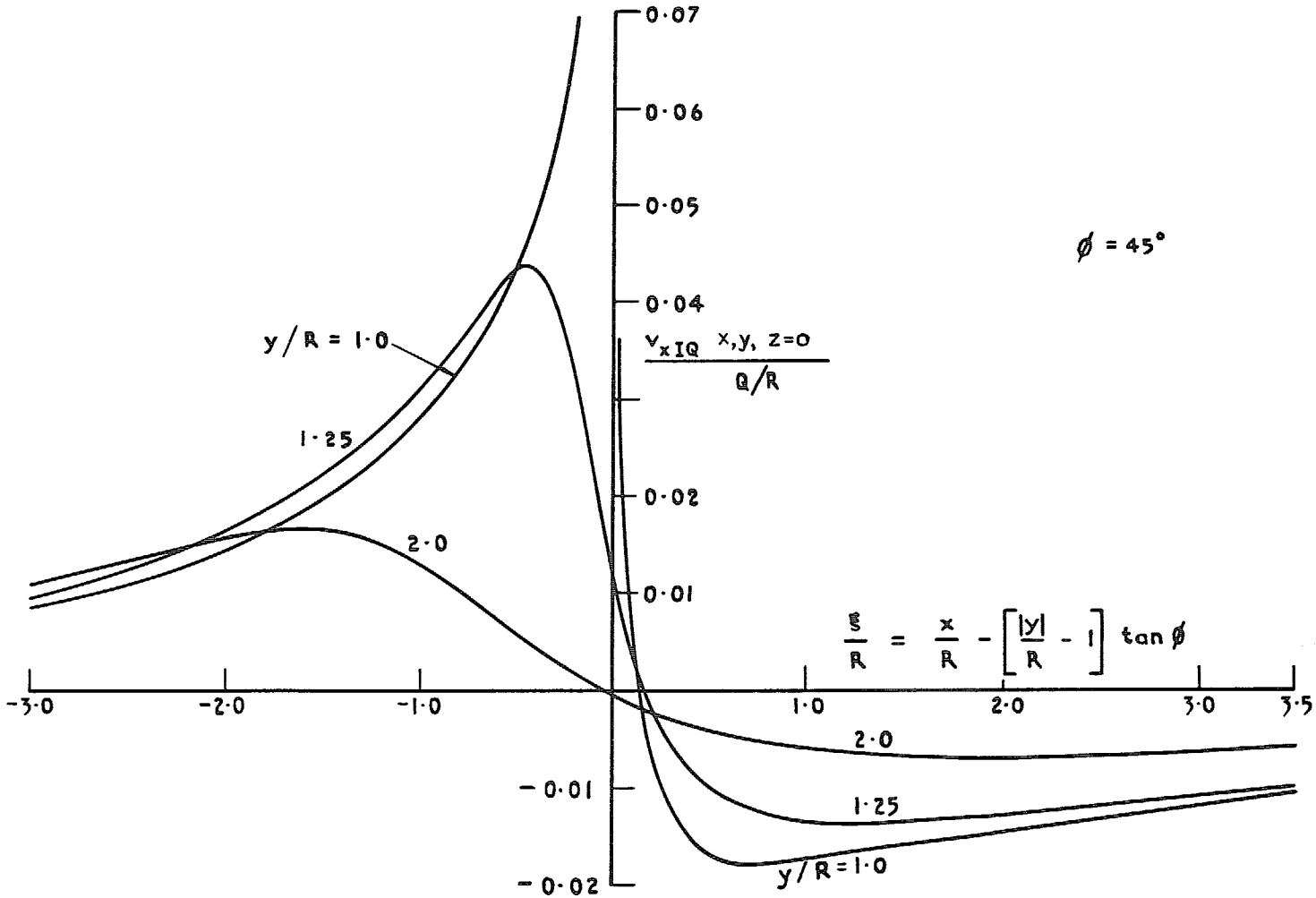

Fig. 4. Additional streamwise velocity in the plane $z = 0$.

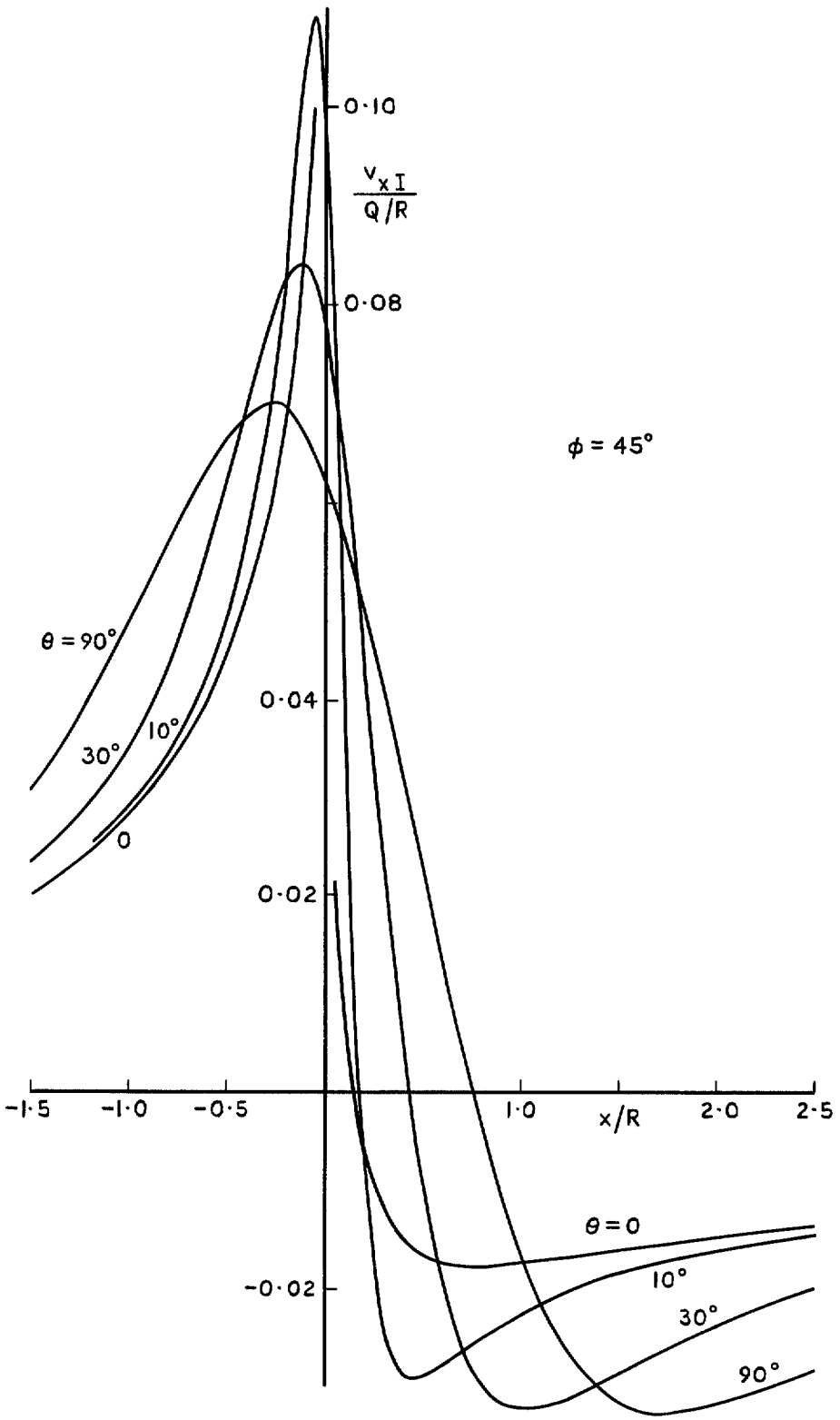

Fig. 5. Interference velocity on fuselage.

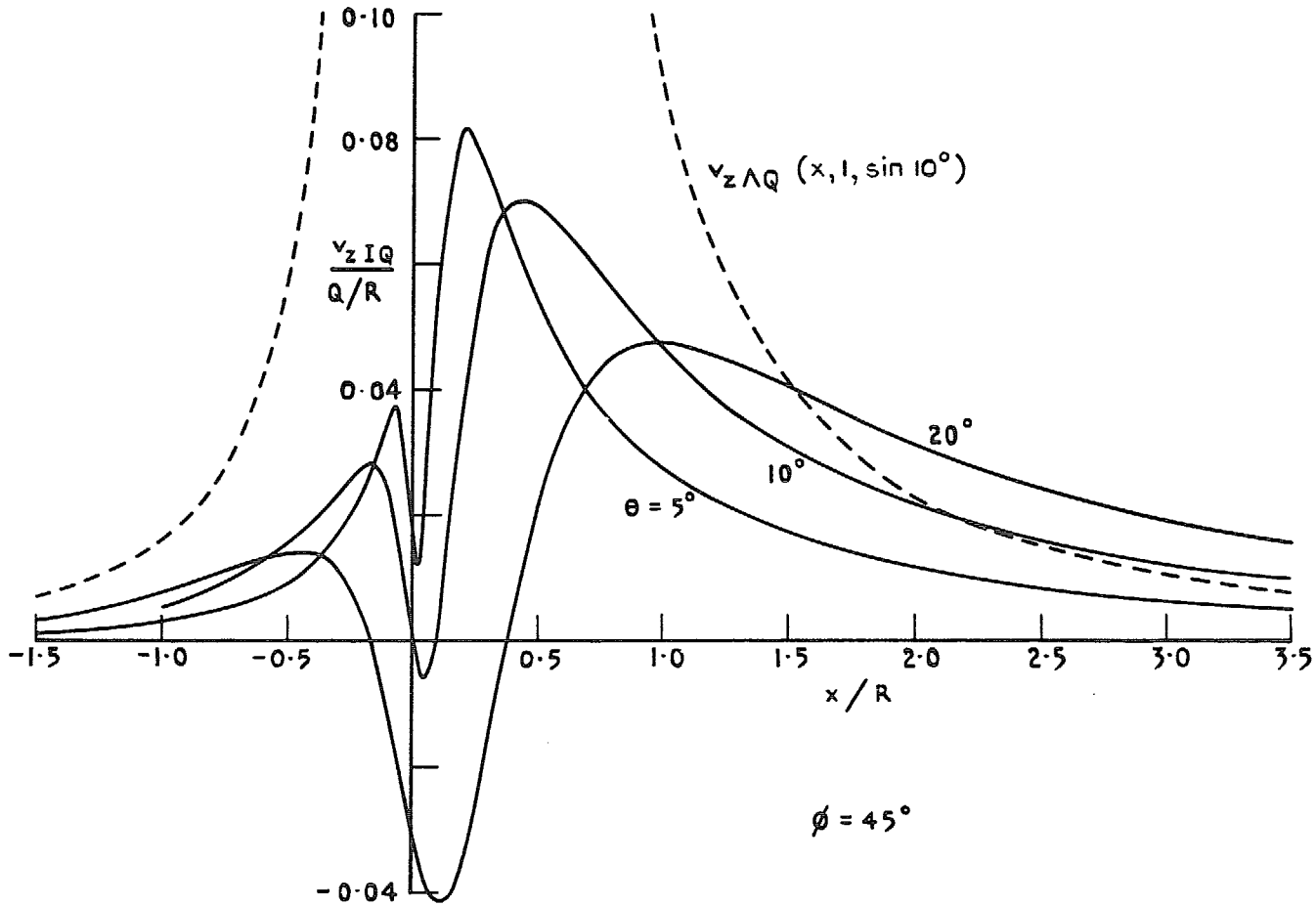

Fig. 6. z-component of the interference velocity at the fuselage.

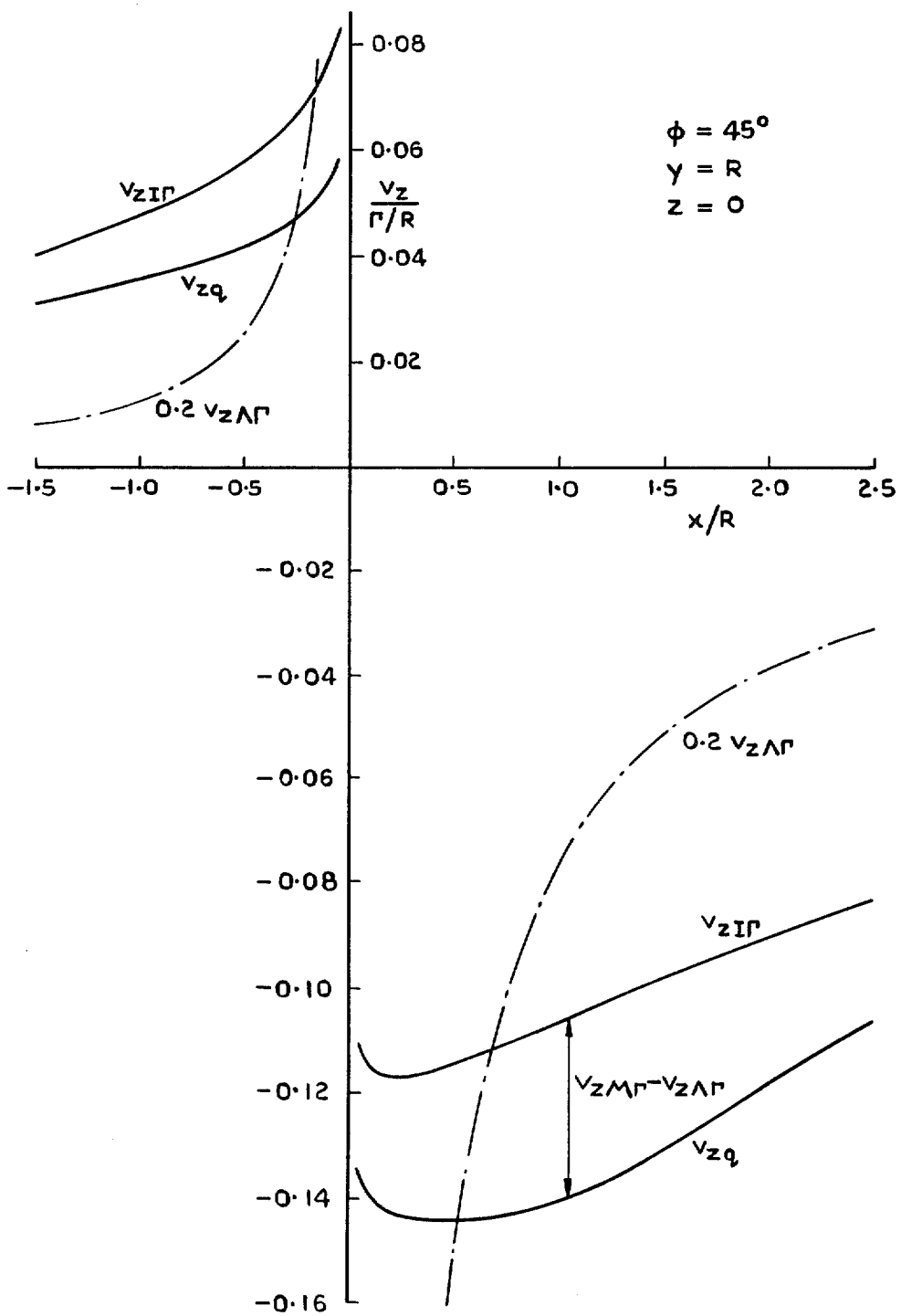

Fig. 7. Additional downwash in the wing–body junction.

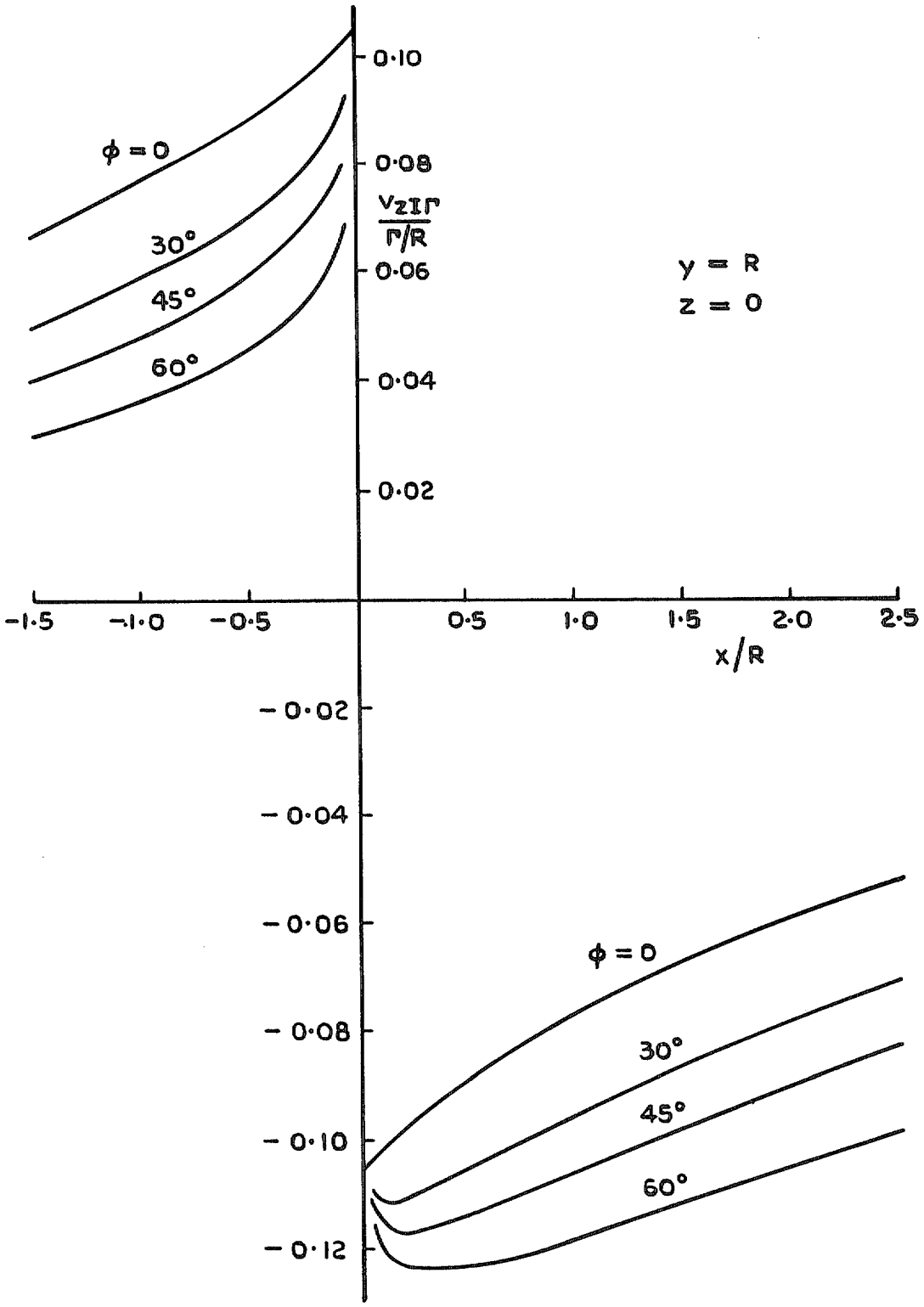

Fig. 8. Additional downwash in the wing–body junction.

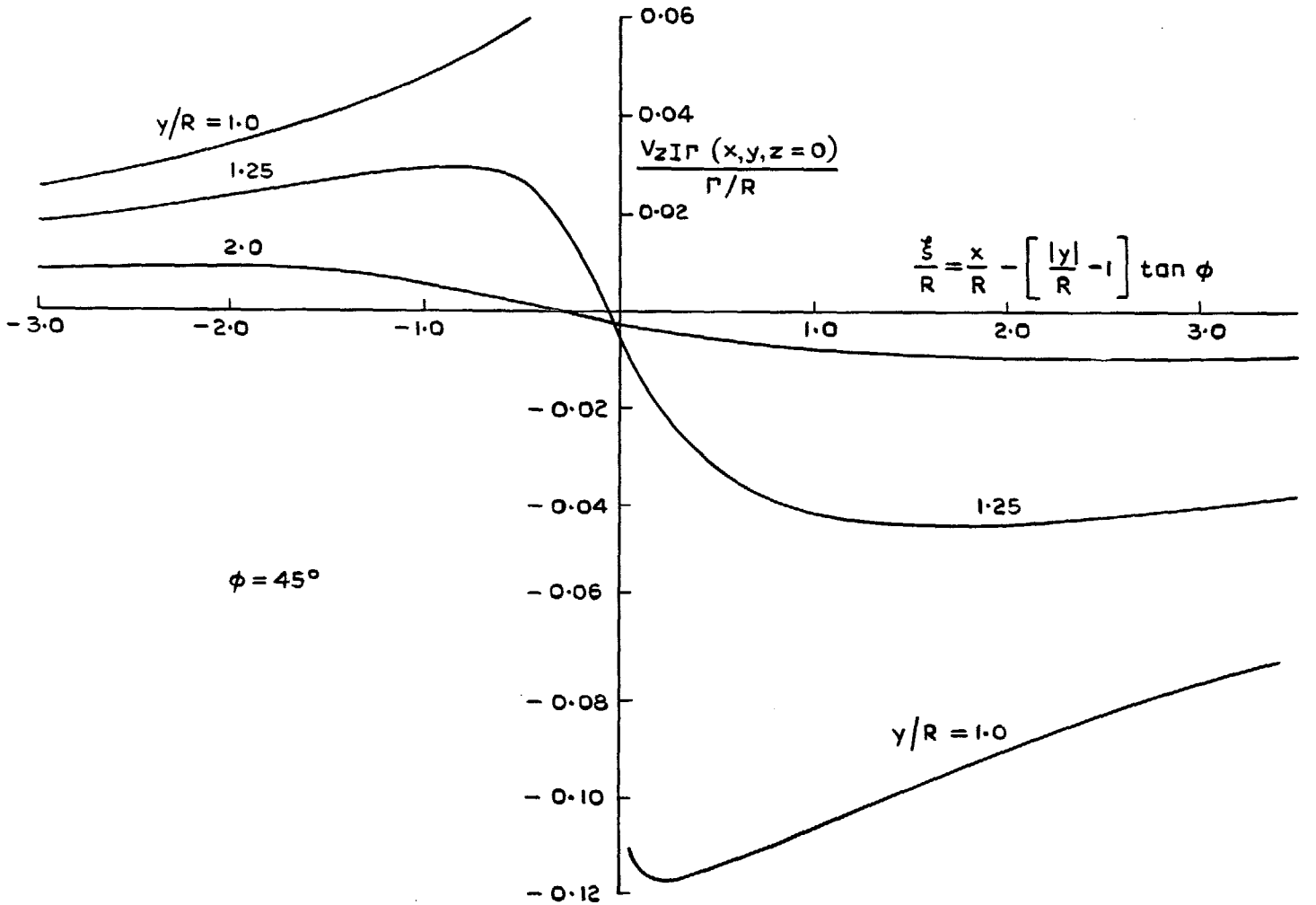

Fig. 9. Additional downwash in the plane $z = 0$.

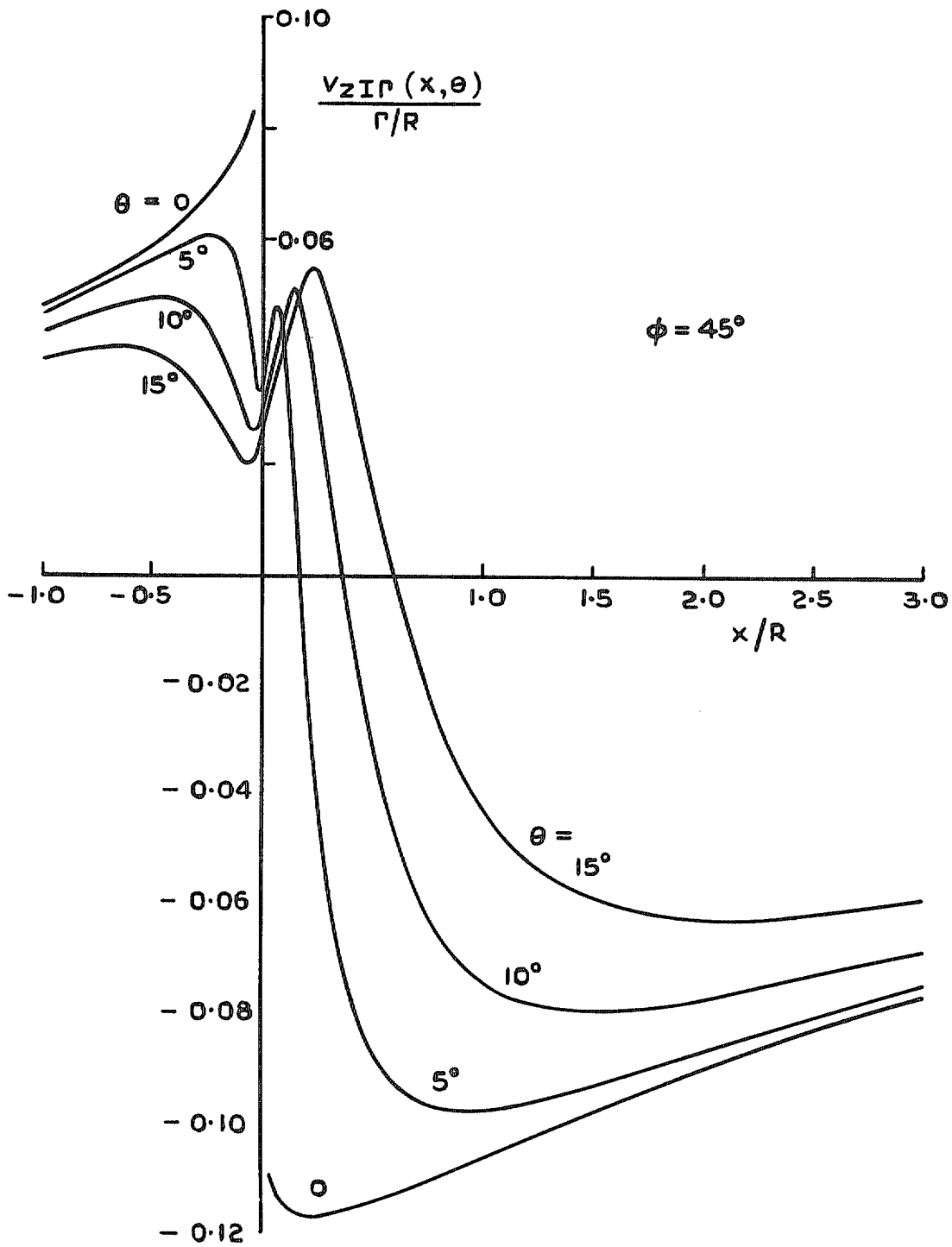

Fig. 10. Additional downwash on the fuselage.

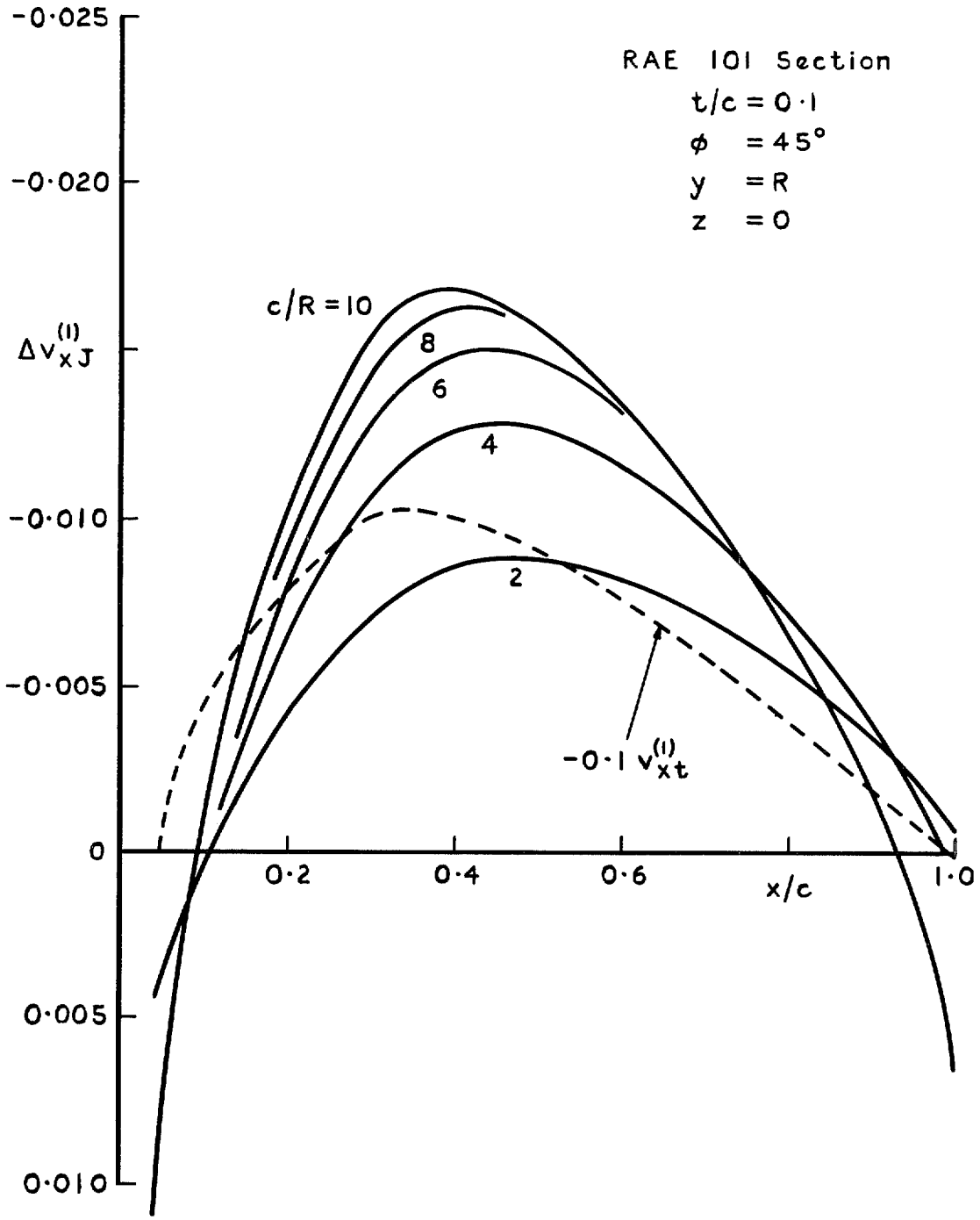

Fig. 11. Interference velocity in the wing–body junction according to first-order theory.

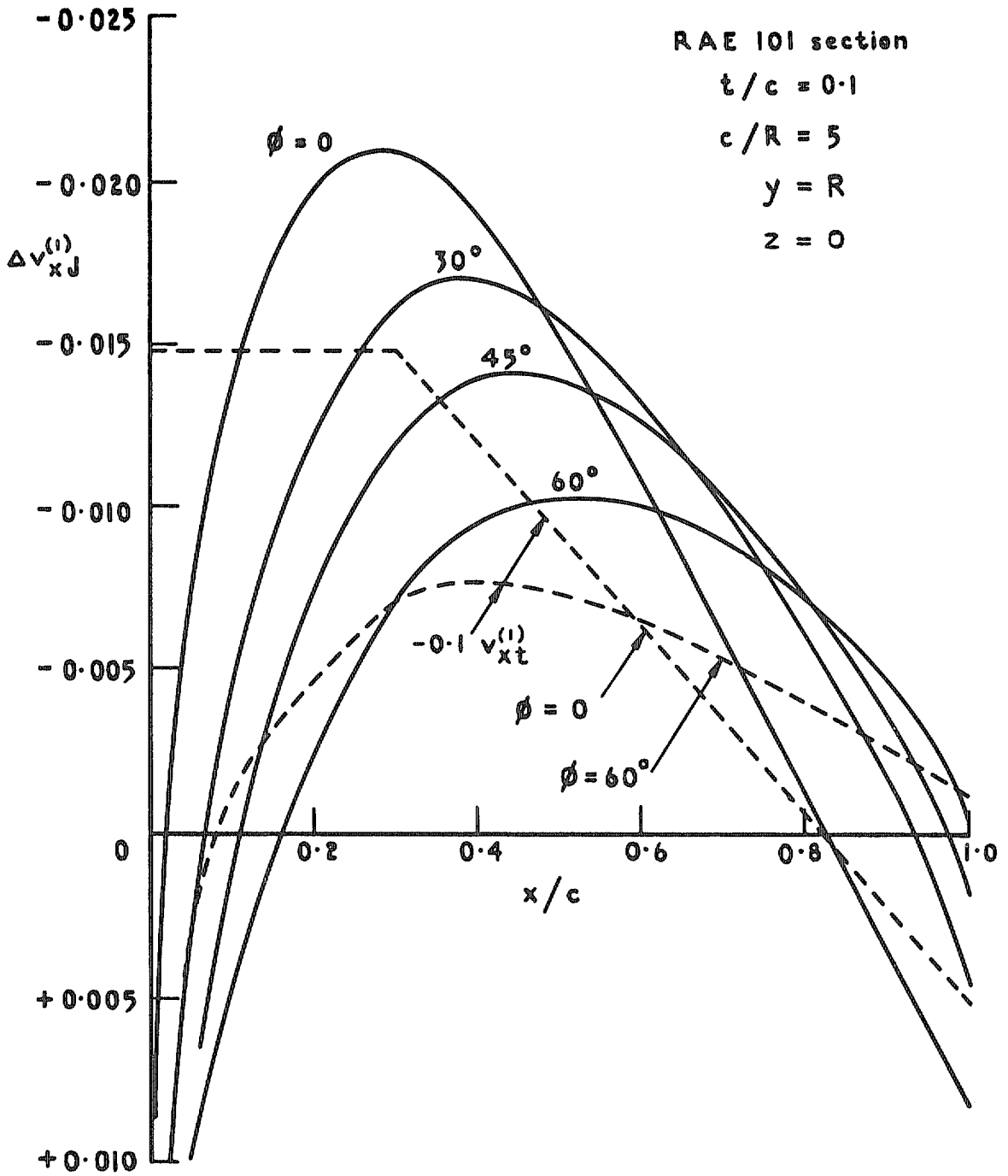

Fig. 12. Interference velocity in the wing–body junction according to first-order theory.

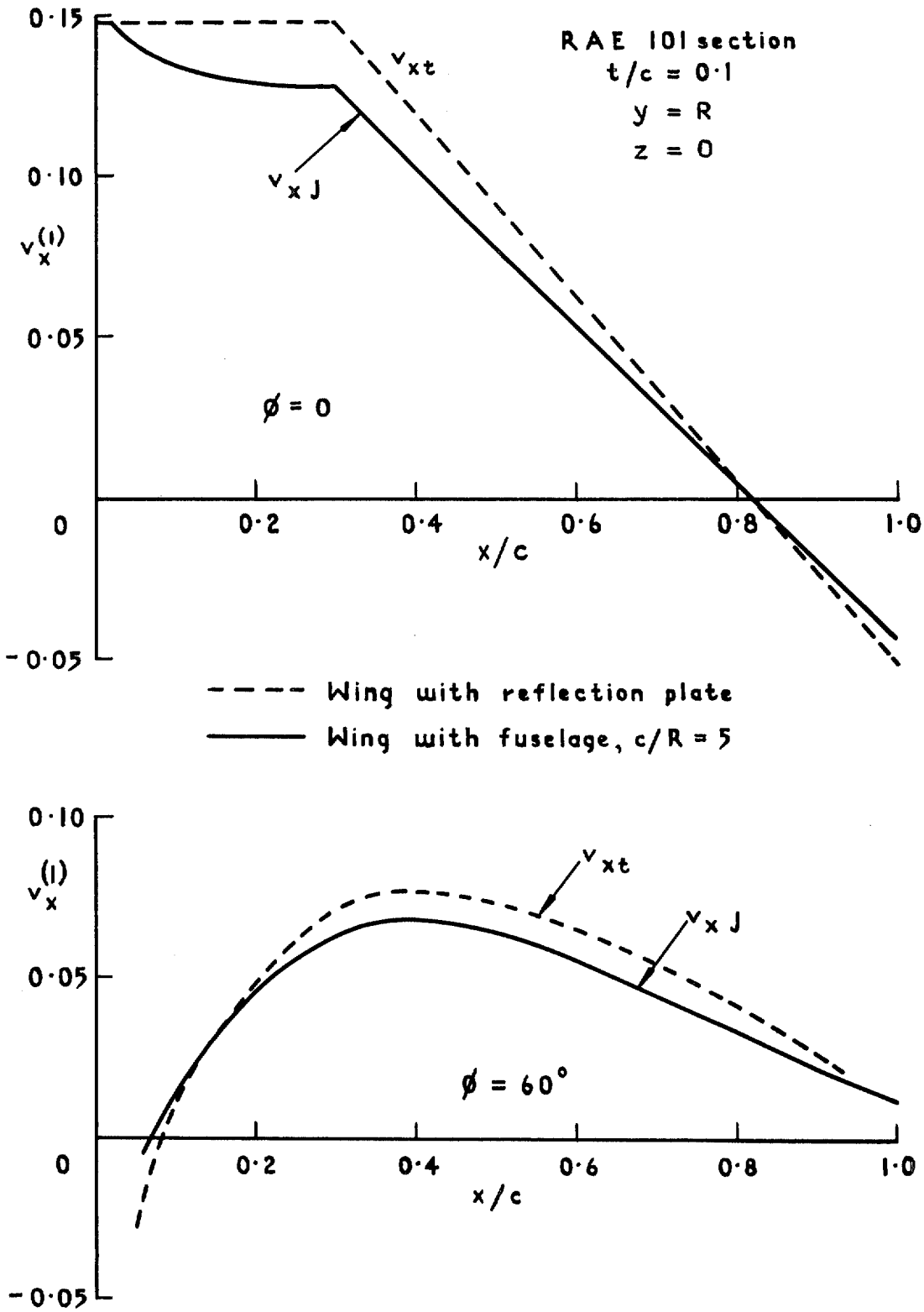

Fig. 13. Velocity in wing–body junction.

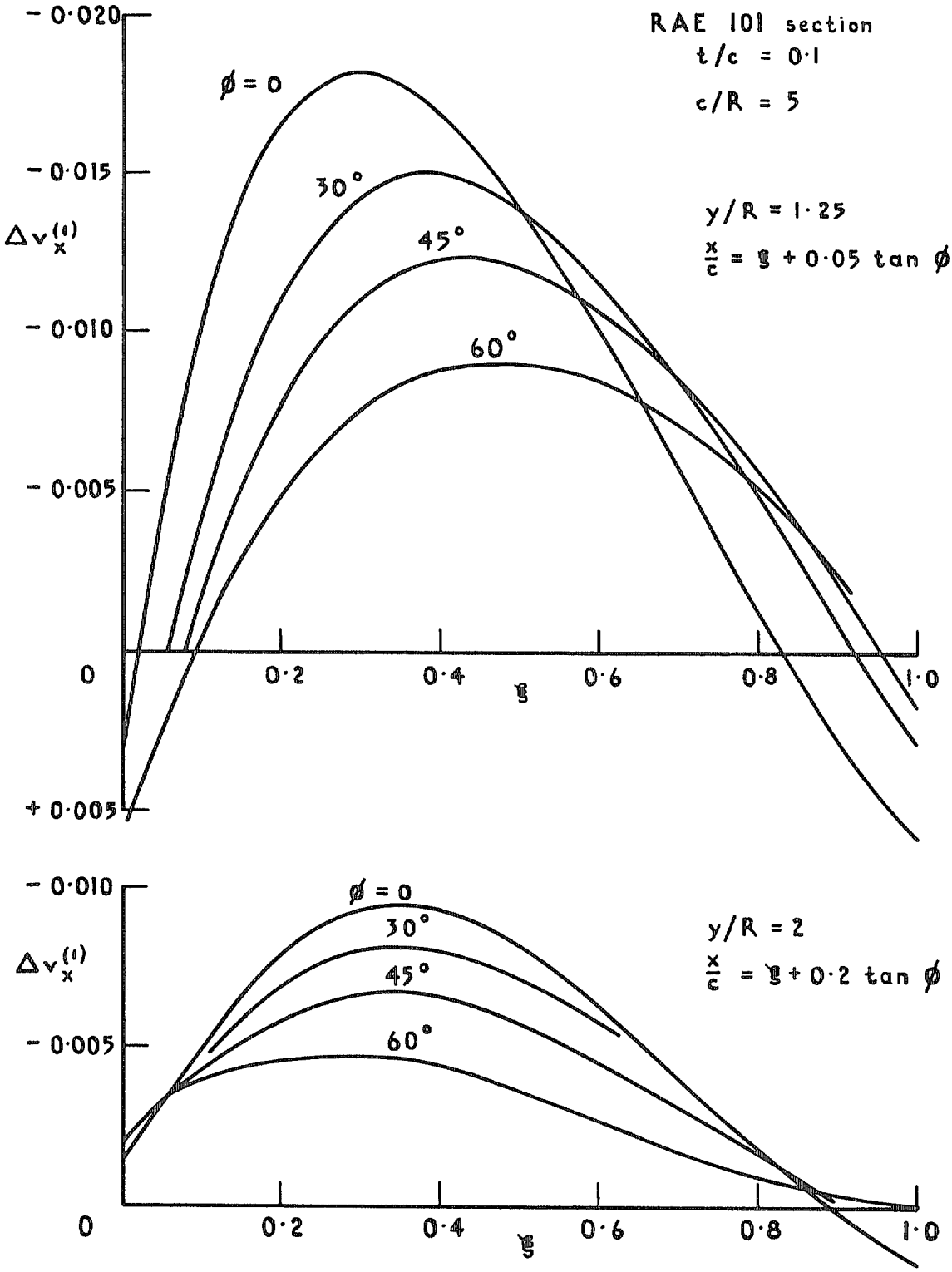

Fig. 14. Interference velocity in the plane of the wing.

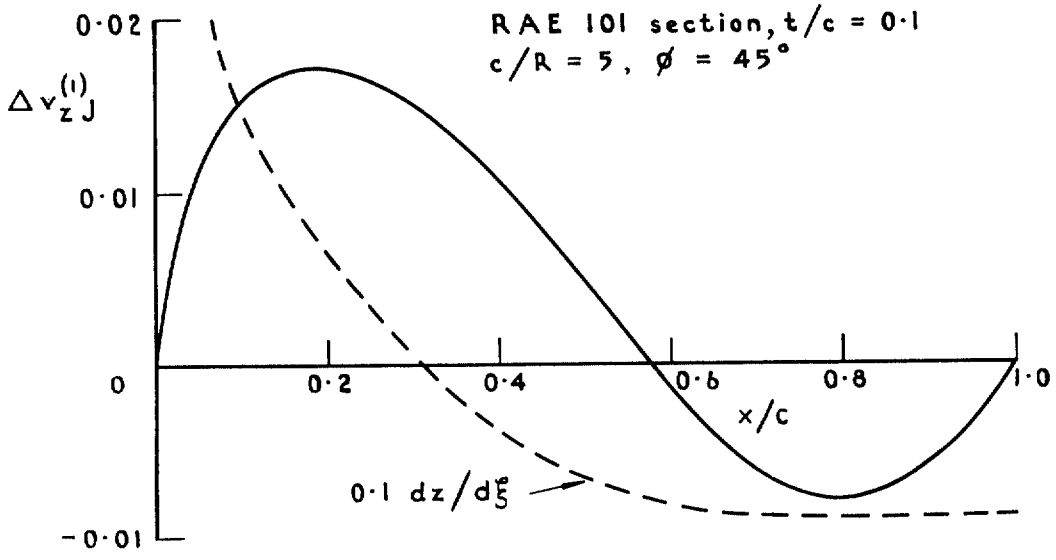

Fig. 15. Interference velocity $\Delta v_z(x, y_J, z_t)$ in the wing–body junction.

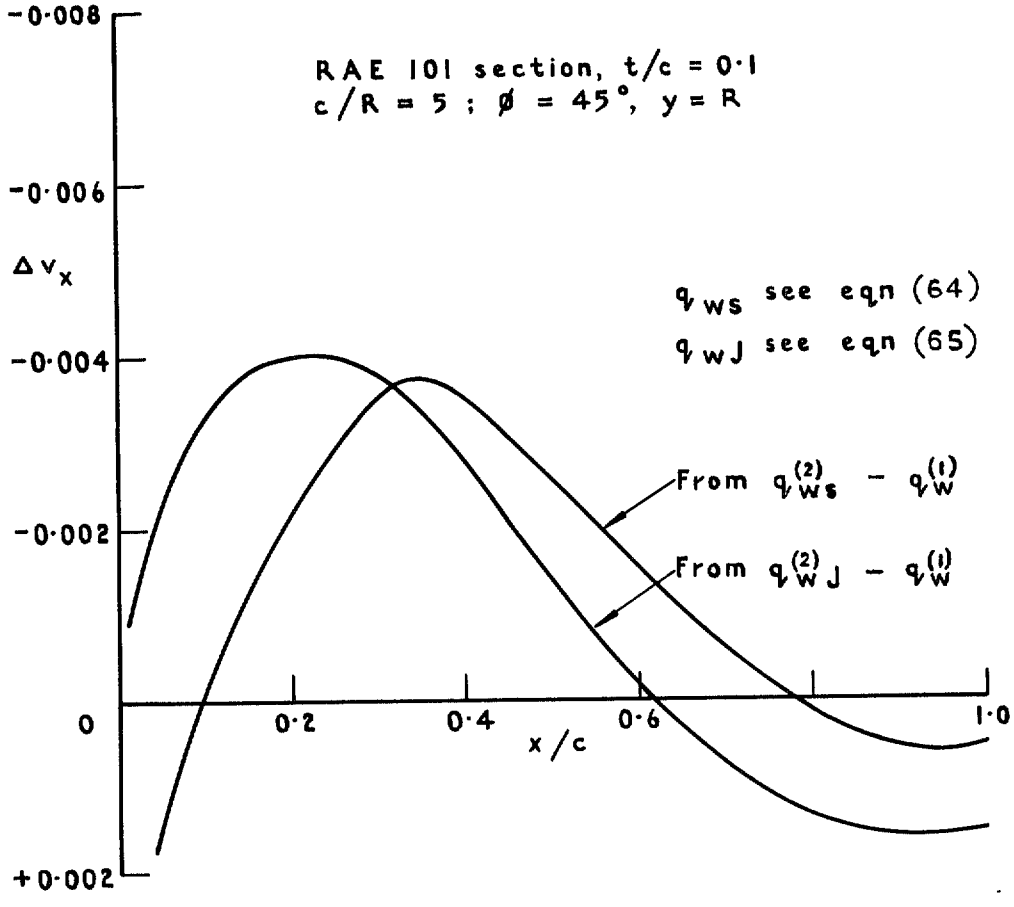

Fig. 16. Change of interference velocity in the wing–body junction ($z = 0$) due to $q_w^{(2)} - q_w^{(1)}$.

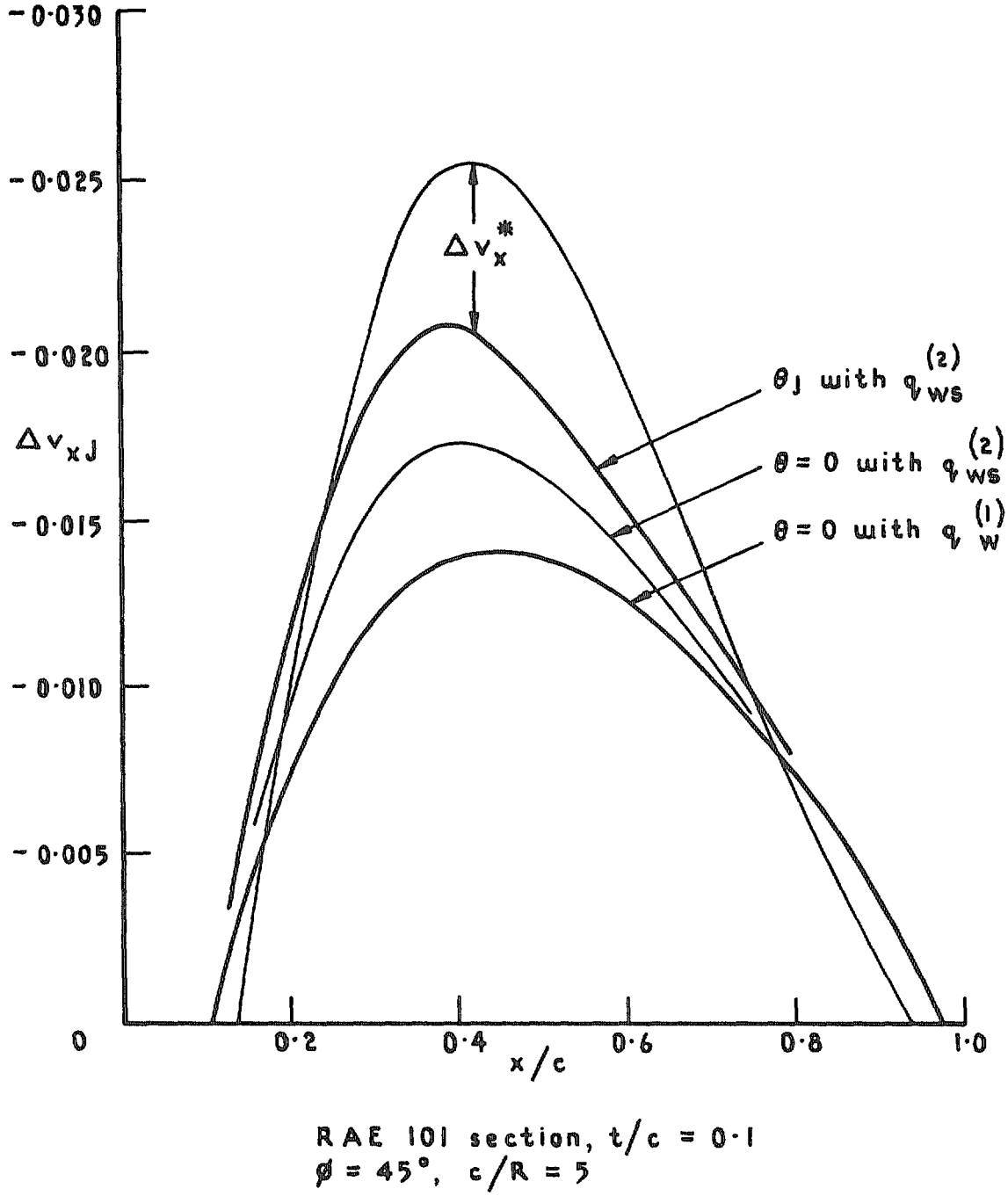

Fig. 17. Interference velocity in the wing–body junction.

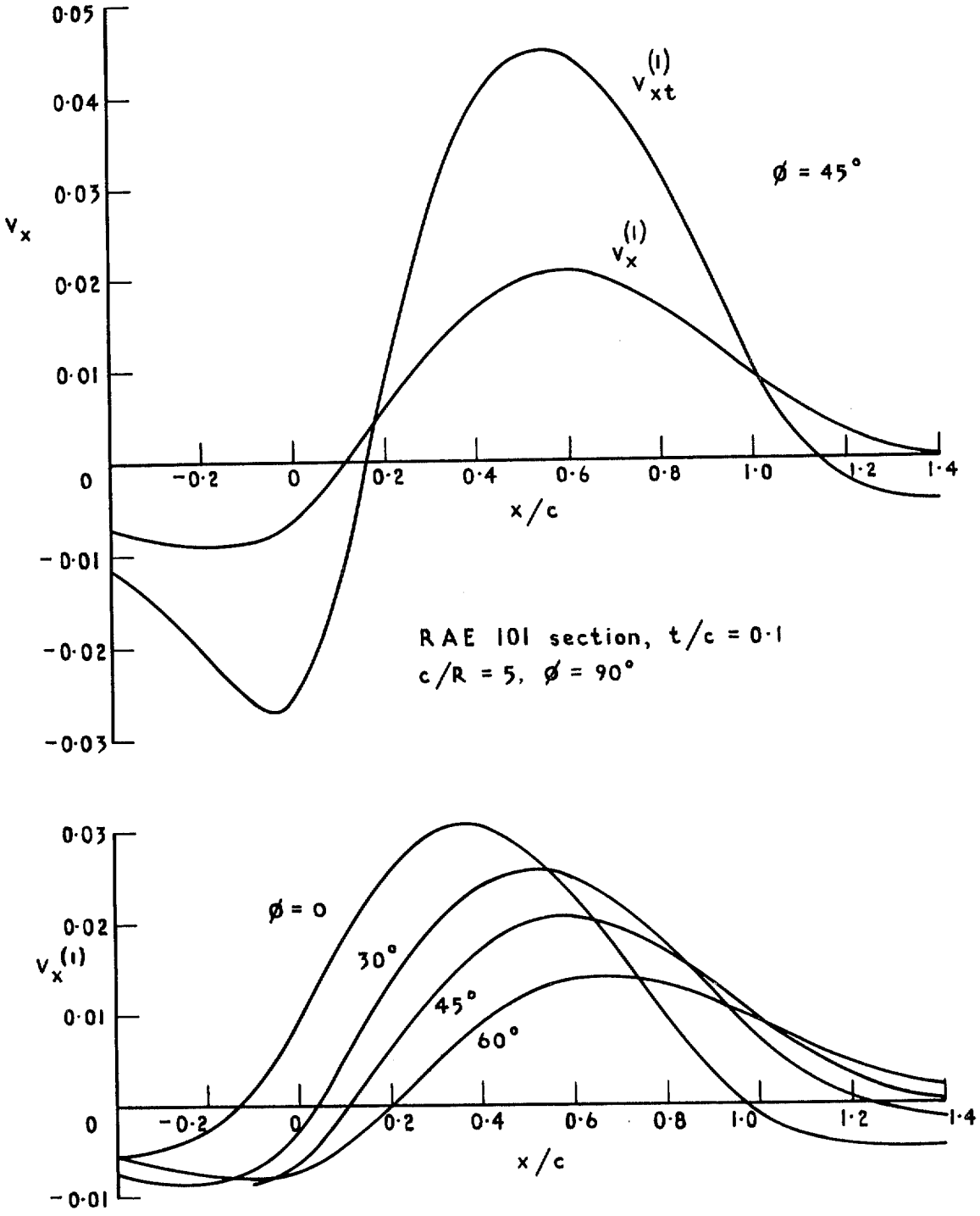

Fig. 18. Velocity at the top of the fuselage.

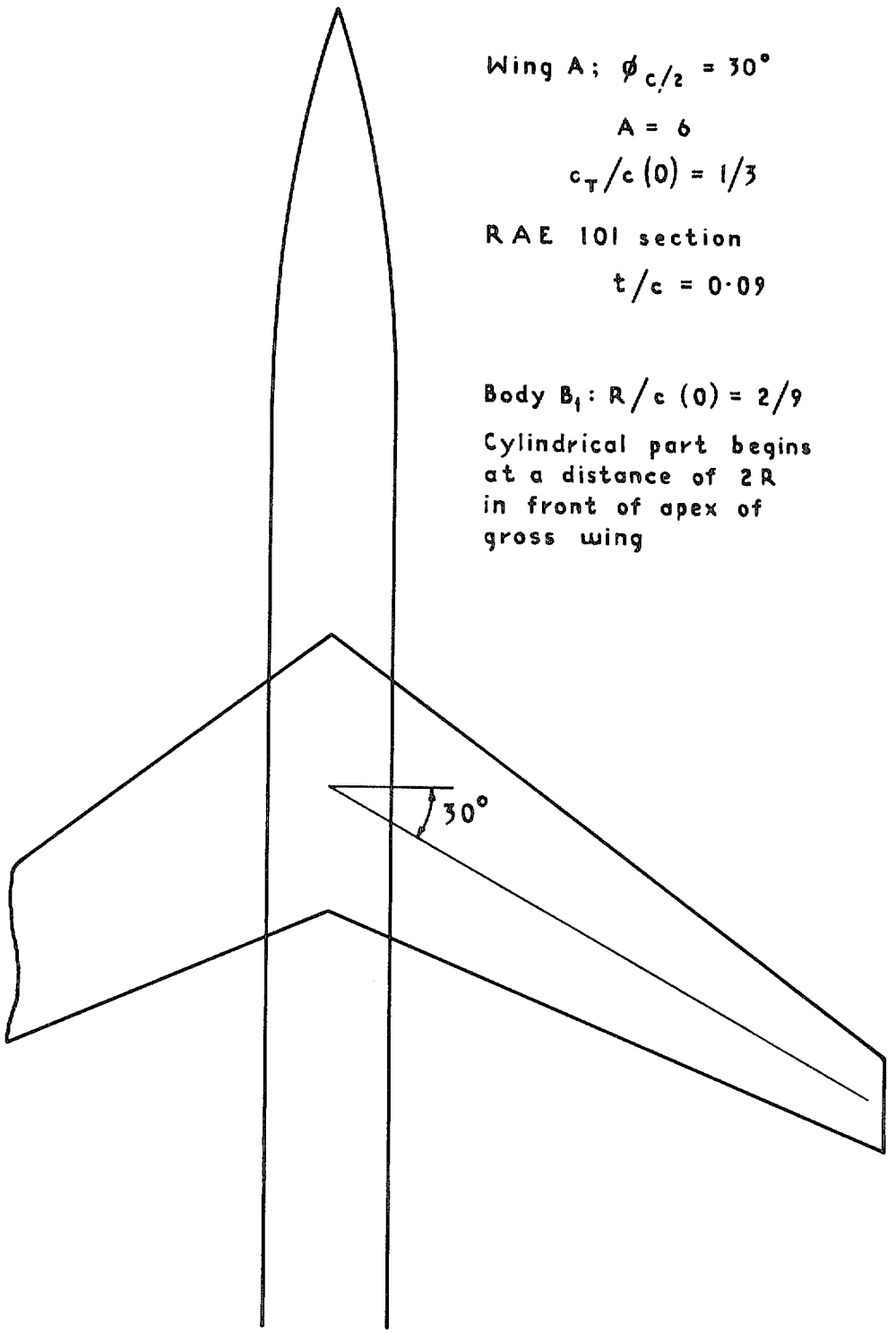

Fig. 19. Geometry of wing fuselage combination AB_1.

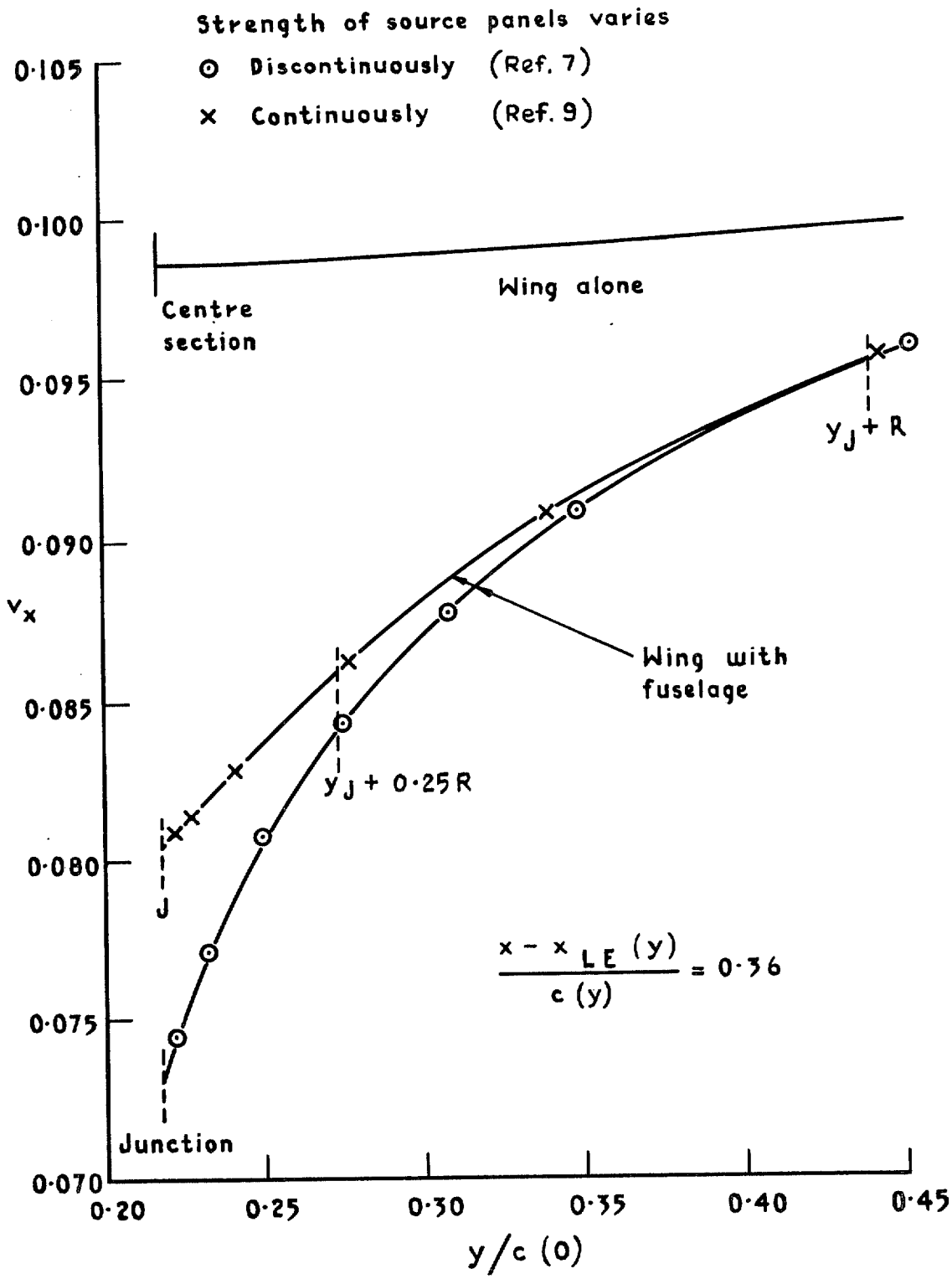

Fig. 20. Streamwise velocity component on the wing–fuselage configuration AB_1 computed by two different panel methods.

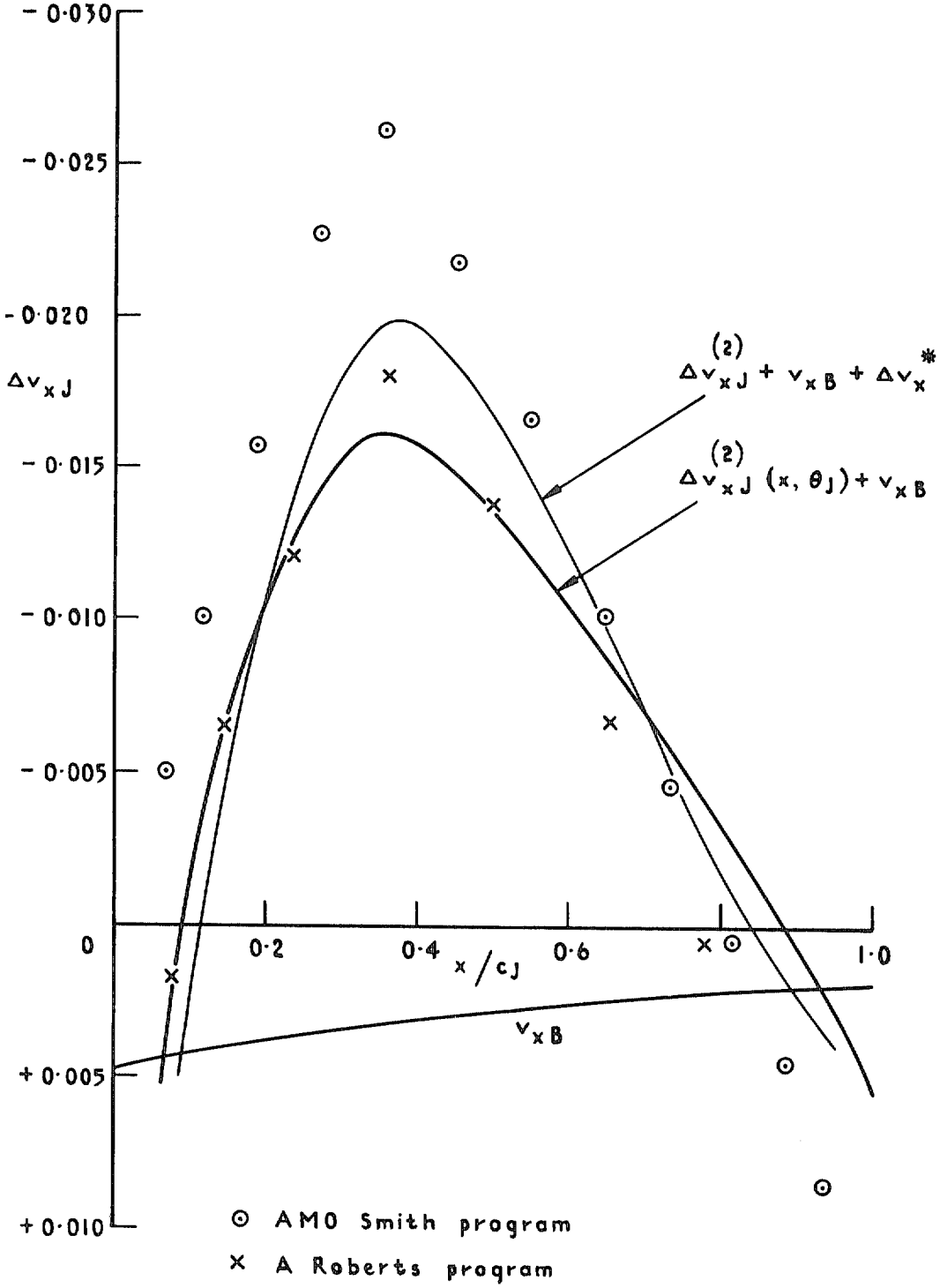

Fig. 21. Interference velocity in the wing–body junction for the configuration AB_1.

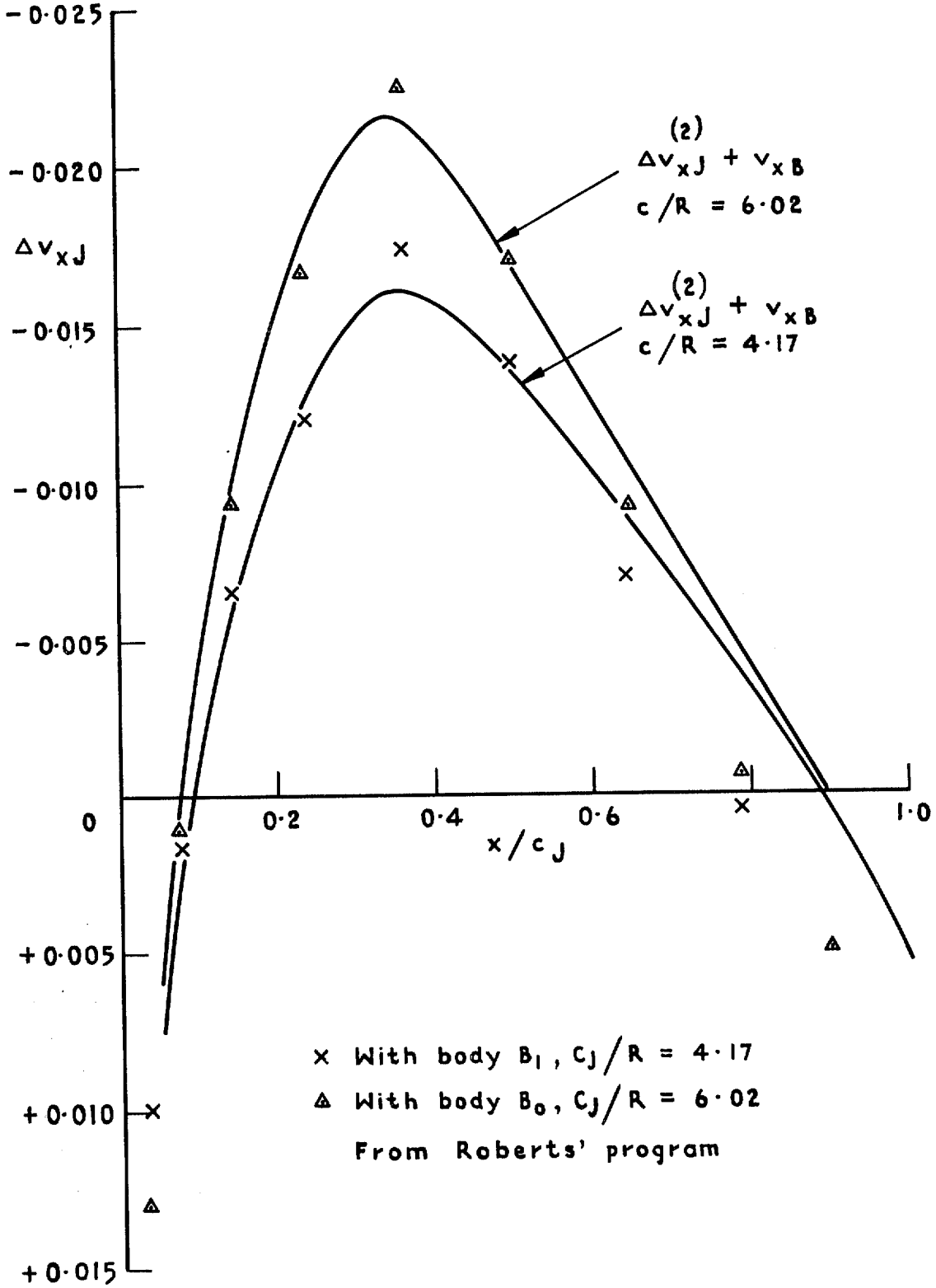

Fig. 22. Interference velocity in the wing–body junction.

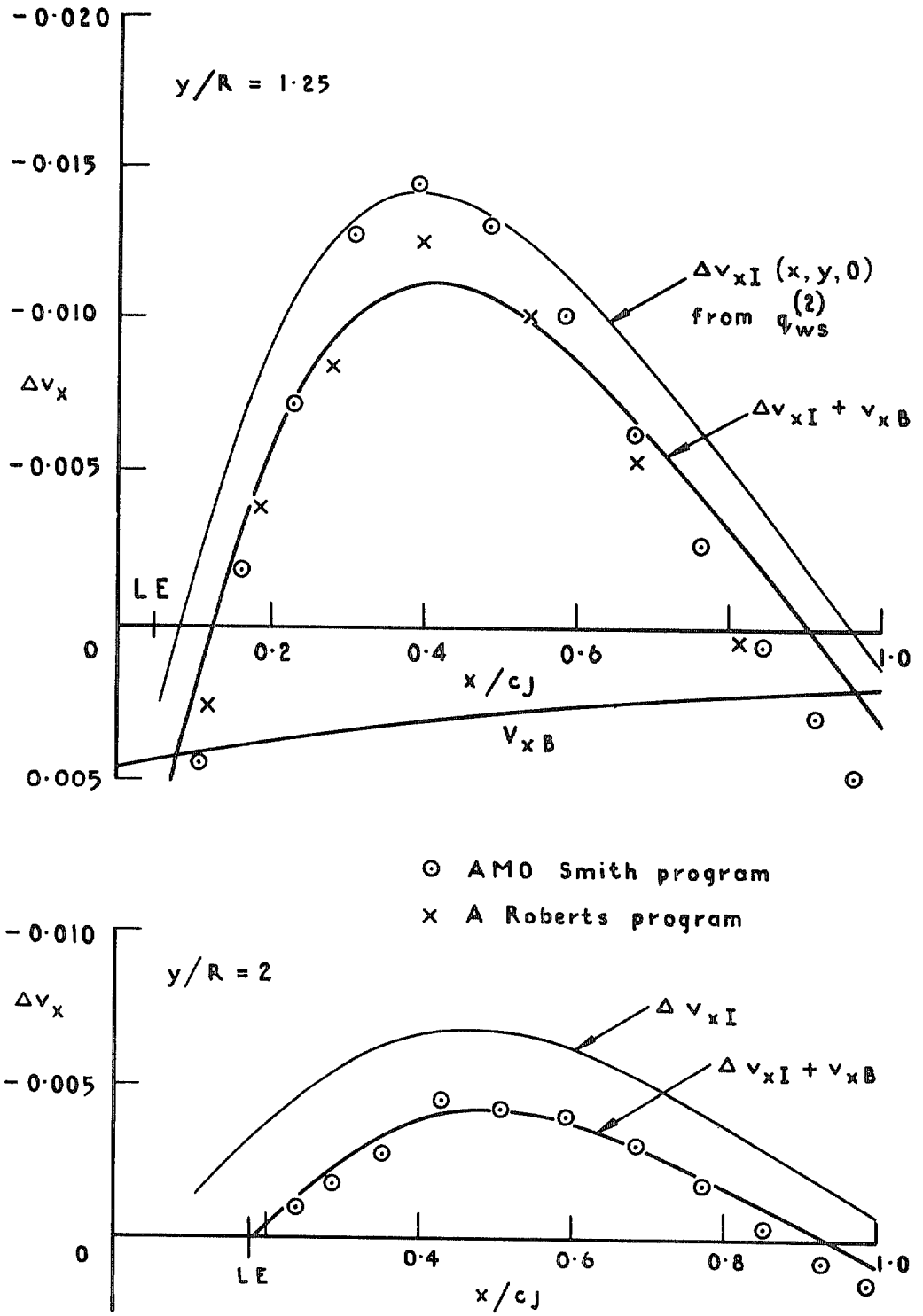

Fig. 23. Interference velocity on wing A with fuselage B_1.

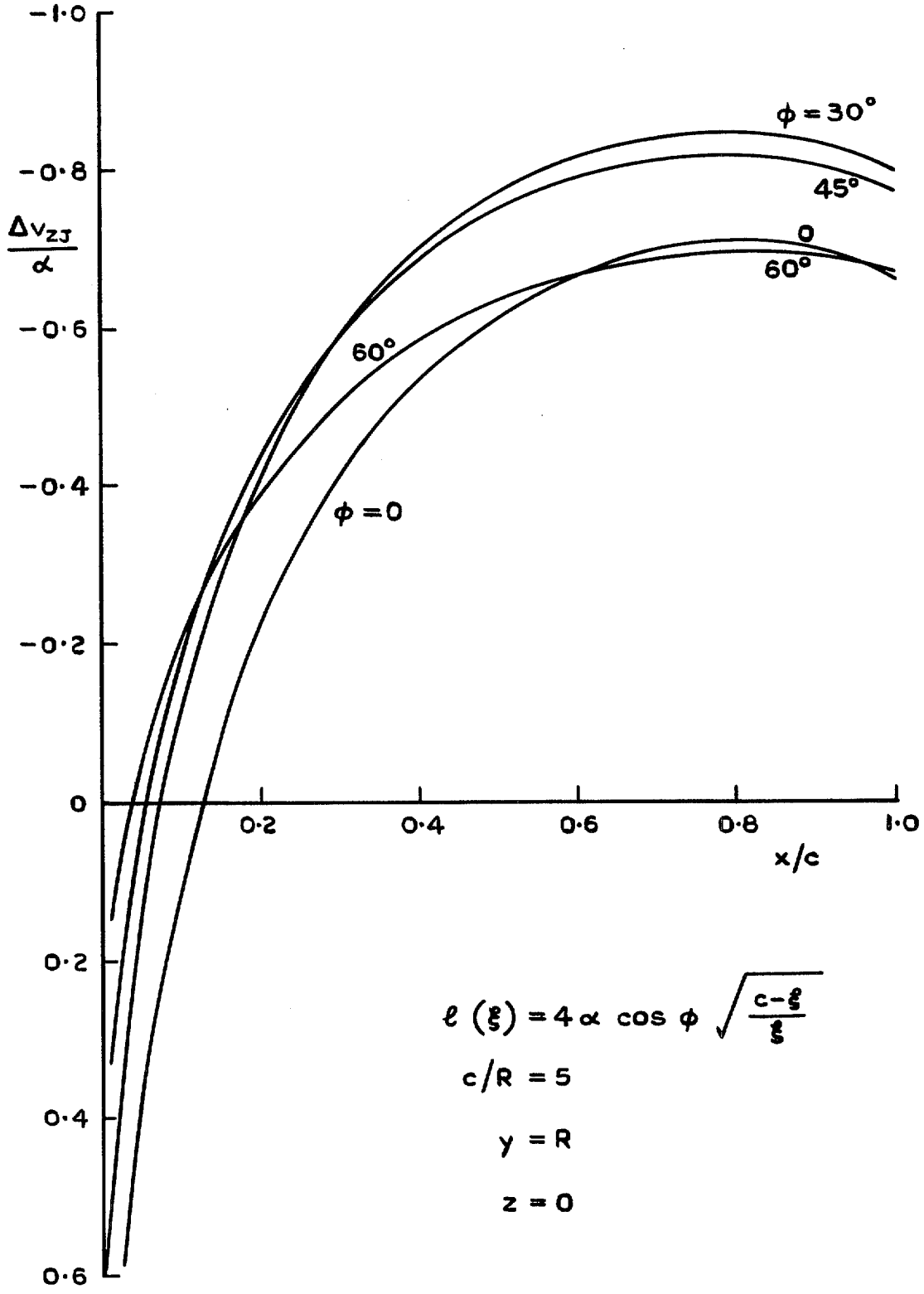

Fig. 24. Additional downwash in the wing–body junction.

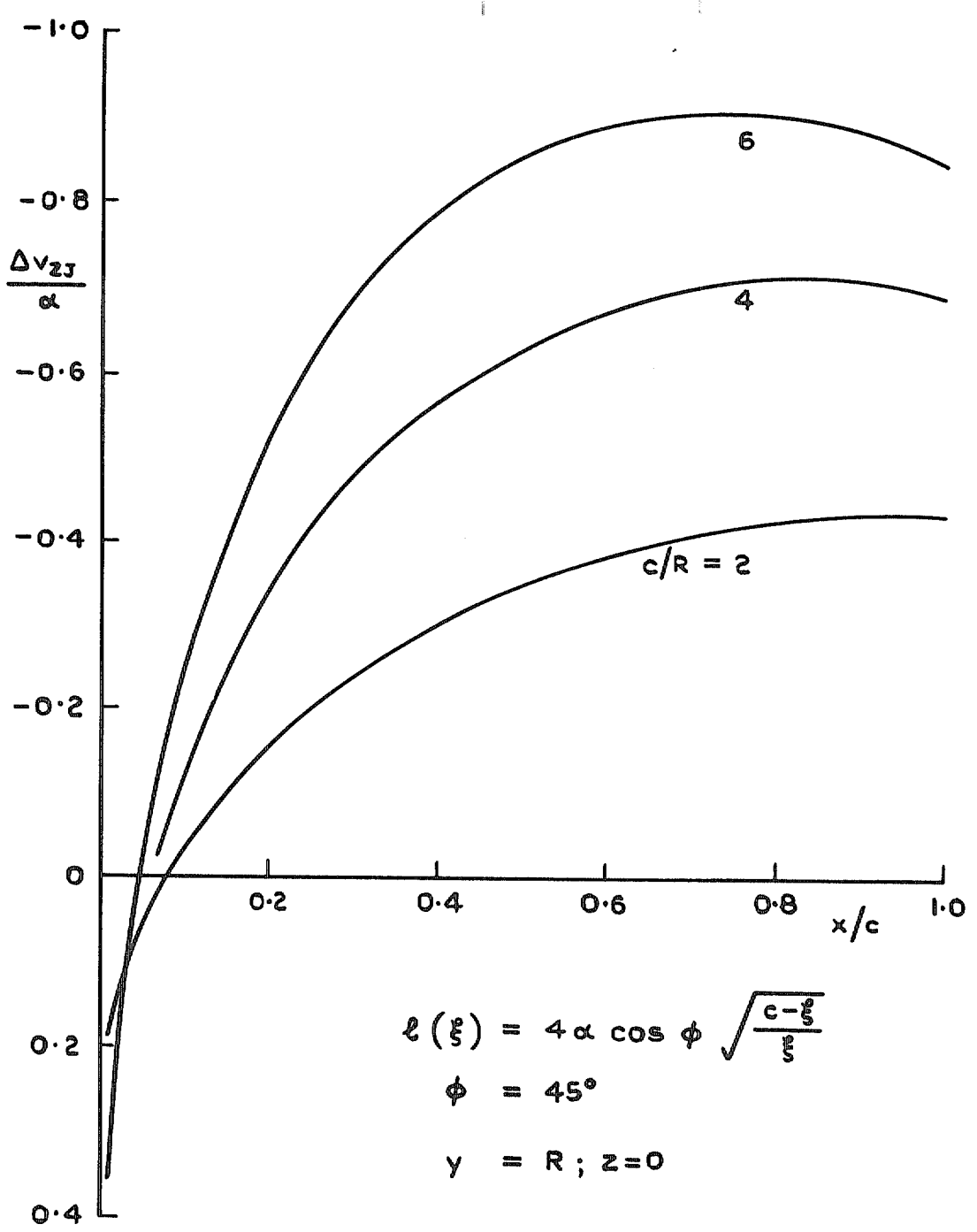

Fig. 25. Additional downwash in the wing–body junction.

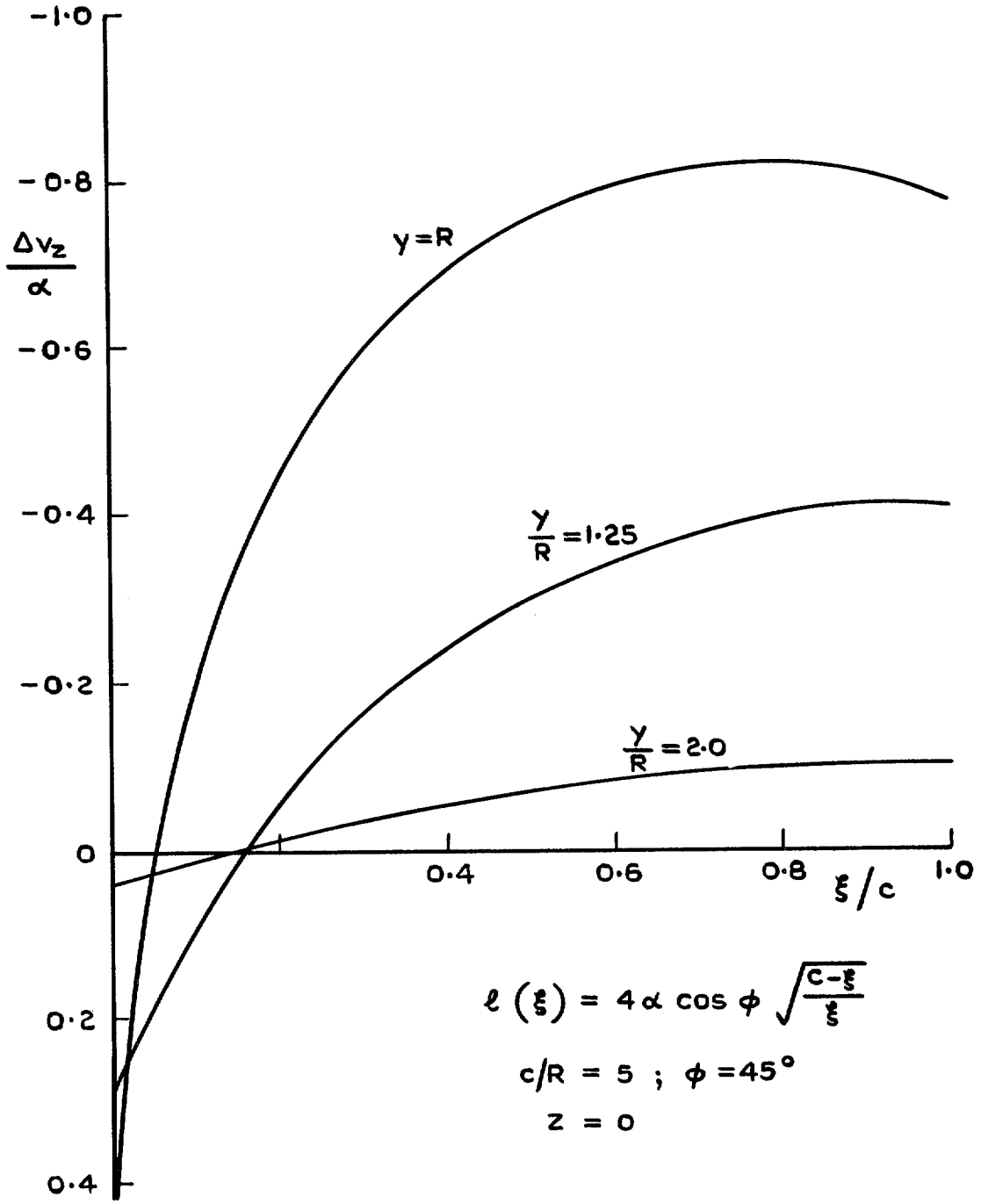

Fig. 26. Additional downwash in the wing plane.

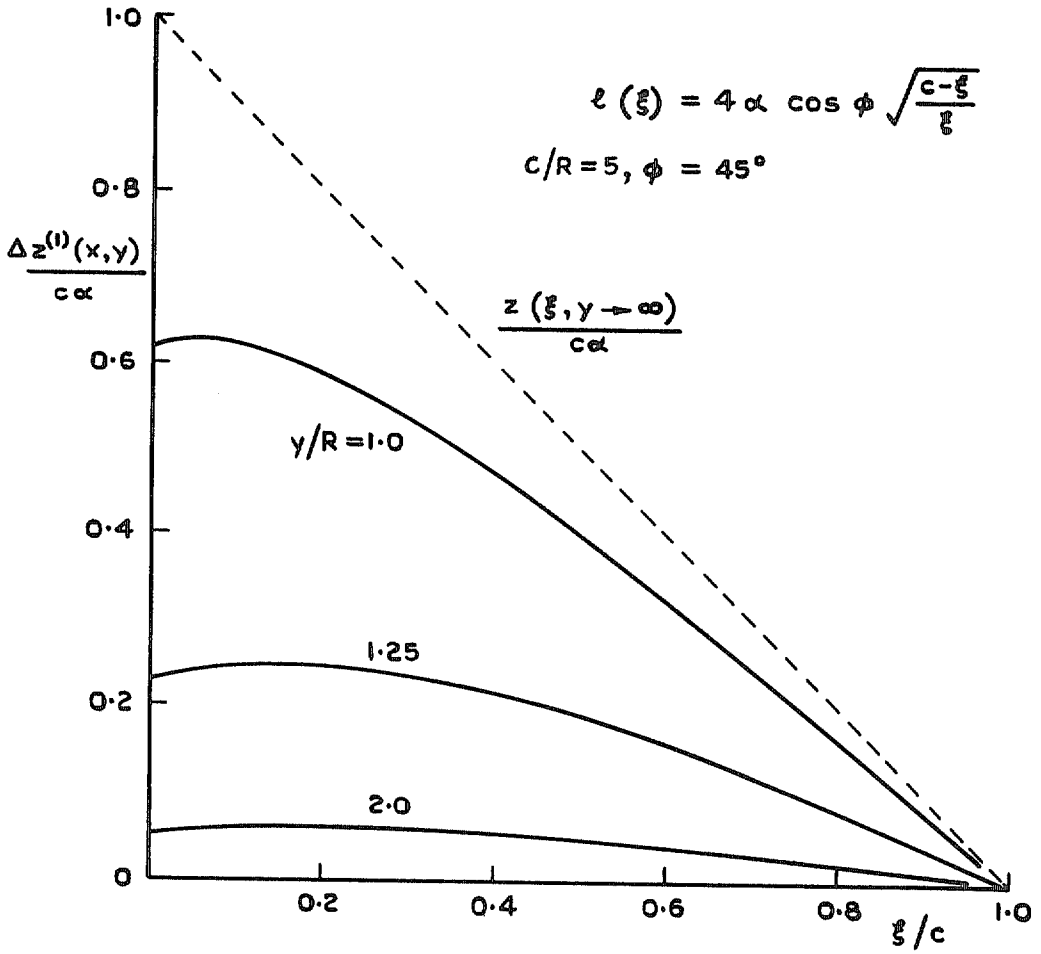

Fig. 27. Additional wing warp.

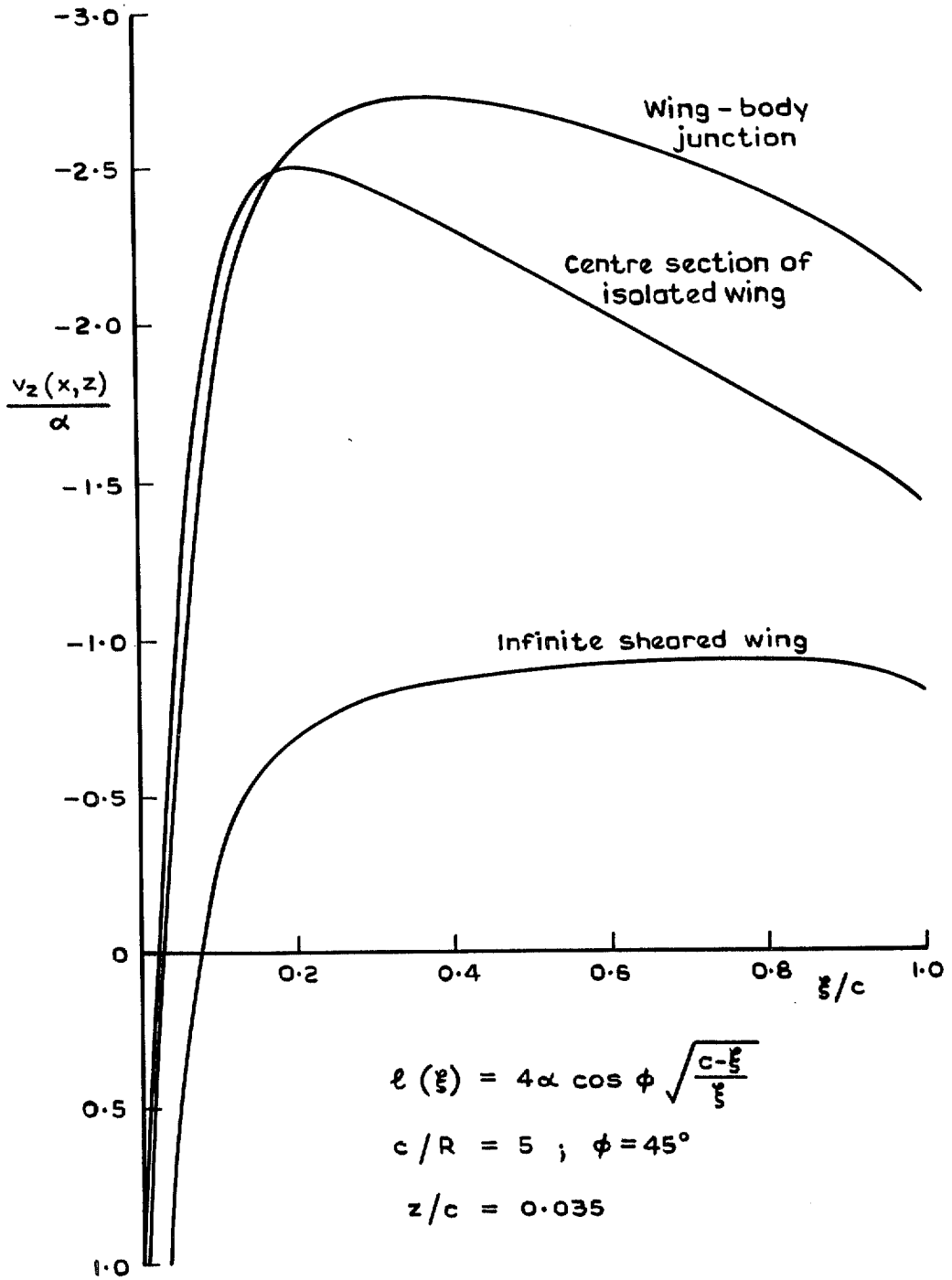

Fig. 28. Downwash distributions at various spanwise stations.

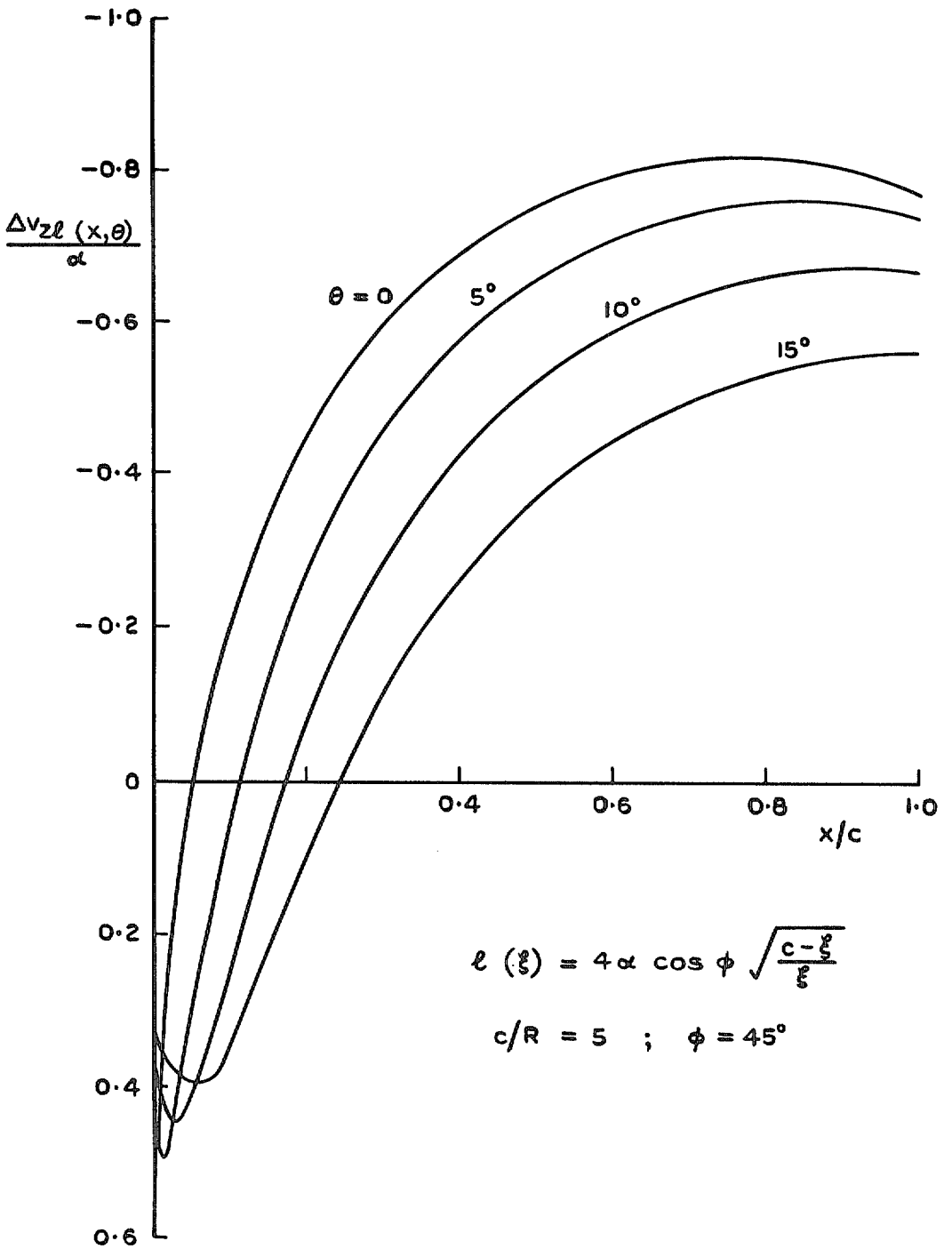

Fig. 29. Downwash distributions in the wing–body junction.

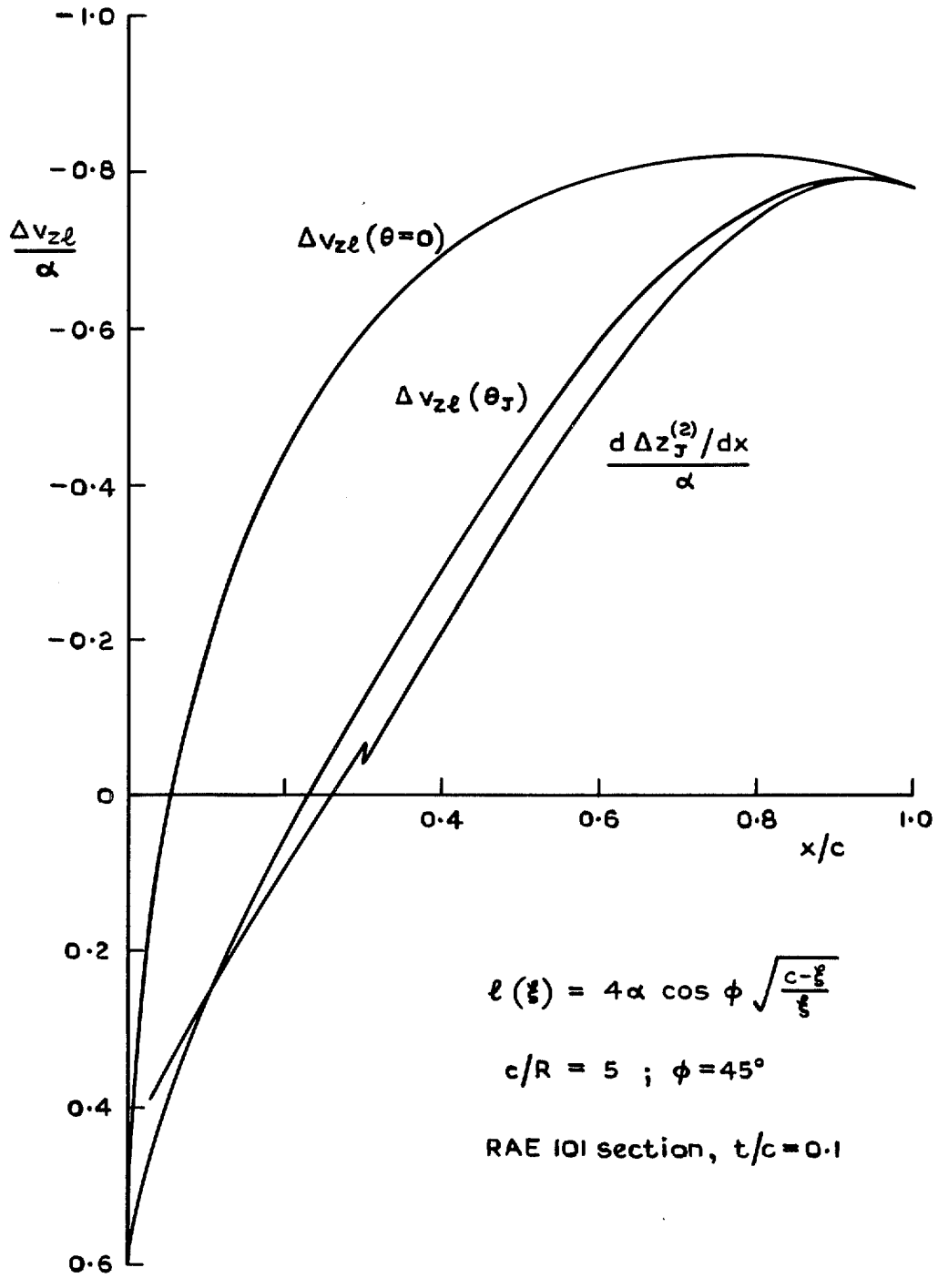

Fig. 30. Downwash distributions in the wing–body junction.

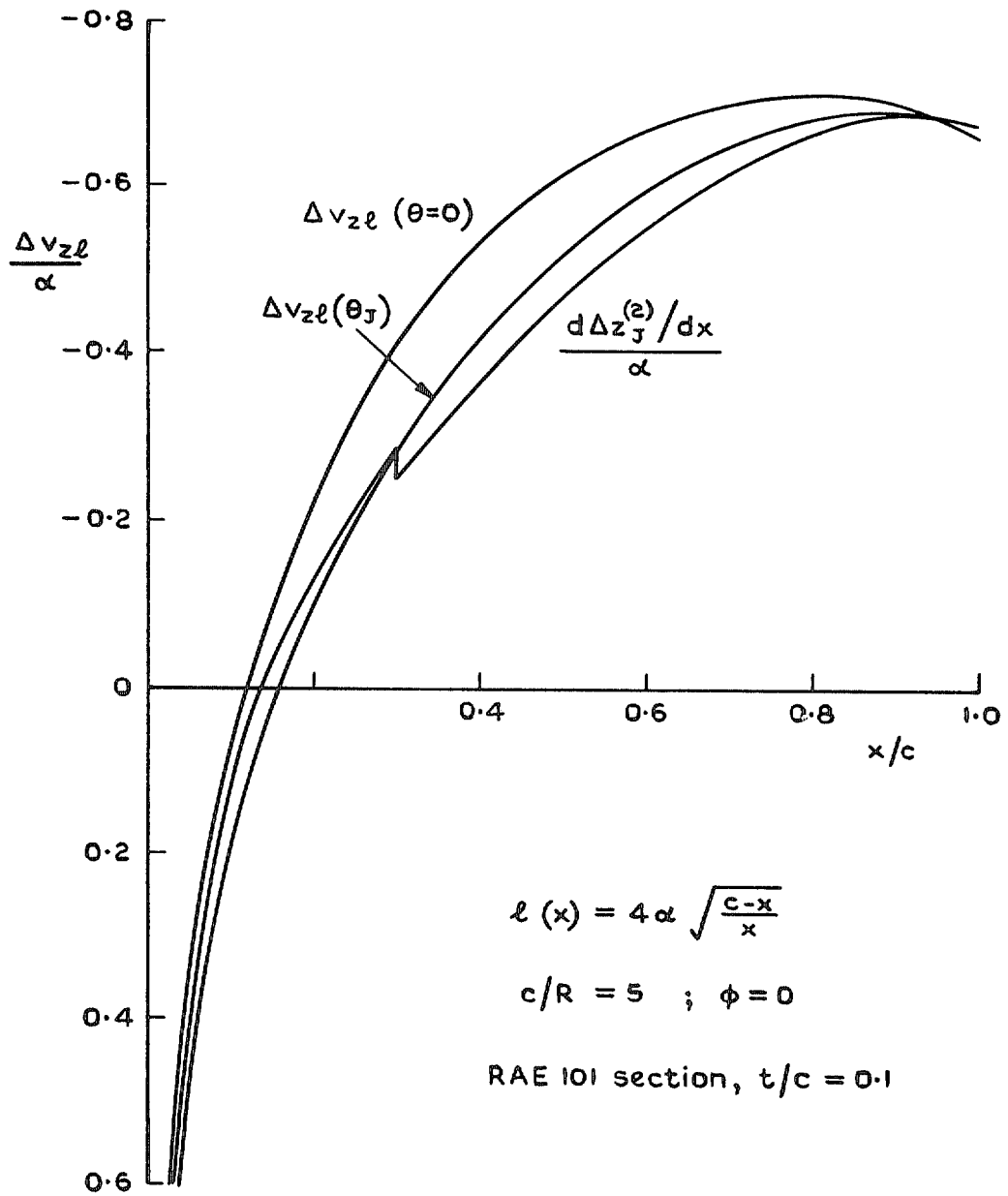

Fig. 31. Downwash distributions in the wing–body junction.

Printed in England for Her Majesty's Stationery Office by J. W. Arrowsmith Ltd., Bristol BS3 2NT
Dd. 289031 K.5. 2/76.

HER MAJESTY'S STATIONERY OFFICE

Government Bookshops

49 High Holborn, London WC1V 6HB
13a Castle Street, Edinburgh EH2 3AR
41 The Hayes, Cardiff CF1 1JW
Brazennose Street, Manchester M60 8AS
Southey House, Wine Street, Bristol BS1 2BQ
258 Broad Street, Birmingham B1 2HE
80 Chichester Street, Belfast BT1 4JY

Government publications are also available through booksellers

R. & M. No. 3781
ISBN 0 11 470926 2